INFORMATION TO USERS

This manuscript has been reproduced from the microfilm master. UMI films the text directly from the original or copy submitted. Thus, some thesis and dissertation copies are in typewriter face, while others may be from any type of computer printer.

The quality of this reproduction is dependent upon the quality of the copy submitted. Broken or indistinct print, colored or poor quality illustrations and photographs, print bleedthrough, substandard margins, and improper alignment can adversely affect reproduction.

In the unlikely event that the author did not send UMI a complete manuscript and there are missing pages, these will be noted. Also, if unauthorized copyright material had to be removed, a note will indicate the deletion.

Oversize materials (e.g., maps, drawings, charts) are reproduced by sectioning the original, beginning at the upper left-hand corner and continuing from left to right in equal sections with small overlaps.

Photographs included in the original manuscript have been reproduced xerographically in this copy. Higher quality 6" x 9" black and white photographic prints are available for any photographs or illustrations appearing in this copy for an additional charge. Contact UMI directly to order.

Bell & Howell Information and Learning
300 North Zeeb Road, Ann Arbor, MI 48106-1346 USA

UMI®
800-521-0600

UNIVERSITÉ DE MONTRÉAL

COMBUSTION OF NATURAL GAS IN A TURBULENT FLUIDIZED BED REACTOR

RAHMAT SOTUDEH GHAREBAAGH

DÉPARTEMENT DE GÉNIE CHIMIQUE

ÉCOLE POLYTECHNIQUE DE MONTRÉAL

THÈSE PRÉSENTÉE EN VUE DE L'OBTENTION

DU DIPLÔME DE PHILOSOPHIAE DOCTOR (Ph.D)

(GÉNIE CHIMIQUE)

DÉCEMBRE 1998

UNIVERSITÉ DE MONTRÉAL

ÉCOLE POLYTECHNIQUE DE MONTRÉAL

Cette thèse intitulée :

COMBUSTION OF NATURAL GAS IN A TURBULENT FLUIDIZED BED REACTOR

Présentée par: SOTUDEH GHAREBAAGH Rahmat
en vue de l'obtention du Diplôme de: Philosophiae Doctor
a été dûment acceptée par le jury d'examen constitué de:

M. PERRIER Michel, Ph.D., président
M. CHAOUKI Jamal, Ph.D., membre et directeur de recherche
M. LEGROS Robert, Ph.D., membre et co-directeur de recherche
M. KLVANA Danilo, Ph.D., membre
M. BEHIE Leo, Ph.D., membre

DÉDICACE

In His Name, The Most High

Dedicated to the Memory of My Beloved Father

ACKNOWLEDGMENT

I would like to express my appreciation to my supervisor Professor Jamal Chaouki for his guidance, help, manifest ideas and moral support. I also thank Dr. R. Legors for his help at the early stage of my Ph.D. studies. Our research collaboration with Mr. Navid Mostoufi has been a most enjoyable experience. His collaboration and help are very much appreciated. The catalytic presence of Dr. Bi from UBC at Ecole Polytechnique was also very useful. The success of this project relied on the participation of the followings:

- Pierre for his assistance in laboratory with high temperature experiments, his useful discussion and endless help.
- Giordano and Yannick for laboratory assistance.
- Daniel, Jean and Robert for technical assistance.
- Special credit also goes to my friends, Saeid and Deiva for their help.

On a more personal note, I would like to thank my dear friend Mr. Mahmoud Mayanloo and his respected family at Laval University for their continued help and moral support.

The Ministry of Culture and Higher Education of I. R. of IRAN is also acknowledged for making Mr. R. Sotudeh-Gharebaagh's graduate studies possible in Canada. This research

work was supported by a grant provided by National Science and Engineering Research Council (NSERC) of Canada and Dupont Inc.

I would also like to thank the members of my jury, Professors Michel Perrier, Danilo Klvana and Leo Behie of University of Calgary, for taking the time to critique this thesis.

I owe a debt of gratitude to my parents and parents in-law and all members of our family. Without their support and encouragement, the completion of this degree was impossible.

Finally foremost, I am deeply grateful and indebted to my wife, for her tremendous support, sacrifice and patient and my two beloved children *Hadi* and *Hanieh* during our stay in Canada.

RÉSUMÉ

La combustion du gaz naturel dans un lit fluidisé s'avère intéressante sur le plan industriel en matière de récupération d'énergie ou encore de valorisation énergétique des déchets ayant un faible pouvoir calorifique. Il s'agit aussi d'un excellent sujet pour la modélisation de réactions rapides et très exothermiques en lit fluidisé. L'isothermicité des lits fluidisés et leur capacité à contenir les réactions exothermiques les a rendu très populaires pour des applications dans l'industrie pétrochimique, la chimie de synthèse et la génération de chaleur. De plus, la nécessité d'assurer des hauts taux de production, un bon contact gas-solide, des temps de résidence relativement courts ainsi que la facilité de manipuler les particules solides et les catalyseurs tendent à désigner le régime turbulent comme le régime de choix en matière de fluidisation. Pour les raisons ci-haut mentionnées, la combustion du gaz naturel peut être mise en pratique de façon très avantageuse dans un lit fluidisé turbulent opérant à des températures inférieures à 1000°C permettant ainsi de respecter les exigences environnementales.

L'objectif principal du présent projet de recherche était d'établir la faisabilité de la combustion du gaz naturel dans un lit fluidisé de particules inertes opérant dans le régime turbulent à des températures entre 800 et 1000°C. Pour ce faire, les objectifs spécifiques suivants ont été étudiés:

1. L'évaluation de la contribution des particules inertes aux réactions de combustion.

2. La détermination des cinétiques des différentes réactions impliquées.

3. La détermination du régime de fluidisation idéal pour la combustion du gaz naturel.

4. La caractérisation de l'hydrodynamique et du *mélange des gaz* des buses d'injection orientées vers le bas introduits dans le lit fluidisé et des gaz de fluidisation.

5. La simulation du réacteur en jumelant le mécanisme réactionnel au modèle hydrodynamique.

L'évaluation de la contribution des particules inertes aux réactions de combustion a été réalisée en étudiant la combustion de débits à faible teneur en méthane (2-4% dans l'air) dans un réacteur à lit fixe chargé de particules inertes. Les données expérimentales ainsi obtenues en utilisant comme particules inertes du sable ou des particules d'alumine ont démontré un faible effet catalytique à base température (<700°C). Par contre, pour des températures intermédiaires (entre 750 et 850°C), un effet d'inhibition s'avère considérable. Pour des températures supérieures à 1000°C, les effets catalytiques et d'inhibition sont négligeables. Un mécanisme réactionnel réduit a été adopté et modifié afin d'expliquer les données expérimentales. Ainsi, les cinétiques (ordres de réaction,

facteur pré-exponentiel et énergie d'activation) d'une vingtaine de réactions ont été identifiées.

La détermination du régime de fluidisation idéal a été réalisée en faisant la combustion du gaz naturel dans les régimes turbulents et à bulle à des températures entre 800 et 1000°C. Avant de faire la combustion, des tests hydrodynamiques ont été réalisés à hautes températures afin de déterminer les vitesses de transition au régime turbulent. Les résultats expérimentaux démontrent la grande qualité des lits fluidisés à maintenir l'isothermicité du milieu réactionnel. De plus, la puissance générée dans le régime turbulent est de loin supérieure à celle générée dans le régime à bulle, et ce tout en respectant les normes environnementales. Lors des tests de combustion, les profiles axiaux de CO ont été mesurés.

Par souci pour la sécurité et en raison d'applications industrielles limitées, l'étude de la combustion dans le mode *non mélangé* (l'oxygène et le gaz naturel sont alimentés d'une manière séparée) a été préféré au mode *mélangé* (l'oxygène et le méthane sont d'abord mélangés avant leur injection dans le lit). Afin de mieux comprendre la combustion dans le mode *non mélangé*, l'hydrodynamique des buses d'injection orientées vers le bas a été longuement étudiée en utilisant comme particules du sable et du FCC. Le but de cette partie de l'étude était de caractériser les modes d'injection, bullage et jet, au moyen de mesures de pression, de test de mélange et de réaction. Les résultats expérimentaux indiquent qu'en présence de bullage, les bulles tendent à conserver leur identité, c'est-à-

dire que le transfert de matière entre les bulles est plutôt faible, tandis que sous des conditions de jet, une zone très turbulente est développée autour des buses d'injection, favorisant ainsi le transfert de matière et aussi l'attrition des particules. Étant donné les répercussions à l'échelle industrielle, les conditions de bullage ont été étudiées afin de caractériser la dispersion axiale et radiale des gaz injectés dans un lit fluidisé opérant à hautes températures. Un modèle à trois phases a été utilisé afin de déterminer les longueur de *mélange*. Les influences de la géométrie de l'injecteur et de la taille de particules ont aussi été étudiées.

L'étape ultime consistait à développer un modèle mathématique permettant de prédire la performance du réacteur en combinant un mécanisme réactionnel de la combustion du gaz naturel à un modèle hydrodynamique représentant tant le lit que l'injecteur. Le modèle a permis de prédire de façon appréciable les effets reliés aussi bien aux réactions impliquées qu'à l'hydrodynamique du lit et des régions d'injection des gaz.

ABSTRACT

Combustion of natural gas in fluidized bed reactors emerges as a promising technology for heat generation, waste-to-energy applications by low calorific fuel upgrading and also can be considered as an excellent example of highly exothermic reactions. Effective handling of highly exothermic chemical reactions in these reactors has made the fluidized bed technology gain a high rate of application in petroleum and petrochemical industry. Furthermore, the need to ensure high throughput at industrial scale, improved gas-solid contact, relatively short residence time and ease of solid and catalyst handling, points the turbulent fluidization regime as the most appropriate one. Combustion of natural gas in a turbulent bed reactor can be carried out at temperatures well below 1000 °C and hence capable of meeting all environmental requirements such as CO and NO_X emission levels.

The main objective of present study is to assess the feasibility of high temperature combustion of natural gas in turbulent fluidized bed reactors of inert particles. Specific objectives are as follows:

- To evaluate the combustion behaviour of inert particles and to determine the reaction scheme.
- To determine the appropriate hydrodynamic regime of fluidization and combustion mode for natural gas combustion.

- To characterize gas sparger hydrodynamics and mixing.
- To predict the reactor performance by coupling the kinetics and the hydrodynamics.

The kinetic evaluation of inert particles was achieved by studying the combustion of a lean mixture of methane in a fixed bed reactor of inert particles. The experimental data obtained in this way shows the accelerating catalytic effect of inert particles, i.e. sand or alumina, is quite small. In addition, the inhibition effect is considerably higher at moderately high temperatures (<850 °C) and it may be neglected at high temperatures well above 1000 °C. A reduced reaction scheme was also adapted and modified in order to explain the experimental data.

The appropriate hydrodynamic regime of fluidization was determined by promoting natural gas combustion in bubbling and turbulent fluidization regimes at relatively high temperatures (800-1000°C). Prior to combustion tests in these two fluidization regimes, the onset of turbulent fluidization was determined experimentally at high temperatures. The experimental results show that the fluidized bed reactors offer excellent thermal uniformity and temperature control. Furthermore, the power generated by the turbulent fluidization regime is much higher than that for bubbling fluidized bed reactors while respecting all environmental requirements. In these combustion tests, the CO profile was also measured inside the bed.

Due to safety concerns and also limited industrial applications of premixed combustion, the non-premixed combustion is only considered in this investigation. In order to understand the non-premixed combustion, the sparger hydrodynamics were extensively studied using FCC and sand particles. The aim of this part of the study was to characterize different discharge modes, bubbling and jetting conditions around the sparger using a pressure measurement technique, mixing and reaction studies. For industrial scale reactors, the dominant discharge mode is the bubbling conditions around the sparger. Under these considerations, experimental studies show that the bubbles tend to retain their identity. Under jetting conditions, a highly turbulent area may be formed around the sparger leading to high degree of attrition. Due to the large industrial impact of bubbling conditions, the radial and axial dispersion of gas in a hot fluidized bed reactor of 20-cm diameter of FCC and sand particles was investigated using a gas chromatography with CH_4 or CO_2 as tracers. A three-phase model was used to obtain the mixing length for these experiments. The effect of sparger configuration and particle size was also investigated.

The ultimate step consisted of building a mathematical model in order to simulate the performance of the reactor by combining a reduced natural gas combustion mechanism and bed-sparger hydrodynamics model. The model predicts reasonably the experimental data, explaining the reactions as well as hydrodynamic effects.

CONDENSÉ EN FRANÇAIS

L'élimination des polluants qui résultent de l'incinération de combustibles fossiles constitue un élément clé en ce qui a trait à la saine gestion des ressources et la préservation de l'environnement. Les unités de combustion traditionnelles sont défavorisées en raison de leurs sévères conditions d'opération: températures élevées et hauts niveaux d'émissions atmosphériques. Cependant, parmi les unités de combustion, les lits fluidisés sont celles disposant de la plus grande efficacité énergétique. Les lits fluidisés comportent bon nombre d'avantages dont leur simplicité de construction, leur taille plus compacte, leur flexibilité à accepter des réactifs gazeux, solides ou liquide et leur efficacité de combustion à basse température, minimisant ainsi les NO_X thermiques. De plus, combinés à un combustible tel le gaz naturel, ils peuvent être mis à profit dans diverses applications bénéficiant ainsi d'avantages tels: préparation minimale du comburant, haute efficacité énergétique, opération économique et faibles niveaux d'émission. Une sélection judicieuse des solides formant le lit peut faciliter la capture in-situ des polluants atmosphériques générés par les réacteurs.

De façon générale, les lits fluidisés sont basés sur les mêmes principes. De l'air ou un gaz quelconque est alimenté à travers un distributeur positionné à la base d'un lit de particules fines. Comme le gaz s'écoule vers le haut du réacteur, la fluidisation débute lorsque les particules sont supportées par le gaz et le lit adopte le comportement d'un liquide. Pour ces raisons, ces réacteurs peuvent être opérés sans donner lieu à des points

chauds. En plus de cet atout, les lits fluidisés sont caractérisés par un bon contact gaz-solide et la facilité avec laquelle on peut manipuler les solides. En raison de ces très importants avantages, les lits fludisés sont grandement utilisés dans les procédés industriels tels: le raffinage du pétrole, le traitement de solides, le séchage, le traitement de surface et la combustion. De plus, les lits fluidisés peuvent aussi être considérés comme la meilleure technologie pour des applications au niveau résidentiel à cause des hauts coefficients de transfert de chaleur qui existe entre le lit et les échangeurs de chaleur.

Selon la vitesse superficielle du gaz de fluidisation, différents régimes sont observés. À basse vitesse (~1 cm/s), on a le régime à bulle, on passe au régime turbulent à vitesse élevée (~1 m/s) et aux régimes de fluidisation rapide et de transport à vitesse très élevée (>4 m/s). La majorité des travaux académiques ont été réalisés sur des lit fluidisé à bulles, pour des raisons de simplicité. Ces réacteurs sont caractérisés par la présence de grosses bulles, un contact gas-solide qui laisse à désirer, un haut niveau de rétro mélange et des faibles niveaux de production. À l'inverse, à l'échelle industrielle, la plupart des réacteurs ont été optimisés en opérant dans le régime turbulent, régime caractérisé par la présence de petites bulles donnant au lit plus homogénéité et un bon contact gas-solide. Les lits fluidisés circulants peuvent aussi être envisagés comme alternative pour la combustion du gaz naturel. La combustion des mélanges méthane-air est fortement défavorisée par la présence de particules dans ces réacteurs, étant donné que les surfaces des solides donnent lieu aux réactions de terminaison des radicaux libres. Il en résulte

une diminution de la conversion du mélange réactionnel en fonction du taux de circulation des solides pour des conditions données. On peut donc conclure qu'un faible niveau de circulation de solide correspondant au régime turbulent est favorable afin d'obtenir un niveau de conversion acceptable. De plus, le coût d'investissement d'un lit fluidisé circulant est beaucoup plus important que celui d'un lit fluidisé turbulent.

Le lit fluidisé turbulent semble être le réacteur de choix pour les réactions rapides et exothermiques. Il a comme avantages un bon transfert de chaleur, un bon contact gaz-solide, une excellente isothermicité, des hauts taux de productions, une simplicité de construction, un coût d'investissement faible et des temps de résidence faibles lorsque comparés à des unités de combustion conventionnelles. Grâce à la présence de bulles de petites tailles, son comportement est en première approximation pseudo-homogène, ce qui permet d'obtenir des conversions supérieures à celles des lits à bulles. Pour ces raisons, ce type de réacteur peut être mis à profit comme une méthode innovatrice pour fin de génération d'énergie à partir de gaz naturel seul ou en combinaison à un autre combustible ayant un plus faible pouvoir calorifique. Il en résulterait une énergie plus propre qui répondrait aux exigences environnementales en réduisant la taille requise des incinérateurs et en diminuant les émissions atmosphériques.

Le développement de tels lits fluidisés turbulents doit être perçu comme une technologie gazière ayant un fort potentiel d'applications telles: des bouilloires ou fournaises industrielles co-alimentées, des unités de génération d'eau chaude au niveau domestique.

La technologie devient encore plus intéressante lorsque le gaz naturel est utilisé en combinaison avec des combustibles de basse qualité afin d'en faciliter la combustion d'en le but d'en faire une valorisation énergétique, i.e. génération de vapeur ou d'électricité. Dans cette perspective, il devient pertinent au point de vue énergétique et environnemental de faire la combustion du gaz naturel dans un lit fluidisé turbulent. Avant tout, il est capital de comprendre la combustion du gaz naturel dans un lit fluidisé turbulent. La combustion du gaz naturel dans un lit fluidisé turbulent peut être réalisée dans un lit fluidisé turbulent à des températures bien inférieures à 1000°C facilitant ainsi le respect des normes environnementales en réduisant la génération des NO_X thermiques.

L'objectif principal du présent projet de recherche était d'établir la faisabilité de la combustion du gaz naturel dans un lit fluidisé de particules inertes opérant dans le régime turbulent à des températures entre 800 et 1000°C. Pour ce faire, les objectifs spécifiques suivants ont été étudiés: (1) l'évaluation de la contribution des particules inertes aux réactions de combustion; (2) la détermination des cinétiques des réactions impliquées; (3) la détermination du régime de fluidisation idéal pour la combustion du gaz naturel; (4) la caractérisation de l'hydrodynamique et du *mélange des gaz* des buses d'injection orientées vers le bas introduites dans le lit fluidisé et des gaz de fluidisation; (5) la simulation du réacteur en jumelant le mécanisme réactionnel au modèle hydrodynamique.

L'évaluation de la contribution des particules inertes aux réactions de combustion a été réalisée en étudiant la combustion de débits à faible teneur en méthane (2-4%) dans un

réacteur à lit fixe chargé de particules inertes. Le réacteur consiste en deux tubes concentriques de 0,6 m de long avec des diamètres de 13 mm (interne) et 7 mm (externe) respectivement. Les tubes sont en alumine afin de limiter les effets de surface et de pouvoir supporter des températures importantes. La combustion a lieu dans l'espace qui sépare les tubes et où les particules étudiées sont disposées. Cette configuration rend possible la mesure de la température à l'intérieur du tube interne. Les débits de méthane et d'air sont mesurés et contrôlés au moyen de débitmètres massiques et ne sont mélangés qu'à l'entrée du réacteur. Les échantillons gazeux sont soutirés à la sortie du réacteur et analysés par chromatographie gazeuse. Les données expérimentales ainsi obtenues en utilisant comme particules inertes du sable et des particules d'alumine ont démontré un faible effet catalytique à base température (<700°C). Par contre, pour des températures intermédiaires (entre 700 et 850°C), un effet d'inhibition s'avère considérable. Pour des températures supérieures à 1000°C, les effets catalytiques et d'inhibition sont négligeables. Finalement, un mécanisme réactionnel réduit a été adopté et modifié afin d'expliquer les données expérimentales. Ainsi, les cinétiques (ordres de réaction, facteur pré-exponentiel et énergie d'activation) d'une vingtaine de réactions ont été identifiées.

La détermination du régime de fluidisation idéal a été réalisée en effectuant des tests de combustion du gaz naturel dans les régimes turbulent et à bulle sur une unité pilote à des températures entre 800 et 1000°C. Le réacteur utilisé a un diamètre interne de 200 mm et une hauteur de 2 m. Sa paroi interne est constituée d'une couche réfractaire. Un brûleur d'une puissance nominale de 20 kW est monté à la base du lit afin de faciliter le

préchauffage du lit. Lors des tests de combustion, des particules de sable ayant un diamètre moyen de 543 μm ont été utilisés. Plusieurs ouvertures ont été disposées à différentes positions axiales stratégiques afin de prendre les profils de pression, de composition des fumées de combustion, et d'injecter le gaz naturel au réacteur. Les mesures de compositions étaient effectuées par chromatographie gazeuse, bien que des analyseurs de fumées de combustion ont aussi été mis à contribution. Des thermocouples de type K ont été disposés à différentes positions axiales afin d'obtenir le profil de température. Un capteur de pression a été utilisé afin de suivre l'évolution du niveau de solide dans le lit. Au cours des expériences les mesures de température et de pression ont été sauvegardées par un système d'acquisition de données.

Avant de faire la combustion, des tests hydrodynamiques ont été réalisés à hautes températures afin de déterminer les vitesses de transition au régime turbulent. Les résultats expérimentaux démontrent la grande qualité des lits fluidisés à maintenir l'isothermicité du milieu réactionnel. De plus, la puissance générée dans le régime turbulent est de loin supérieure à celle générée dans le régime à bulle, et ce tout en respectant les normes environnementales. Lors des tests de combustion, les profiles axiaux de CO ont été mesurés.

Par soucis pour la sécurité et en raison d'applications industrielles limitées, l'étude de la combustion dans le mode *non mélangé* (l'oxygène et le gaz naturel sont alimentés d'une manière séparée) a été préférée au mode *mélangé* (l'oxygène et le méthane sont d'abord

mélangé avant leur injection dans le lit). Afin de mieux comprendre la combustion dans le mode *non mélangé*, l'hydrodynamique des buses d'injection orientées vers le bas a été longuement étudiée en utilisant comme particules du sable et du FCC. Pour cette série d'expériences, le montage expérimental était le même que celui décrit dans la section précédente. Le but de cette partie de l'étude était de caractériser les modes d'injection, bullage et jet, au moyen de mesures de pression, de test de réaction. Les résultats expérimentaux indiquent qu'en présence de bullage, les bulles tendent à conserver leur identité, c'est-à-dire que le transfert de matière entre les bulles est plutôt faible, tandis que sous des conditions de jet, une zone très turbulente est développée autour des buses d'injection, favorisant ainsi le transfert de matière et aussi l'attrition des particules. Étant donné les répercussions à l'échelle industrielle, les conditions de bullage ont été étudiées afin de caractériser les dispersions axiale et radiale des gaz injectés dans un lit fluidisé de 200 mm de diamètre interne opérant à haute température. Les tests impliquaient l'injection de gaz tels le CO_2 et le méthane. Un modèle à trois phases a été utilisé afin de déterminer les longueur de mélange. Les influences de la géométrie de l'injecteur et de la taille de particules ont aussi été étudiées.

L'étape ultime consistait à développer un modèle mathématique permettant de prédire la performance du réacteur opérant dans le régime fluidisé turbulent et en mode non mélangé. Le modèle proposé consiste en une combinaison d'un mécanisme réactionnel de la combustion du gaz naturel à un modèle hydrodynamique représentant tant le lit que l'injecteur. Le sous-modèle hydrodynamique prend ses racines dans les expériences

effectuées au laboratoire et en utilisant des informations provenant de la littérature, tandis que le sous modèle réactionnel décrivant la combustion du gaz naturel ainsi que la formation des polluants atmosphériques est tiré de la littérature et des résultats expérimentaux obtenus dans le cadre de ce projet. La validité du modèle a été démontrée en le confrontant aux résultats expérimentaux obtenus. Le modèle a permis de prédire de façon appréciable les effets reliés aussi bien aux réactions impliquées qu'à l'hydrodynamique du lit et des régions d'injection des gaz.

TABLE OF CONTENT

LIST OF TABLES

LIST OF FIGURES

LIST OF APPENDICES

CHAPTER II NOMENCLATURE

$[A_k]$	molar concentration of k^{th} species, ($kmol/m^3$)
[M]	effective concentration of mixture, ($kmol/m^3$)
A	constant
A_k	symbolic representation of k^{th} species
a_{nk}	NASA polynomial coefficients to fit of thermodynamic data, (n=1,2,3, ...7)
$C°_{pk}$	standard state specific heat at constant pressure of the k^{th} species, (J/mol.K)
d_p	mean particle size, (μm)
E_i	activation energy in the rate constant of the i^{th} reaction, (J/mol)
$E_{icorr.}$	corrected activation energy in rate constant of i^{th} reaction, (J/mol) (Ei+ΔE)
F	molar flow rate, (mol/s)
f	ratio of heterogeneous reaction rate to homogeneous reaction rate
F_{cent}	blending function
F_{CH40}	initial methane molar flux, (mol/s)
$H°_k$	standard state enthalpy of the k^{th} species, (J/mol)
i	reaction index
I	total number of reactions
k	ratio of inner tube to outer tube
k	species index
K	total number of species
k_0	lower limit reaction rate constant, (depends on reaction)

K_{ci}	equilibrium constant in concentration units for the i^{th} reaction
k_{fi}	forward reaction rate constant of i^{th} reaction, (depends on reaction)
k_{ri}	reverse reaction rate constant of i^{th} reaction, (depends on reaction)
k_i	pre-exponential factor in the rate constant of the i^{th} reaction
k_{pd}	pressure dependent reaction rate expression, ($kmol/m^3.s$)
K_{pi}	equilibrium constant in pressure units for the i^{th} reaction, (depends on reaction)
k_∞	upper limit reaction rate constant, (depends on reaction)
L	length, (m)
n_i	temperature exponent in the rate constant of the i^{th} reaction
P	pressure, (pa)
P_a	atmospheric pressure, (pa)
p_r	reduced pressure
R	Outer tube diamter, mm
R	universal gas constant, (J/mol.K)
R_2	universal gas constant, (cal/mol.K)
r_i	i^{th} elementary reaction rate ($kmol/m^3.s$)
r_k	net production rate of k^{th} species, ($kmol/m^3.s$)
r_{max}	maximum value in elementary reaction rate vector ($kmol/m^3.s$)
$S°_k$	standard state entropy of the k^{th} species, (J/mol.K)
T	temperature, (°C)
T_b	reactor temperature, (K)

v	reactor volume, (m^3)
W	mass of solid particles in the bed, (kg)
X_{CH40}	initial methane mole fraction

Greek Symbols

τ	mean residence time (s)
α	constant
Δ	refers to changes occuring in passing from reactants to products in i^{th} reaction
ΔE	difference between E for heterogeneous and homogeneous reactions, (KJ/mol)
β	constant
β_0	constant
β_{ki}	enhanced third body coefficients of the k^{th} species in the i^{th} reaction
δ	threshold value used for mechanism reduction <1
γ	constant
η	contact time index (W/F_{CH40}) (g.s/mol)
ν''_{ki}	stoichiometric coefficients of the k^{th} product species in i^{th} reaction
ν'_{ki}	stoichiometric coefficients of the k^{th} reactant species in i^{th} reaction
θ	constant in equation

Subscripts

0	refers to lower limit for pressure dependent reactions
a	refers to alumina particles
het	refers to heterogeneous reactions
hom	refers to homogeneous reactions
i	i^{th} reaction
k	k^{th} species
∞	refers to upper limit for pressure dependent reactions

CHAPTER III NOMENCLATURE

D	reactor diameter, m
d_p	mean particle size, μm
F_{CH4}	methane molar flow rate (mol/s)
P	power generated during the combustion process (kW)
T	bed temperature, K
T_0	ambient temperature, K
U	superficial gas velocity, m/s
U_c	onset of turbulent fluidization, m/s
U_j	jetting velocity, m/s
X	methane conversion
z	height along the bed, m

Greek Letters

ΔH(T)	heat of combustion at temperature T

CHAPTER IV NOMENCLATURE

C	concentration ($kmol/m^3$)
D	bed diameter (m)
d_b	bubble diameter, m
D_e	effective diffusion coefficient of gas (m^2/s)
d_j	nozzle diameter (m)
d_p	particle diameter (μm)
g	acceleration due to gravity, (m/s^2)
K_{be}	bubble to emulsion mass transfer coefficient, s^{-1}
L_j	characteristic jet length (mm)
P	pressure (Pa)
T	temperature (K)
U	gas velocity (m/s)
U_c	onset of turbulent fluidization (m/s)
U_j	discharge velocity (m/s)
U_{mf}	minimum fluidization velocity (m/s)
U_{mj}	minimum jetting velocity (m/s)
U_{or}	orifice velocity (m/s)
z	axial position (m)

Greek letters

δ	bed volume fraction in bubble phase
ρ	particle density (kg/m^3)
ε	porosity (-)
ρ_f	gas density (kg/m^3)
μ_g	gas viscosity (Pa.s)

Subscripts

e	emulsion
g	grid
s	sparger

CHAPTER V NOMENCLATURE

A	cross sectional area, m^2
C	concentration, $kmol/m^3$
D	reactor diameter, m
d_b	bubble diameter, m
D_e	effective diffusion coefficient, m^2/s
d_j	discharge hole diameter, mm
d_p	mean particle size, μm
E_i	activation energy in the rate constant of the i^{th} reaction, (J/mol)
g	acceleration due to gravity, m/sec^2
H	bed height, m
h_0	bed height above sparger, m
I	total number of reactions
K	total number of species
K_{be}	bubble to emulsion mass transfer coefficient, s^{-1}
k_i	pre-exponential factor in the rate constant of the i^{th} reaction
L_j	characteristic jet length (mm)
n_i	temperature exponent in the rate constant of the i^{th} reaction
P	pressure, pa
q_{bj}	induced gas flow from bed to jet, m^3/s
r_i	i^{th} chemical reaction rate, $kmol/m^3.s$

R_k net production rate of k^{th} species, $kmol/m^3.s$

T bed temperature, K

U gas velocity, m/s

U_j jetting velocity, m/s

x axial postion from the sparger tip toward jet penetration length, m

z axial coordinate, m

Greek letters

μ gas viscosity, pa.s

θ jet half angle from the axial position

δ bed volume fraction in the bubble phase

ε voidage

ν''_{ki} stoichiometric coefficients of the k^{th} product species in i^{th} reaction

ν'_{ki} stoichiometric coefficients of the k^{th} reactant species in i^{th} reaction

ρ solid density , kg/m^3

Subscripts

0 initial conditions

abs absolute value

e emulsion phase

fg	gas phase in the jet
g	gas phase
g	grid bubbles
i	reaction index
j	refers to jet
bx	bed properties as a function of x
jx	average inside of the jet
k	species index
mf	minimum fluidization
r	radial position, m
s	solid
s	sparger bubbles

CHAPTER 1: INTRODUCTION

1.1 Introduction

Safe control, efficient reduction and economical destruction of pollutant emissions from the devices burning various fossil fuels are major focuses of environmental concern and legislation. In response to such environmental requirements and based on increased availability of natural gas, different attractive and cost-effective technologies such as basic co-firing and gas reburn (*American Gas association, 1991*) have been initiated. Co-firing, which means combining natural gas with fuels e.g. coal being burnt in the combustion chamber is regarded as an *in-situ* destruction method of pollutants and gives the system significantly more flexibility than flue gas desulphurization or switching to low sulfur or high grade fuels. Gas reburn is also becoming an important and commercially feasible technology for reducing NO_X emissions (*Makansi, 1989*) in large-scale industrial waste-to-energy plants. Since the combustion of natural gas produces virtually no sulfur oxide and reactive hydrocarbon or particulate, these two methods can be considered as the modified combustion technique being applied to different fossil fuel burning devices to reduce the pollutant emissions.

Attempts to burn natural gas in conventional devices are hindered by the hostile environments of these furnaces, including high temperatures and high levels of flue gas emissions. Such high temperatures make the combustor to become less resistant to corrosion and to be deformed by temperature-related stresses that occur during normal furnace operation. However, among the fossil fuel burning devices, fluidized beds are the most promising energy-conversion options available today. They also offer a variety of advantages, including their simplicity of construction, their smaller size, their flexibility in accepting solid, liquid or gaseous fuels and their high combustion efficiency at a remarkably low temperature while minimizing thermal NOx generation. In addition, they can be widely used with natural gas for wide range of applications, providing some unique advantages such as, minimal fuel preparation requirements, high energy efficiency, economical system operation and lower emission levels. Moreover, judicious selection of bed material can result in the in-bed capture of gaseous pollutant species generated in fluidized bed reactors.

Basically, all fluidized bed reactors operate based on the same principles in which gas or air is fed upward through a distributor at the bottom of the bed of finely divided particles. As the gas flows upward, fluidization occurs as the particles begin to move in liquid-like behavior. The process leads to high heat transfer to the particles because of increased heat transfer coefficients. The reactors could also be operated isothermally without developing hot-spots (Foka et al, 1994a; Gonzalez, 1995; Grace, 1990; Avidan, 1982) and are fully capable of meeting all environmental requirements. These characteristics,

the versatility and unique features of the fluidized bed technique have led to its application in a wide range of industrial processes in petroleum refining, solids blending, drying, coating techniques and combustion. Furthermore, the fluidized bed can also be considered as the best technology for residential sector applications because of the high heat transfer rate between the bed and the heat exchanger (Molerus, 1995). The hot water obtained in this way can be used for heating or sanitary purposes.

Various fluidization regimes are observed as the superficial gas velocity increases ranging from the bubbling to fast fluidization. The fluidized bed reactors are specific to these fluidization regimes. Most works in academia have been focussed on bubbling fluidized bed reactors. These reactors are described by the existence of large bubbles, a poor gas-solid contact, high gas back mixing and a low throughput and therefore, they are not suitable for fast reactions where high conversion is expected. Most industrial processes operate under turbulent fluidized bed (TFB) conditions where a more homogeneous appearance with small bubbles and a good gas-solid contact exists *(Grace, 1990)*. Circulating Fluidized Bed (CFB) reactors can also be considered as an advanced alternative method for natural gas combustion. The combustion of methane-air mixture is strongly inhibited by solid particles in these reactors considering the fact that at solid surfaces reactive radicals recombine together shortly. Consequently, at given operating conditions, the conversion decreases with solid circulation rate (Feugier et al., 1987) and it can be concluded that a very low solid circulation rate, which corresponds to TFB

conditions, should be used for obtaining the high conversion. Moreover, when compared to TFB reactors, higher cost is associated with CFBC units for solid handling.

TFB reactors seem to be an ideal reactor for fast exothermic reactions at high temperatures. They have the advantages of the exceptionally high heat transfer, intimate gas and solid contact, excellent thermal uniformity and temperature control, high overall productivity, versatility, much lower capital cost and relatively short mean residence time as compared to the conventional combustion systems for a given geometry. Their overall homogeneous behavior makes the gas-solid contact to become more efficient by further enhancing the overall conversion (Gonzalez, 1995; Foka et al. 1994). Therefore, these reactors can provide an innovative method of converting natural gas, alone or with dirty fuels, to electricity with higher net efficiency in order to address the national and environmental concerns by providing more reasonable combustor size and lower pollutant levels.

The operation and process development for TFB can be considered as a promising technology for natural gas utilization with very large economic impact such as, industrial applications to co-fired boilers and furnaces, domestic applications to hot water generation for heating and sanitary purposes. The technology becomes more attractive when firing natural gas itself or with other low quality fuels for energy recovery and wastes disposal purposes. The low quality fuels, which may be easily burnt in fluidized bed reactors, are the lower grade and high-sulfur solid fuels, wood, pulp, paper and

municipal solid wastes, liquid and gaseous wastes. Therefore, mixing methane with these fuels makes firing of these materials in the TFB reactors become possible from the energy and environmental perspective. However, for all the claims made about the multiplicity and co-firing capabilities of natural gas in TFB reactors, only fewer applications at the industrial level are being carried out largely without scientific bases. The aim of this study, however, is to gain a more fundamental understanding of this new technology through a combination of experiments and modeling.

1.2 Objectives

The main objective of present study is to assess the feasibility of high temperature combustion of natural gas in TFB reactors. Specific objectives are as follows:

- To evaluate the combustion behaviour of inert particles and to determine the reaction scheme.
- To determine the appropriate hydrodynamic regime of fluidization and combustion mode for natural gas combustion.
- To characterize gas sparger hydrodynamics and mixing.
- To predict the reactor performance by coupling the kinetics and the hydrodynamics.

1.3 Thesis Structure

The thesis is made up of four papers. Besides these papers, which are forming the main body of the thesis in the form of different chapters, there is a general introduction, conclusions, recommendations and one appendix. The content of each part is described below:

- Chapter I consists of a general introduction presenting the global scope of the work and the related features reported in the literature. The objectives of the present studies also outlined.

- Chapter II consists of a paper submitted to Combustion & Flame entitled "Investigation of the Heterogeneous and Homogeneous Combustion of Methane". In this paper, the contribution of inert particles to the natural gas combustion was studied experimentally in a fixed reactor. A reduced reaction scheme was also adapted to explain the experimental data.

- Chapter III presents a publication entitled "Natural Gas Combustion in a Turbulent Fluidized Bed of Inert Particles", which will appear in Chemical Engineering Science. In this paper, the combustion of natural gas was studied in a TFB reactor of inert particles at relatively high temperatures in both bubbling and turbulent regimes.

- In Chapter IV, the publication " Gas Mixing in a Non-Premixed Turbulent Fluidized Bed Reactor" is presented. This article is submitted to Canadian Journal of Chemical Engineering. Sparger hydrodynamics and gas mixing are studied in detail using different technique and a model is presented to predict the mixing length.

- Chapter V consists of the publication entitled "A Mathematical Model for Natural Gas Combustion in a Turbulent Fluidized Bed of Inert Particles". The paper is submitted to Ind. Eng. Chem. Res. The model prediction of the reactor performance is quite satisfactory.

- Conclusions and Recommendations

- Four appendices which give more detail on fixed and fluidized bed studies: complementary detail on fixed bed studies, reactor operation and security manual, pressure fluctuation analysis and sample concentration calculations for all individual phases encountered in non-premixed fluidized bed reactors.

CHAPTER 2: INVESTIGATION OF THE HETEROGENEOUS AND HOMOGENEOUS COMBUSTION OF METHANE

Reference:

Sotudeh-Gharebaagh, R., J. Chaouki and R. Legros, (1998), "INVESTIGATION OF THE HETEROGENEOUS AND HOMOGENEOUS COMBUSTION OF METHANE", Submitted to COMBUSTION AND FLAME (November, 1998).

Keywords:

Methane combustion, inhibition, emulsion phase, reduced mechanism, fixed bed.

2.1 Abstract

The combustion of methane has been studied in a fixed bed reactor to determine the effect of inert particles on the combustion process through heterogeneous and homogeneous reactions. To elucidate these effects on combustion, premixed methane-air mixtures are introduced into a fixed bed of inert particles. Methane and CO_2 mole fractions are measured at the reactor outlet. The experimental data obtained in this way shows that the accelerating catalytic effect of inert particles, i.e. sand or alumina, is quite small. In addition, it is found that the inhibition effect is considerably higher at moderately high temperatures (<850 °C) and it may be neglected at high temperatures well above 1000 °C. A plug flow reactor model with a complete reaction scheme is developed to explain the experimental data. Based on information gathered during the simulation with the complete reaction mechanism, a reduced mechanism is developed and its performance is tested against the complete mechanism. Both mechanisms fail to fully predict the experimental data. Therefore, an improved combined mechanism, which takes into account the heterogeneous and homogeneous reactions chemistry, is proposed based on reduced mechanism. The combined mechanism is able to predict the experimental data satisfactorily for the operating conditions used in this investigation.

2.2 Introduction

Large amount of energy needed for power generation and other applications depends on direct or indirect combustion of natural gas (mainly methane) in combustion devices,

which may lead to some serious environmental problems. To settle these problems, the performance of the combustion devices should be improved in terms of high efficiency and low emission levels through understanding of elementary steps involved in combustion. As environmental regulations become more stringent, a better understanding of the mechanism and conditions, which lead to formation of undesired products, becomes critical for optimization of combustor performances.

Among the combustion devices, fluidized bed systems have so far been developed for efficient combustion of fuel-air mixture with less pollutant formations. Further improvements of combustion efficiency in fluidized bed reactors and reduction in pollutant emissions can be achieved using catalysts as bed materials. However, for power generation units, such combination increases the operating cost and the current accepted practice is to use inert particles as bed materials. These materials are cheap, readily available and applicable to high temperature conditions. Such inert particles, when used in combustion devices, can considerably alter the combustion process because of heterogeneous inhibition reactions. Therefore, a better understanding of how and why these particles influence the gaseous fuel combustion mechanism becomes very important in fluidized bed reactors.

Combustion phenomena are affected by inert particle surface through thermal and kinetic coupling with the homogeneous combustion. The thermal coupling is thought to play an important role in combustion [1]. The kinetic coupling between a surface and gas phase

becomes dominant in operations of fixed or fluidized bed reactors at moderately high temperatures. The coupling can be regarded as catalytic or inhibition effect through intermediate species interaction which is common in both heterogeneous and homogeneous phases. The extent of catalytic reaction contribution from solid inert particles is still unknown. For alumina particles for example, Brougton [2] reported that it has no significant accelerating catalytic effect. However, further work is still needed in order to conclude correctly on catalytic effects of different inert particles on the combustion mechanism.

Besides their catalytic activities, solid particles may inhibit combustion through depleting free radicals' concentration in the homogeneous phase. This effect was thought to explain the increase of homogeneous combustion ignition temperature in the presence of inert solid particles. Herein, the inhibition occurs when radical intermediates, which are crucial for ignition, may diffuse or be transported to the particle surface and be terminated there. The extent of inhibition varies with temperature and particle size distribution within the reactor [3, 4]. Moreover, it might be expected that the inhibition process due to solid surface would strongly affect the conversion of CO to CO_2. It is worth mentioning that the role of particle surface on the formation of undesired by-products such as CO or other intermediates is poorly understood. The undesired by-products may diffuse from or to the surface and hence would alter homogeneous combustion through momentum, energy and mass balance [4]. The inhibition may also occur because of third bodies (mixture of stable species), free radicals and bubble

surfaces in fluidized bed reactors. Lewis and von Elbe [5] stated that the rate of free radical termination by gas phase collision, through third bodies and free radicals, is negligible as compared to termination by solid surfaces. It should also be mentioned that the presence of third bodies could be easily modeled with gas phase kinetics. However, the contribution of heterogeneous processes in inhibition is not yet well understood and more work is needed.

This investigation is devoted to increase the understanding of the combustion behavior of premixed methane-air mixtures in a fixed bed of inert heat carriers in view of their use in the emulsion phase of turbulent fluidized bed reactors. Some qualitative conditions for fluidized bed reactors, i.e., catalytic effect, inhibition and temperature range of operation, may also be derived. An attempt is also made to employ complete and reduced reaction schemes within the reactor model. The reduced and complete mechanisms have never been applied to methane combustion in fluidized bed reactors. So far, Van de Vaart [6] applied a global reaction rate expression for the disappearance of methane in a fluidized bed reactor. The use of only one overall reaction has made prediction of CO, NO_x and other intermediates impossible.

2.3 Theory

Chemical reactions converting fuel to combustion products are complex depending in subtle ways on the conditions under which combustion takes place. An understanding of

the conversion process can be attained by identifying the elementary steps and the corresponding reaction rates. These steps coupled with the governing hydrodynamic equations are needed in order to explain the combustion process in a chemical reactor in detail. A large amount of information is now available in the combustion literature regarding the small molecules, [7, 8] which therefore increases the ability to model the combustion processes using computers. Herein, the most updated and complete reaction scheme is used in order to simulate the combustion mechanism of premixed methane-air mixtures in a fixed bed reactor.

As mentioned earlier, the study is aimed at understanding the combustion behavior of premixed methane-air mixture in fluidized bed reactors with inert sand or alumina particles. Such an understanding can be achieved by obtaining kinetic data at the operating range of interest for these reactors. However, fluidized bed reactors are hydrodynamically complex for deriving the kinetics data needed for combustion simulations. Therefore, the data must be obtained in reactors (e.g. fixed beds) where hydrodynamics can be described confidently [9]. For purpose of this study, the emulsion phase of the fluidized bed reactors is approximated with a fixed bed so that the kinetic measurements become possible. This approximation can be justified considering the fact that the emulsion phase is usually assumed to be at minimum fluidization conditions, where the large amount of solid particles are present. The behavior of the fixed bed, which is operated at steady state and isothermal conditions, is simulated by coupling a plug flow reactor model with a complete or reduced combustion kinetic model. In this

study, the reaction zone, which is a very thin shell of 3mm, is well located at the reactor center. With a very small amount of mixture flowing through the reactor, the flow is fully developed and the reactor remains isothermal. Therefore, it is reasonable to model the flow in the reactor as plug flow. Under these conditions, there is no radial gradient in velocity. These assumptions are so far verified in chemical reaction engineering. In the following section, description of the complete methane combustion mechanism and the approach used to obtain a reduced mechanism is presented.

2.3.1 The complete methane combustion mechanism

The detailed GRI (Gas Research Institute) mechanism for methane combustion, which consists of 279 elementary reaction steps among 49 species, is used in a wide range of experimental conditions encountered in the fixed bed reactor. The GRI mechanism is a product of computational and experimental researches sponsored by the Gas Research Institute (GRI) and several US work-groups have contributed to this mechanism. This is an optimized detailed chemical reaction mechanism capable of the best representation of methane combustion at this time. The validity of GRI approach has been demonstrated for the improvement of methane combustion mechanism. A detailed description of the complete GRI mechanism can be found in [10, 11] and the GRI's annual reports (i.e. [12]). Summary of mathematical expressions needed for calculation of reaction rates and thermodynamic properties, which were derived from [14, 8, 12], are given in Tables 2.1

and 2.2. The physico-chemical and thermodynamic properties needed for calculations are taken from the combustion literature [8, 10, 15].

Table 2.1 Summary of expressions used in simulation

$$\sum_{k=1}^{K} \nu'_{ki} A_k \rightleftharpoons \sum_{k=1}^{K} \nu''_{ki} A_k \qquad (i = 1,2,3,\ldots,I) \tag{2.1}$$

$$r_k = \sum_{i=1}^{I} (\nu''_{ki} - \nu'_{ki})\, r_i \qquad (k = 1,2,3,\ldots,K) \tag{2.2}$$

$$r_i = k_{fi} \prod_{i=1}^{K} [A_k]^{\nu'_{ki}} - k_{ri} \prod_{i=1}^{K} [A_k]^{\nu''_{ki}} \tag{2.3}$$

$$[M] = \sum_{k=1}^{K} \beta_{ki} [A_k] \tag{2.4}$$

$$k_{fi} = k_i T_b^{n_i} \exp\left(\frac{E_i}{R_2 T_b}\right) \tag{2.5}$$

$$k_{ri} = \frac{k_{fi}}{K_{ci}} \tag{2.6}$$

$$k_{pd} = k_\infty \left(\frac{p_r}{1 + p_r}\right) F_{cent} \tag{2.7}$$

$$p_r = \frac{k_{i0}\,[M]}{k_{i\infty}} \tag{2.8}$$

$$k_0 = k_{i0}\, T_b^{mi0} \exp\left(\frac{-E_i 0}{R_2\, T_b}\right)$$
$$k_\infty = k_{i\infty}\, T_b^{mi\infty} \exp\left(\frac{-E_{i\infty}}{R_2\, T_b}\right) \tag{2.9}$$

Table 2.1 (continued)

$$\log F = [1+]^{-1} \log F_{cent} \tag{2.10}$$

$$\begin{aligned} c &= -0.4 - 0.67 \log F_{cent} \\ n &= 0.75 - 1.27 \log F_{cent} \end{aligned} \tag{2.11}$$

$$F_{cent} = (1-\alpha) \exp\left(-\frac{T_b}{\beta}\right) - \alpha \exp\left(-\frac{T_b}{\gamma}\right) + \exp\left(-\frac{\theta}{T_b}\right) \tag{2.12}$$

$$\frac{dF_k}{dt} = r_k \tag{2.13}$$

$$\frac{dp}{dL} = -\beta_0 \frac{P_a}{p} \tag{2.14}$$

Table 2.2 Summary of expression used to calculate the thermodynamic properties

$$K_{ci} = K_{pi}\left[\frac{P_a}{RT_b}\right]^{\sum_{k=1}^{K}(\nu''_{ki}-\nu'_{ki})} \tag{2.15}$$

$$\ln K_{pi} = \frac{\Delta S^{\circ}_i}{R} - \frac{\Delta H^{\circ}_i}{RT_b} \tag{2.16}$$

$$\frac{\Delta S^{\circ}_i}{R} = \sum_{k=1}^{K}(\nu''_{ki}-\nu'_{ki})\frac{S^{\circ}_k}{R} \tag{2.17}$$

$$\frac{\Delta H^{\circ}_i}{RT_b} = \sum_{k=1}^{K}(\nu''_{ki}-\nu'_{ki})\frac{H^{\circ}_k}{RT_b} \tag{2.18}$$

$$C^{\circ}_{pk} = R(a_{1k} - a_{2k}T_b + a_{3k}T_b^2 - a_{4k}T_b^3 + a_{5k}T_b^4)$$

$$H^{\circ}_k = RT_b\left(a_{1k} - \frac{a_{2k}}{2}T_b - \frac{a_{3k}}{3}T_b^2 - \frac{a_{4k}}{4}T_b^3 - \frac{a_{5k}}{5}T_b^4 - \frac{a_{6k}}{T_b}\right) \tag{2.19}$$

$$S^{\circ}_k = R\left(a_{1k}\ln T_b - a_{2k}T_b - \frac{a_{3k}}{2}T_b^2 - \frac{a_{4k}}{3}T_b^3 - \frac{a_{5k}}{4}T_b^4 + a_{7k}\right)$$

2.3.2 The reduced methane combustion mechanism

The complete mechanism, which generates a great amount of chemical information, is not quite suitable for all modeling efforts since it requires high computation costs. In fact, not all the reactions contribute equally to the combustion process. Some of them may contribute significantly, some do marginally and the rest do not contribute at all. In addition, some of species reach almost stationary mole fractions by very rapid elementary

steps, while for others, this change happens slowly by elementary steps that determine their overall reaction rate. This is an important and unique property of the system and it will then be used for mechanism reduction. The component with small net rate may cause severe problem in solving large system of differential equations. Due to such unusual behavior of large reaction systems which needs high computing costs, number of methods has been initiated for mechanism reduction. In recent review given by Tomlin et al. [16], an up-to-date picture of all the main mathematical tools, which have been widely used in the combustion literature, has been provided for the construction, investigation and reduction of complex reaction mechanisms. There are also reviews, which discuss some of these methods in details [18, 19, 20, 21]. Almost all reduction techniques i.e. [22] have been developed and tested for combustion modeling and their applicability to combustion in chemical reactors are questioned. Apparently, there is still a continuing need for reliable and reduced mechanism which must be capable of predicting experimental data over the range of operating conditions for hydrodynamically complex chemical reactors.

In order to develop a reduced mechanism for the purpose of this investigation, the forward and reverse reactions, which have small contributions, are identified by examining their respective reaction rates. This can be achieved through sufficient rate information generated during the simulation with the complete mechanism by setting a threshold value (δ). The method is reliable for finding redundant reactions (Tomlin et al.

[16]) and non-contributing reactions can be identified by evaluating the following criterion for all grid points of the calculation:

$$\frac{|r_i|}{|r_{max}|} \leq \delta \qquad (2.20)$$

2.3.3 Solution method

The resulting ordinary differential equations (ODEs), in Table 2.1, are solved numerically to determine the evolution of the system for any assumed initial conditions. For a large number of components considered in the model, it should be mentioned that the existence of wide range of reaction rates in the ODEs leads to severe difficulties in solving them by conventional integration methods. Therefore, a finite difference method is used to calculate emissions of CO, unburned CH_4 and CO_2 with the complete and reduced mechanisms.

2.4 Experimental

The experimental study was carried out in a fixed bed reactor. A schematic of the experimental reactor is shown in Figure 2.1. The reactor consists of two concentric 0.6 m long tubes with 13 mm I.D. and 7 mm O.D., respectively and its walls are made of alumina in order to limit wall catalytic effects. Combustion takes place between the two concentric tubes in where the sand particles are placed. This configuration allows the

temperature inside the inner tube to be measured. Heating is provided by a high temperature furnace with a single heated zone of 222 mm long. The methane and air gas flows were measured with mass flow controllers and mixed before the reactor inlet. Total flow rates ranging from 100 and 500 *ml/min* premixed mixture with 2 to 4 % methane were introduced into the reactor. Gas samples were drawn at the reactor outlet. A gas chromatograph equipped with a thermal conductivity detector (TCD) was used to monitor the methane and CO_2 mole fractions. The CO emission level was calculated by

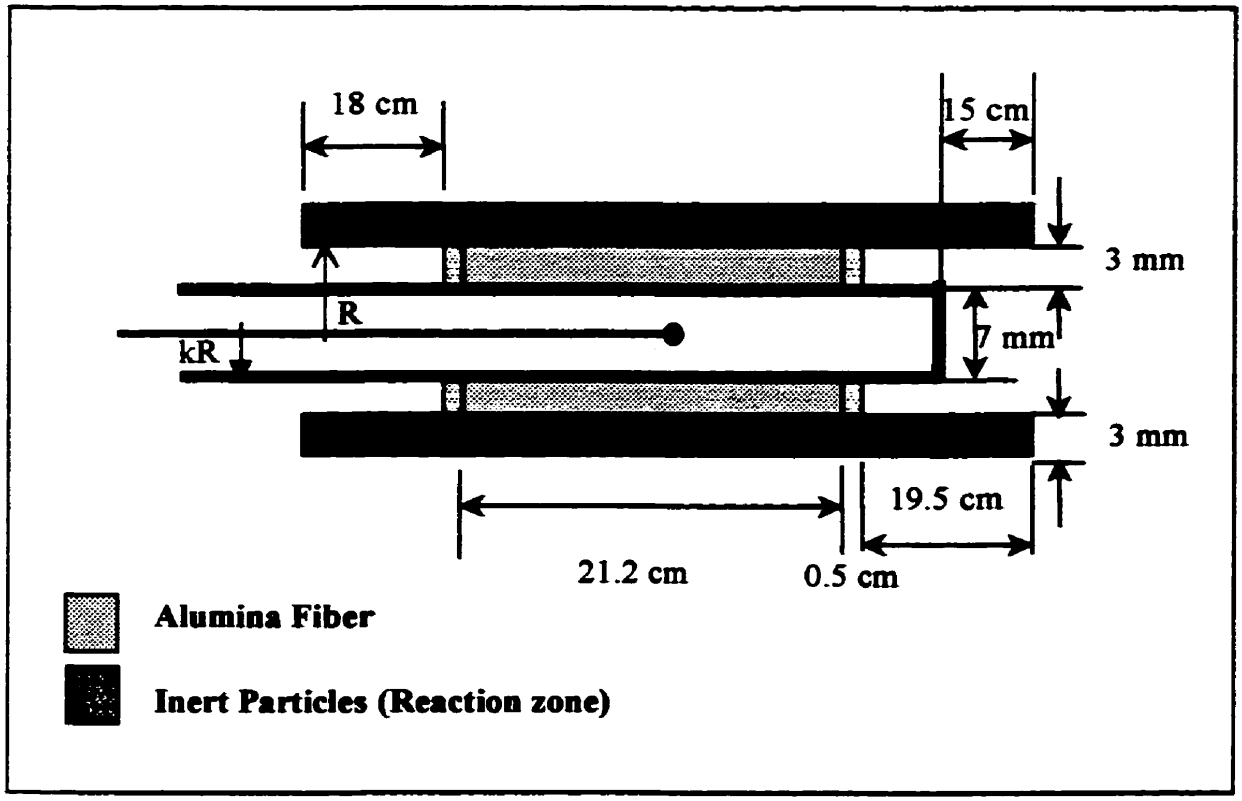

Figure 2.1 Schematic of the experimental fixed bed reactor.

mass balance. Sand particles, which consist of mainly silica, in various size cuts with an average particle size of 230, 330, 523 μm are used during the combustion tests. Chemical composition of the sand particles is given in Table 2.3. Some experiments were also performed with the empty reactor in order to quantify the wall effects on the combustion reaction process.

Table 2.3 Chemical composition of sand particles used in this study

Composition	%
SiO_2	99.710
Fe_2O_3	0.050
Al_2O_3	0.072
CaO	0.010
TiO_2	0.006
MgO	0.019
K_2O	0.030
Na_2O	0.006
LiO	0.096

Furthermore, to amplify the contribution made by reactor walls on combustion, the reactor was filled with alumina powder, with an average particle size of 362 μm, which is the same material used in the reactor construction. For all experiments, the inner tube and furnace temperatures were measured under steady state conditions. Due to quite small amount of fuel introduced into the reactor and the presence of no flow within the inner tube, the mean value of the measured temperatures is taken as reactor temperature and used throughout this study. It is also important to note that due to low specific heat

of gas and small hydraulic diameter and radiation effects, the gas rapidly reaches to the reaction zone temperature [16].

2.5 Numerical Performance of Reduced Mechanism

A reduced reaction mechanism was developed based on the complete GRI mechanism from the detailed inspection of the rate information for C-H-O reactions. These information are gathered during the simulation with the complete mechanism with the objective of obtaining the smallest set of reactions capable of reproducing closely the main combustion characteristics predicted by the complete mechanism. This was done by removing the less significant reactions and identifying those components that are contributing the most to the overall combustion process. Upon excluding non-contributing species from the complete mechanism, the stiffness of the numerical system is also greatly reduced which then leads to a substantial reduction in computation time. The procedure, as applied for the reduced mechanism construction, removes C_2 path from the combustion chemistry. It is well recognized that the C_2 path, which is a sequence of less well-understood steps, becomes important for sufficiently fuel rich mixtures [1, 15]. The mechanism reduction with δ=0.02 has already been used in combustion literature for mechanism reduction [23] that generated a set of 22 species, 104 reactions. It is important to note that the reduction technique is sensitive to the threshold value. Applying a uniform threshold value for different test conditions may either result in redundant reactions being left in the scheme or an oversimplified reaction scheme.

Therefore, depending on test conditions, a suitable threshold value should be used for mechanism reduction. The present reduction has been performed using δ=0.005 for combustion of methane in an isothermal plug flow reactor. The following test conditions are used: initial methane mole fraction=2%, atmospheric pressure and for a wide range of reactor temperatures (600 to 900°C). This procedure generated a set of 17 species, 37 reactions, which is shown in Table 2.4. This is the reduced mechanism used throughout this investigation for comparison purposes. However, two threshold values have also been examined which generated a set of 15 species and 21 reactions and a set of 23 species and 55 reactions with δ=0.05 and δ=0.0005, respectively. The computational time needed to perform the simulation using the three sets of reduced mechanism just described was almost the same. In addition, there are not much difference in the number of species kept and it was then decided to use the reduced mechanism generated with δ=0.005 for this study. The developed reduced mechanism is compared with GRI using a series of conversion data calculated in a plug flow reactor for CO, CH_4 and CO_2. The results are shown in Figure 2.2, where a reasonable agreement is obtained between reduced and full mechanism predictions.

Table 2.4 The reduced mechanism consisting of 37 elementary steps

i	Reactions Considered	k_i (cm-mol-s)	n_i	$E_i \times 10^{-3}$	$E_{icorr.} \times 10^{-3}$
1	$O+HO_2+M_4<=>OH+O_2+M_4$	2.00E+14	0	217.28	
2	$O+H_2O_2+ M_4<=>OH+HO_2+ M_4$	9.63E+06	2.0	16.74	234.02
3	$O+CH_3<=>H+CH_2O$	8.43E+13	0	0	
4	$O+CH_4<=>OH+CH_3$	1.02E+0977	1.5	35.98	
5	$O+CO+M_1<=>CO_2+M_1$	6.02E+14	0	12.55	
6	$O+CH_2O+ M_4<=>OH+HCO+ M_4$	3.90E+13	0	14.81	232.09
7	$O_2+CH_2O<=>HO_2+HCO$	1.00E+14	0	167.41	
8	$H+O_2+M_2<=>HO_2+M_2$	2.80E+18	-.9	0	
9	$H+2O_2<=>HO_2+O_2$	3.00E+20	-1.7	0	
10	$H+O_2+H_2O<=>HO_2+H_2O$	9.38E+18	-.8	0	
11	$H+O_2+N_2<=>HO_2+N_2$	3.75E+20	-1.7	0	
12	$H+O_2+ M_4<=>O+OH+ M_4$	8.30E+13	0	60.31	277.59
13	$H+HO_2<=>O_2+H_2$	2.80E+13	0	4.47	
14	$H+HO_2+ M_4<=>2OH + M_4$	1.34E+14	0	2.66	219.94
15	$H+H_2O_2<=>HO_2+H_2$	1.21E+07	2.0	21.76	
16	$H+H_2O_2+ M_4<=>OH+H_2O+ M_4$	1.00E+13	0	15.1	232.38
17	$H+CH_4<=>CH_3+H_2$	6.60E+08	1.6	45.36	
18	$H+CH_2O<=>HCO+H_2$	2.30E+10	1.1	13.7	
19	$OH+H_2<=>H+H_2O$	2.16E+08	1.5	14.35	
20	$2OH<=>O+H_2O$	3.57E+04	2.4	-8.83	
21	$OH+HO_2<=>O_2+H_2O$	2.90E+13	0	-2.1	

Table 2.4 (continued)

22	$OH+CH_4<=>CH_3+H_2O$	1.00E+08	1.6	13.05	
23	$OH+CO<=>H+CO_2$	4.76E+07	1.2	0.29	
24	$OH+CH_2O<=>HCO+H_2O$	3.43E+09	1.2	-1.87	
25	$HO_2+CH_3<=>O_2+CH_4$	1.00E+12	0	0	
26	$HO_2+CH_3+ M_4<=>OH+CH_3O+ M_4$	2.00E+13	0	0	217.28
27	$HO_2+CO+ M_4<=>OH+CO_2+ M_4$	1.50E+14	0	98.75	316.03
28	$HO_2+CH_2O<=>HCO+H_2O_2$	1.00E+12	0	33.5	
29	$CH_3+O2+ M4<=>O+CH_3O+ M_4$	2.68E+13	0	120.5	337.78
30	$CH_3+O2<=>OH+CH_2O$	3.60E+10	0	37.4	
31	$CH_3+H2O2<=>HO_2+CH_4$	2.45E+04	2.5	21.67	
32	$CH_3+CH2O<=>HCO+CH_4$	3.32E+03	2.8	24.5	
33	$CH_3+CH3OH<=>CH_3O+CH_4$	1.00E+07	1.5	41.59	
34	$HCO+H_2O+ M_4<=>H+CO+H_2O+ M_4$	2.24E+18	-1.0	71.13	288.41
35	$HCO+M_3<=>H+CO+M_3$	1.87E+17	-1.0	71.13	
36	$HCO+O_2<=>HO_2+CO$	7.60E+12	0	1.67	
37	$CH_3O+O_2<=>HO_2+CH_2O$	4.28E-13	7.6		-14.77

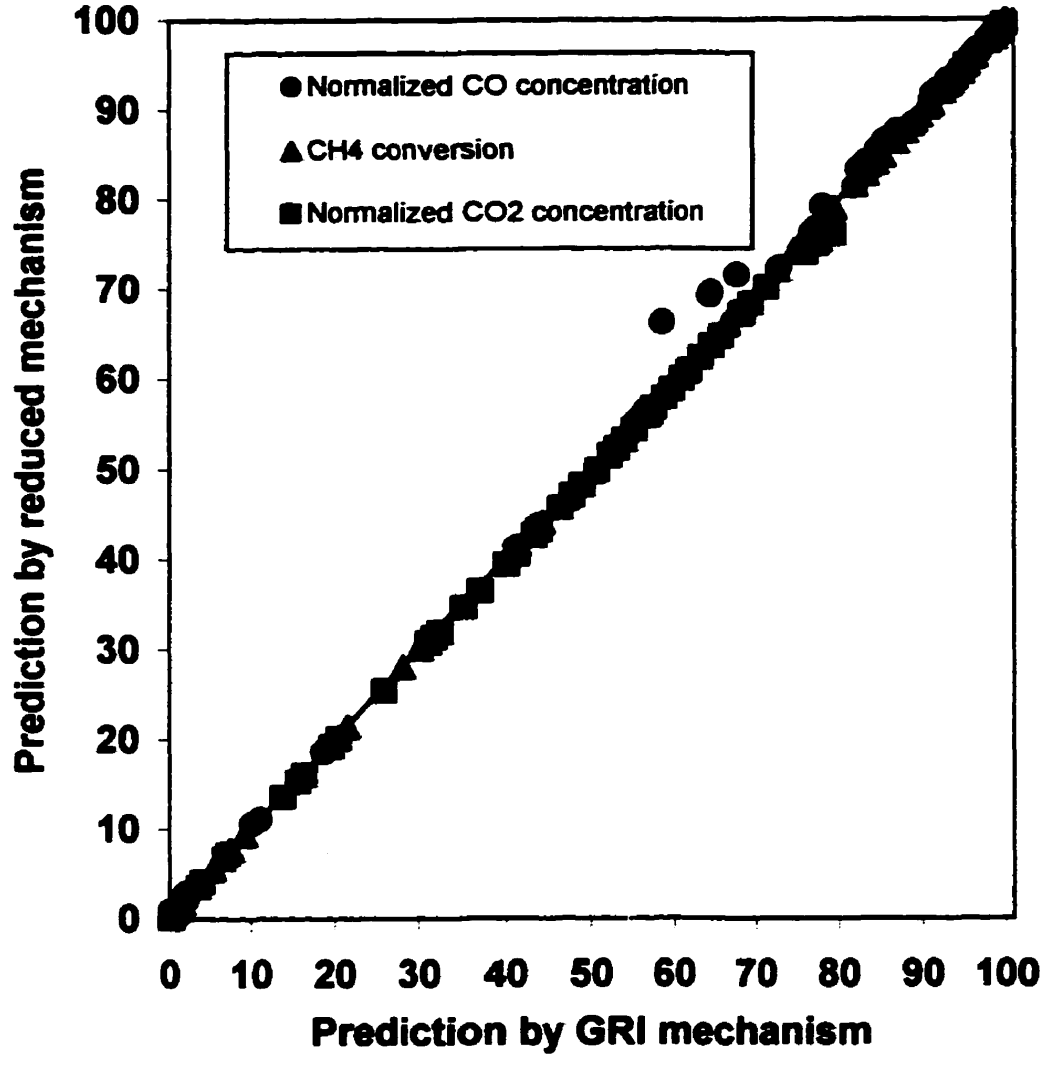

Figure 2.2 Comparison of the methane conversion, normalized CO and CO_2 concentrations predicted from the GRI mechanism to the prediction obtained from the reduced mechanism for sand and alumina particles (X_{CH40}= 2%, η=1e7, τ=3 and τ_a=2.4)

2.6 Results And Discussion

In this section, experimental combustion data obtained in the fixed bed reactor are discussed and compared with gaseous concentration profiles predicted by the complete and reduced mechanisms for a variety of operating conditions. It is worth to mention that the experiments were repeated several times to ensure the reproducibility of the data and identical results were obtained. Figure 2.3 shows the experimental data for the empty reactor and the reactor filled with sand particles of 523 μm. Two approaches were taken to simulate the behavior of the empty reactor: plug flow model and laminar flame model. The detail of the laminar flow model for the experimental unit is presented by Sotudeh [16]. Comparing the simulation results of these two different approaches shows slight difference. This suggests that considering a plug flow model is a very good estimation for this system since the gas velocity is very small. The figure also shows the predictions obtained with the GRI mechanism for 2% initial methane mole fraction and mean residence time of 3 sec. The following conclusions can be derived from this figure:

1) For the empty reactor, agreement comparison between experimental and predicted data is reasonable close to the inflection point, and the difference can be attributed to the fact that the reactor walls may contribute to combustion. No information may be found in the literature in order to explain this disparity.

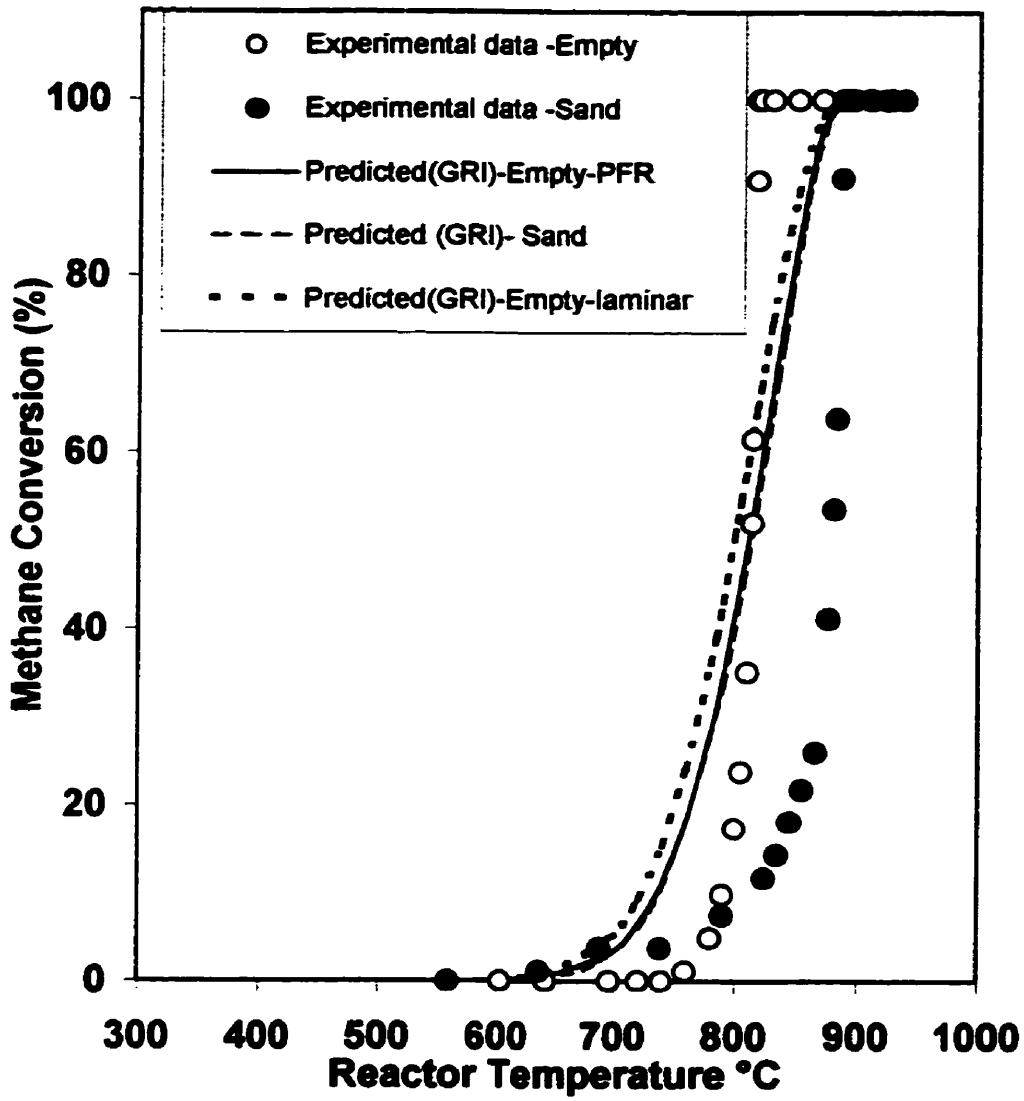

Figure 2.3 Comparison of experimental methane conversion data with sand particles and empty reactor to the predictions obtained from the GRI mechanism (dp=523, X_{CH4O}= 2%, η=1e7 and τ=3)

2) By comparing the experimental data reported in the figure, three different temperature intervals can be identified:

a) T <~750 °C: Some accelerating catalytic effects can be seen in this interval. The contribution is quite small and seems negligible.

b) ~750 °C < T < ~875 °C: At this moderately high temperature range, conversion at the empty reactor differs from the fixed bed reactor. It seems that solid and wall surfaces alter homogeneous combustion by reducing free radical concentrations. Such effects may lower conversion as shown in the figure. Vlachos et al. [1] reported that the operating conditions and spatial heterogeneity (presence of solid surface) can largely affect product distributions. For example, removal of H atoms and CH_3 radicals by adsorption [1] can increase the ignition temperature. The inhibition effects as reported here are also consistent with the overall trend observed for the premixed combustion in fluidized bed reactors [24, 25].

c) T > ~875: Under these conditions, comparison between theory and experiment is satisfactory since the free radical generation dominates the free radical destruction process and inhibition becomes less pronounced.

3) For the fixed bed reactor, the GRI mechanism fails to provide good predictions for the first and second intervals and accurate predictions could be obtained by coupling homogeneous and heterogeneous kinetics. For third temperature interval, excellent agreement is seen between experiments and model predictions, where the complete conversion is achieved.

In figure 2.4, experiments were also reported for alumina and different sand particles. The base of comparison is the contact time index. Alumina was tested as bed material for amplifying the reactor wall effects. Alumina basically behaved like sand particles meaning that the reactor walls may also contribute to combustion. For all particles reported in this figure, the GRI mechanism fails to provide good agreement at the second interval. This figure also shows that above a certain critical temperature, homogeneous combustion takes place i.e. $T > 875$ °C. Hesketh and Davidson [26] showed that above a certain critical temperature, the emulsion phase exhibits homogeneous combustion behaviour in a fluidized bed reactor. This critical temperature is difficult to be determined because of the complexity associated with the hydrodynamics of fluidized bed reactors. The results from the present investigation give a good indication of this behaviour.

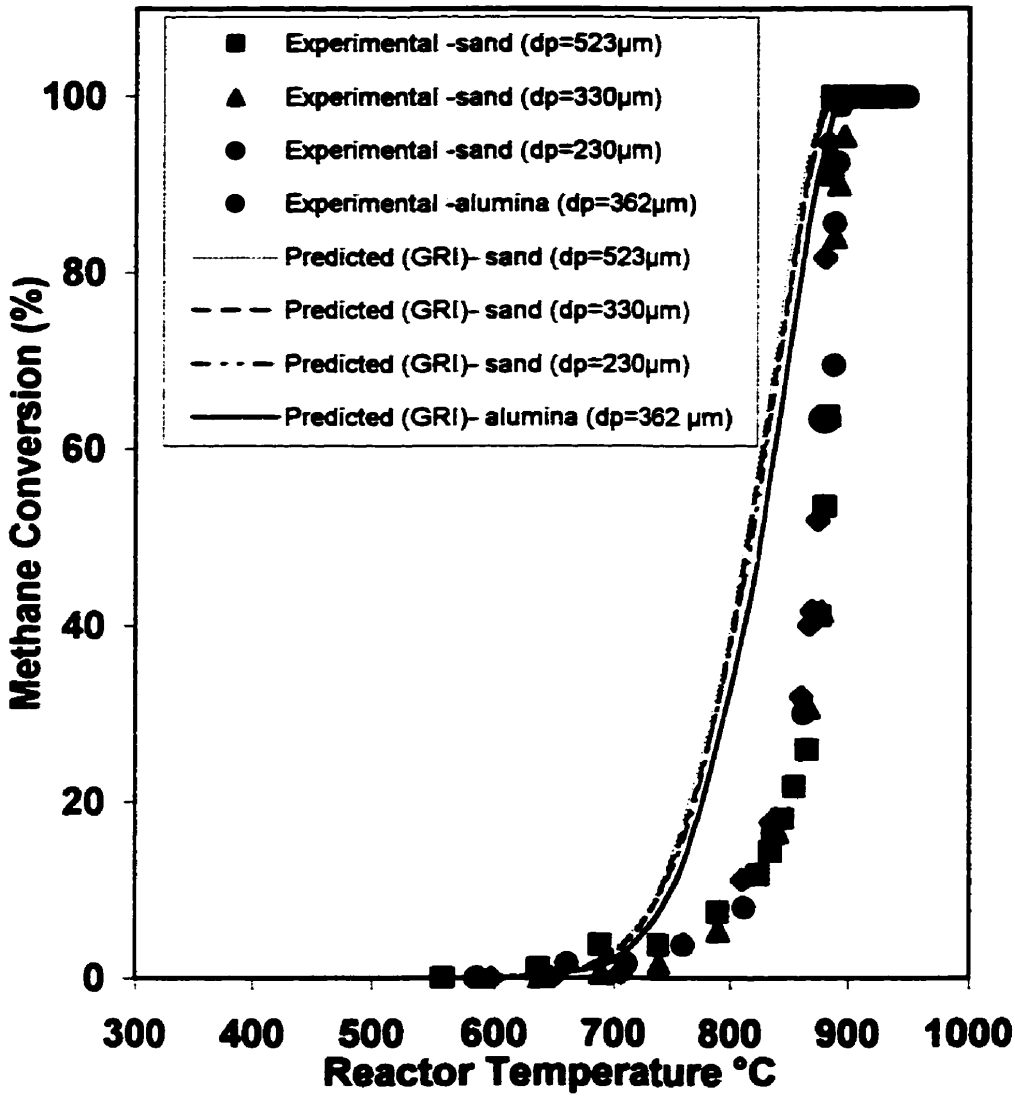

Figure 2.4 Comparison of experimental methane conversion data with different sand and alumina particles to the predictions obtained from the GRI mechanism (X_{CH4O}= 2%, η=1e7, τ=3 and τ_a=2.4)

In Figure 2.5, a comparison between CO mole fraction calculated by mass balance and predictions obtained from the complete mechanism is presented. The CO mole fraction is low compared to model prediction for T<875 °C. This is a very interesting finding since it shows that at this temperature range, combustion over sand particles may lead to less CO emission (almost half) as compared with homogeneous combustion. This effect can be attributed to the low concentration of OH radicals, which is considered as the main oxidant species of CO. The OH radicals are substantially reduced by recombination reactions at the particle surface. In the combustion of hydrocarbons, consumption of CO is very small compared to its formation at lower temperatures. Therefore, this effect leads to a maximum in CO emission level. A gas analyzer was also used to verify this maximum of CO emission by direct measurement. However, it was not possible to obtain exact values of CO emissions from the analyzer, since the amount of flue gas needed for gas analyzer is higher than the total outlet flow from the reactor. Therefore, the use of gas analyzer alters the fixed bed hydrodynamics. The results obtained from the gas analyzer confirmed the existence of a maximum.

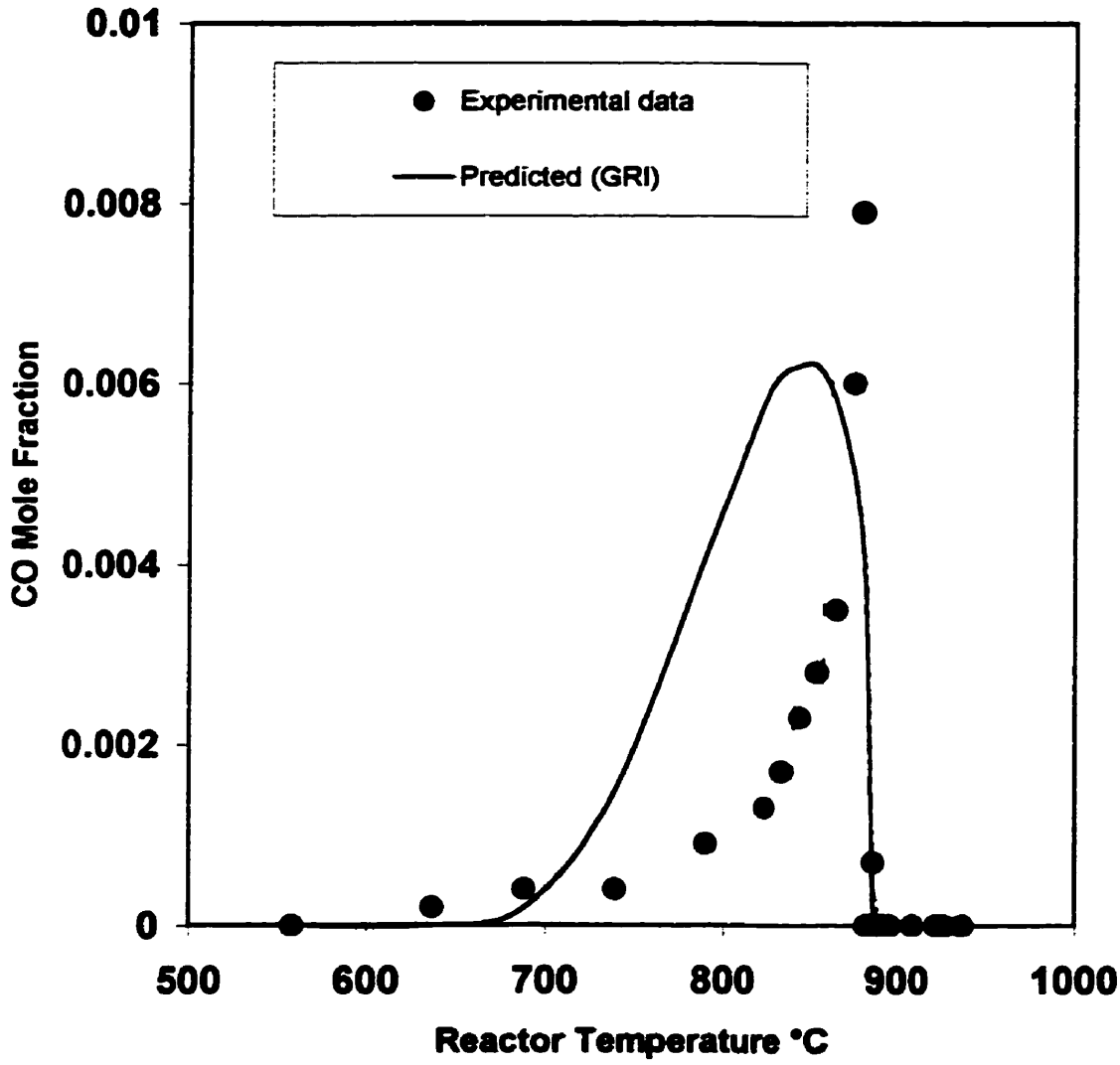

Figure 2.5 Comparison of CO mole fraction at reactor exit to predictions obtained from the GRI and reduced mechanism (Sand particles, dp=523, X_{CH40}= 2%, η=1e7 and τ=3)

Figure 2.6 shows a comparison of experimental conversion between data for different sand particles and the prediction obtained by the reduced mechanism for η=4e6. This figure does not show large difference regarding the particle size effect at second temperature interval. By comparing experimental data reported in figure 2.4 with those here, it is seen that the second temperature interval becomes narrower.

Figure 2.7 shows the effect of the contact time index and the mean residence time. These values are smaller for fluidized bed reactors. By approximating the emulsion phase of a turbulent fluidized bed reactor with a fixed bed reactor for the purpose of this study, one may conclude that the emulsion phase becomes the subject of inhibition and higher temperature is needed to obtain high methane conversion in this phase. This figure may also suggests that the methane conversion in the emulsion phase of turbulent fluidized bed reactors may require high temperatures even above 1000 °C. This may be justified by considering a very short residence time in these reactors and further mass transfer resistance between bubble and emulsion phases. This means that, in the emulsion phase of fluidized beds of inert particles at temperatures below ~1000 °C the combined homogeneous and heterogeneous reaction rate is smaller than in the case of solely homogeneous gas phase reactions. This is consistent with the information found in fluidization literatures where it has been reported that homogeneous reaction in the emulsion phase starts well above 1100 °C.

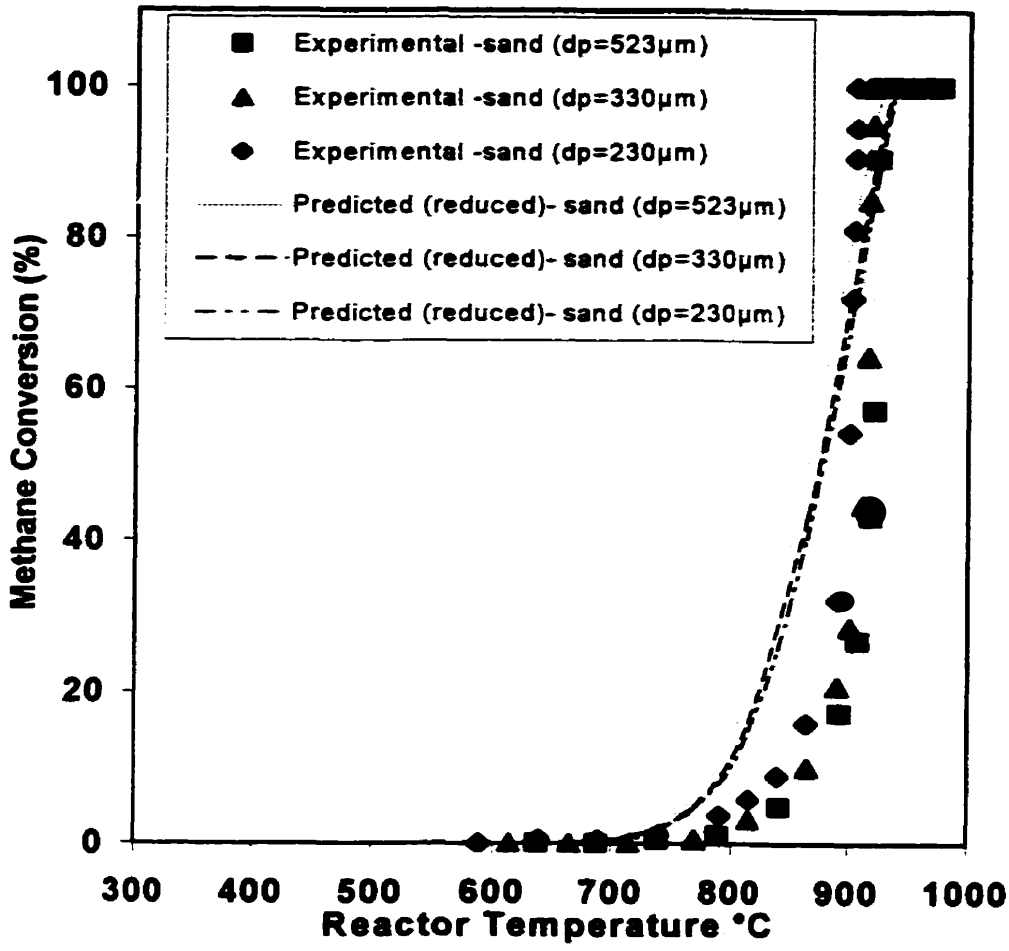

Figure 2.6 Comparison of experimental methane conversion data with different sand particles to the predictions obtained from the reduced mechanism (X_{CH40}= 2%, η=4e6 and τ=1.2)

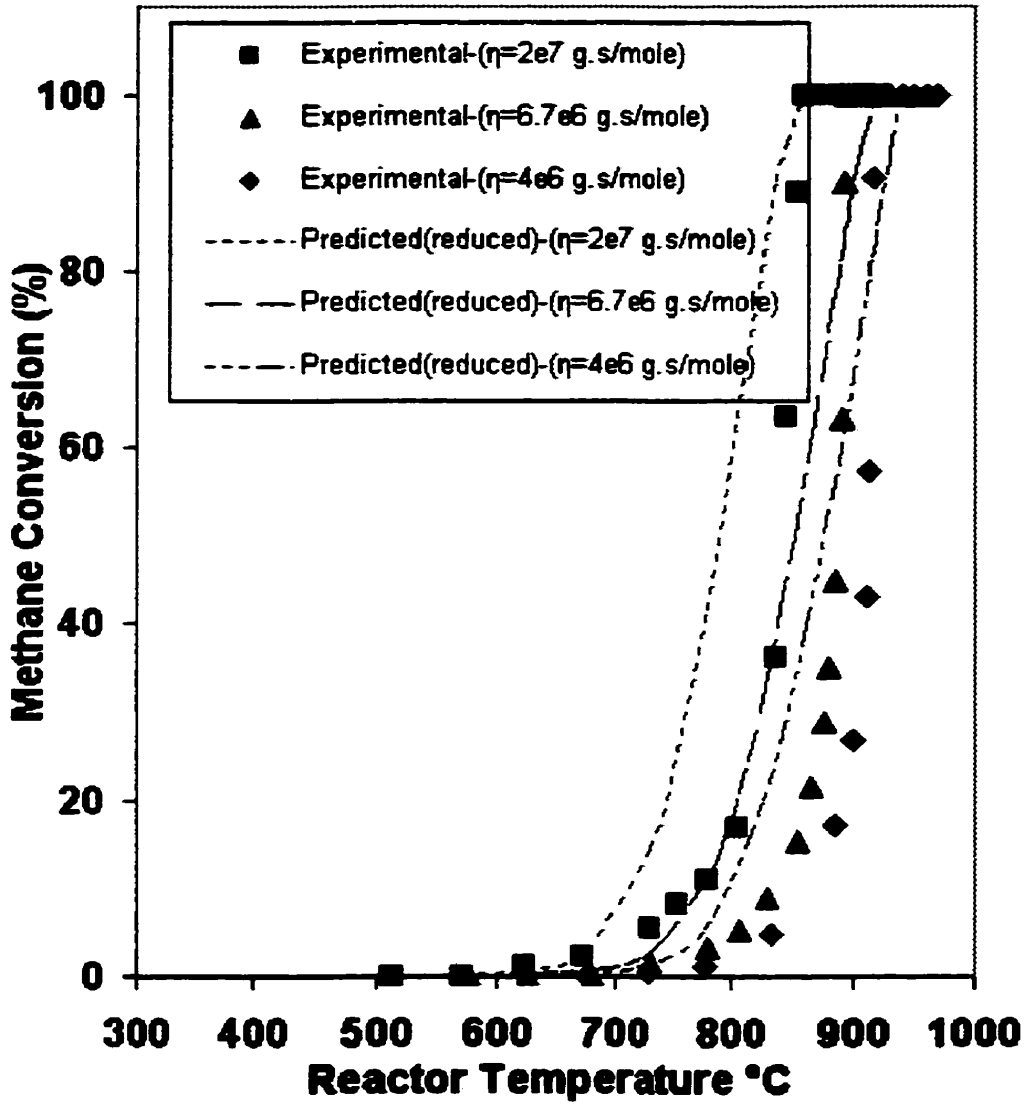

Figure 2.7 Comparison of experimental methane conversion data with sand particles to the predictions obtained from the reduced mechanism for different contact time index and mean residence time values (dp=523, X_{CH40}= 2%, η=2e7, 6.7e6, 4e6 and τ=6, 2, 1.2, respectively).

Figure 2.8 gives a comparison between experimental conversion data with sand particles (d_p=330 μm) and predictions obtained with the reduced mechanism for 2% and 4% initial methane mole fraction. The base of comparison is the mean residence time. This figure shows that the experimental and predicted conversion is independent of initial methane mole fraction, meaning that the overall methane combustion reaction is first order with respect to methane concentration. For lean mixtures, this is an accepted assumption for combustion studies, where homogeneous reactions are encountered and inert particles are absent.

Figures 2.3 to 2.8 clearly show that the GRI and reduced mechanisms fail to predict the experimental data accurately at the second temperature interval. The failure is attributed to the fact that the reaction mechanisms are constructed based on homogeneous elementary reaction rates. These rates are widely available in the literature due to their applications in traditional gas combustion devices and no heterogeneous elementary reactions are included in these mechanisms. To fully predict the experimental data, one should include the heterogeneous elementary reaction kinetics in the modeling. Therefore, a combined reaction mechanism needs to be constructed based on kinetic information of both homogeneous and heterogeneous reactions. Unfortunately, no heterogeneous kinetic information is available in the open literature for test conditions used for the present study.

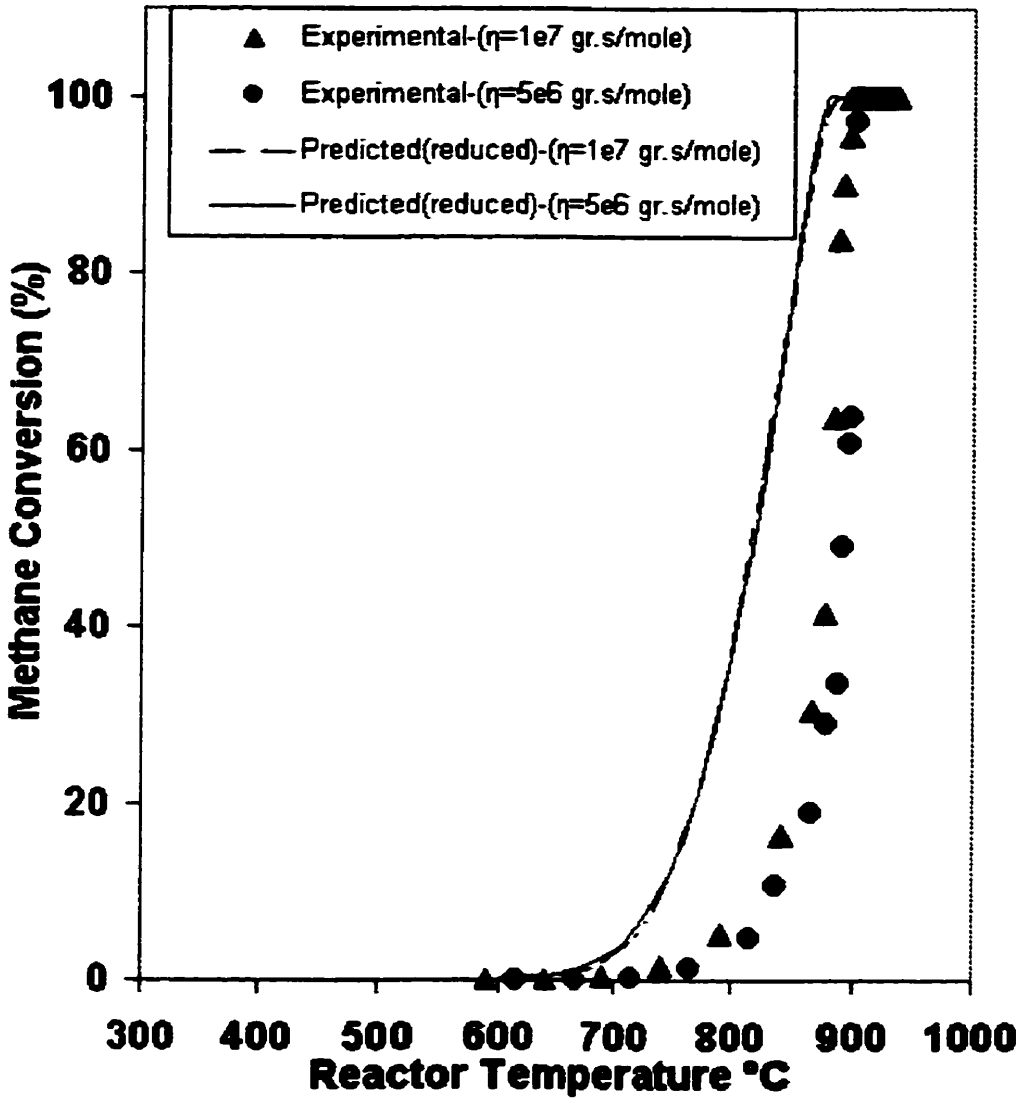

Figure 2.8 Comparison of experimental methane conversion to the prediction obtained from the reduced mechanism (Sand particles, dp=330, X_{CH40}=2 and 4% and τ=3)

For the purpose of this study, we decided to choose a certain number of reactions in the reduced mechanism and to modify their reaction rates for presenting the heterogeneous effects in the simulation. It is believed that wall quenching results in a reduction of free radicals near the wall and surface [1,5]. OH, O, H and CH_3 consumption retards homogeneous ignition [1]. The inhibition of homogenous combustion of CH4 in the presence of catalyst is caused by consumption of the intermediate species, which probably H atoms and CH_3 radicals being the most important [1]. It seems that in the presence of inert particles, the most important radicals probably are OH radical and H atom. Numerical optimization based on reduced mechanism with chosen experimental targets shows that OH radicals play a major role in the inhibition process for the conditions used in this study. This suggests that the production rate of OH radicals should be modified in order to construct a modified combustion mechanism. Therefore, the reaction no. 1, 2, 6, 12, 14, 16, 26, 27, 29 and 34 were chosen and their reaction rates have been modified in the reduced mechanism. For each reaction considered, the frequency factor and the activation energy should be modified. That means the estimation of 20 independent variables for reaction rate data. Such estimation is a tedious and awkward task and an effective strategy might be used. Since the activation energies for the set of reactions considered in the modification have mostly the same order of magnitude, though it has been decided to modify the reaction rates with a global

correction factor. This factor is defined as the ratio of the heterogeneous reaction rate to the homogeneous reaction rate:

$$f = \frac{r_{het}}{r_{hom}} = A \exp\left[\frac{-\Delta E}{RT}\right] \qquad (0<f<1) \qquad (2.21)$$

The optimal values for A and ΔE are: ($A=4.32759\times10^{9}$ and $\Delta E = 217.2$). At temperatures ~900°C, the value for f is equal to 1, which means that the reduced homogenous mechanism is capable of predicting the experimental data and no heterogeneous chemistry is needed for simulation. The activation energy is of the order of magnitude found in the combustion literature [25, 26]. The modified activation energies for the modified mechanism are presented in Table 2.4. The results obtained based on this improved mechanism are presented in figures 2.9 and 2.10.

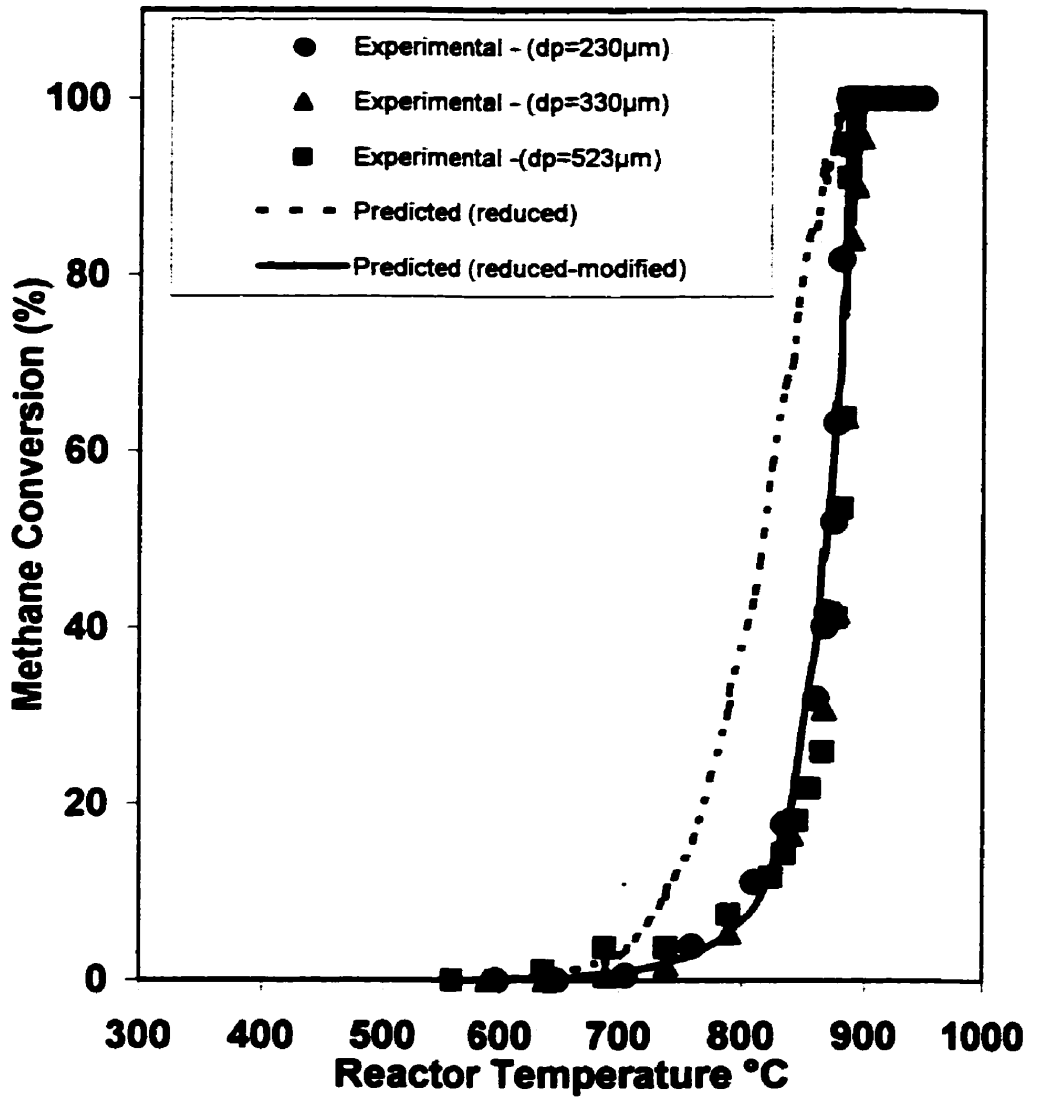

Figure 2.9 Comparison of experimental methane conversion data with different sand particles to the predictions obtained from the reduced and combined mechanism (X_{CH4O}= 2%, η=1e7 and τ=3)

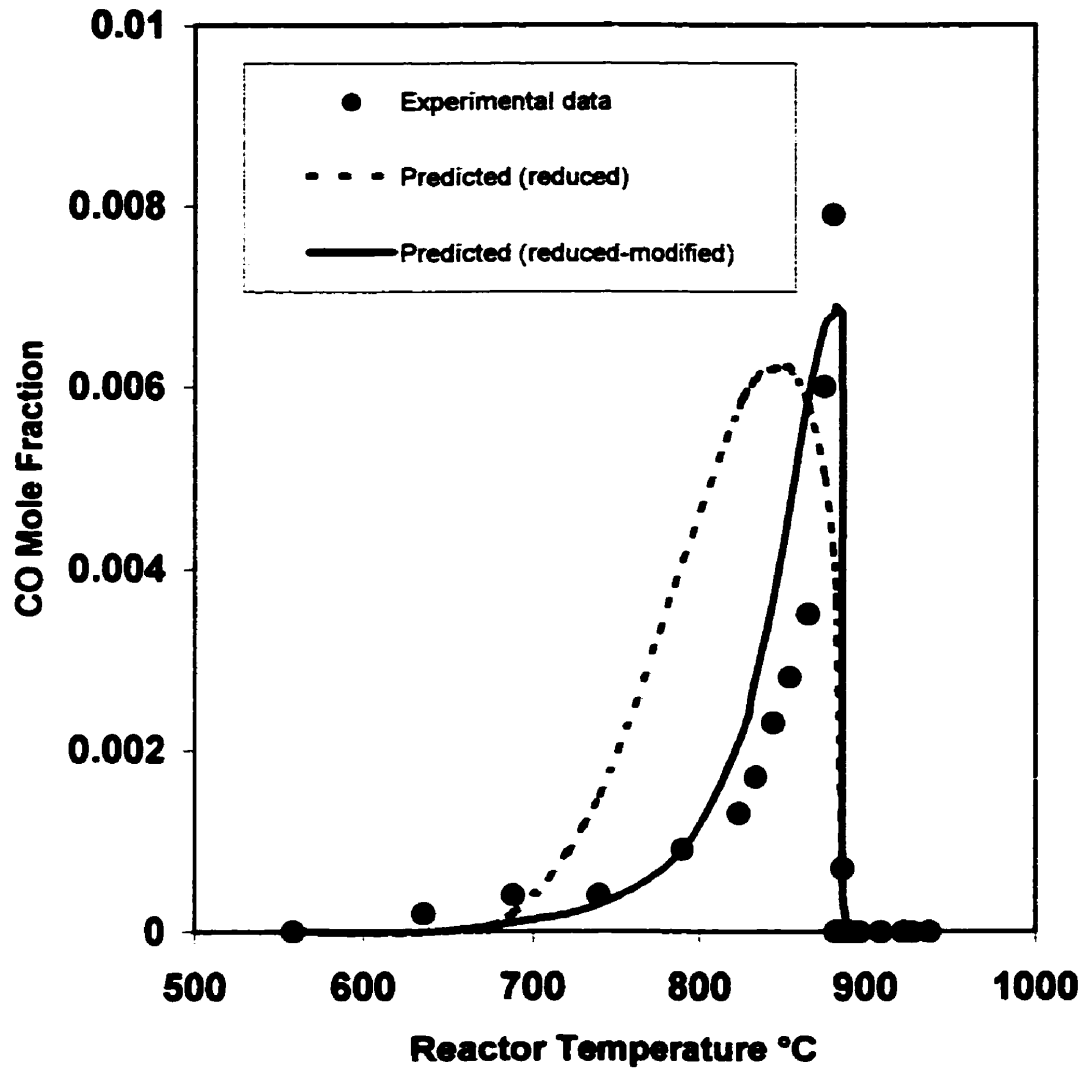

Figure 2.10 Comparison of CO mole fraction with sand particles to the predictions obtained from the reduced and combined mechanism (dp=523, X_{CH4O}= 2%, η=1e7 and τ=3).

In figure 2.9, a comparison between the experimental data and predictions obtained from reduced and combined mechanisms is presented. The base of comparison is the contact time index. As shown in the figure, the combined mechanism is a well-improved version of the reduced mechanism and its agreement with the experimental data is excellent. This justifies the choice of reactions to present the heterogeneous chemistry in the combined reaction scheme. This also means that the OH radicals have a low concentration due to inhibition process as compared with purely homogeneous reactions.

Figure 2.10 shows a comparison of CO mole fraction calculated by mass balance and the predictions obtained by the reduced and combined mechanism. Again, this figure shows that the reduced reaction scheme is largely improved by introducing the modified reaction rates for heterogeneous chemistry. The comparison between the combined mechanism prediction and the experimental data is quite satisfactory.

2.7 Conclusions

A series of measurements has been completed for methane combustion in a fixed bed reactor with different inert particles and under various operating conditions. A plug flow reactor model coupled with complete and reduced mechanisms is used to simulate the performance of this reactor. The main conclusions of this study as derived from the experimental observations and theoretical considerations can be summarized as follows:

- The experimental results show that at temperatures below ~ 750°C, sand particles may act as catalysts to increase conversion but their contribution is quite small. In fluidized bed reactors of sand particles for the temperature range of interest between 800 to 1000 °C, such contribution seems negligible.

- At moderately high temperatures (~ 750-850 °C), the free radical concentrations are lowered by their termination on solid surface and therefore, inhibition becomes important. This behaviour becomes critical if one decides to operate the combustion devices in this temperature range. Therefore, combined heterogeneous and heterogeneous kinetics are needed to fully understand the combustion process in these devices.

- At high temperatures above ~ 875 to 900 °C, the rate of free radical formation becomes dominant as compared to the free radical destruction on solid surfaces or reactor walls. Under these conditions, the inhibition process plays a less important role and may then be neglected. This is a common practice for the combustion devices operating at high temperatures well above 1000 °C.

- The results of this study may suggest that in the emulsion phase of fluidized beds of inert particles at temperatures below ~1000 °C the combined homogeneous and heterogeneous reaction rates are less significant for methane combustion.

- A reduced methane combustion mechanism comprising of 37 reversible reactions and 19 species is developed and compared with the prediction provided by the complete GRI mechanism. It is concluded that the reduced mechanism is sufficiently accurate, despite its small sizes for predicting the behaviour of homogeneous reactions.

- A combined heterogeneous and homogeneous mechanism is designed to describe methane combustion in presence of sand particles. The combined mechanism predicts the methane conversion very accurately and predicts the CO emissions trend correctly.

2.8 Acknowledgements

The authors are grateful to Professor D. Klvana and Mr. P. Sauriol for their help with the experimental work. This work was supported by a grant provided by National Science and Engineering Research Council (NSERC) of Canada. Ministry of Culture and Higher Education of I. R. of IRAN is also acknowledged for making Mr. R. Sotudeh-Gharebaagh studies possible in Canada.

2.9 References

1 Vlachos, D. G., Schmidt, L. D. and Aris, R., AIChE, vol. 40, No. 6, 1994.

2 Broughton, J., Ph.D. dissertation, Newcastle upon Tyne, 1972.

3 Chantravekin P. and Hesketh R. P., Chem. Phys. Processes Combust. 527-530, 1993.

4 Tringham, D. J. Ph.D. dissertation, Leeds, 1982.

5 Lewis, B. and G. von Elbe, "combustion flame and explosions of gases", 3rd edition, Academic Press, London, 1987.

6 Van der Varrt D.R., Ind. Eng. Chem. Res., 31, 1992, 999-1007.

7 Leeds university, http://chem.leeds.ac.uk/Combustion/Combustion.html, 1997.

8 Gardiner, W.C., " Combustion Chemistry", Springer-Verlag, 1984.

9 Grace J. R., " Fluidized Beds as Chemical Reactors", Chapter 11 in Gas Fluidization Technology, Edited by Geldart, D., Wiley, 1986.

10 GRI-Mech, http://www.me.berekely.edu/gri_mech/data/rxn_table.html, 1997.

11 Frenklach M., H. Wang, C.T. Bowman, R.K. Hanson, G.P. Smith, D.M. Golden, W.C. Gardiner and V. Lissianski, 25th International Symposium on Combustion, Poster WIP-3-26.

12 Gas Research Institute, Annual

13 Report, September 1994 - August 1985.

14 Kee, R. J., Rupley, F.M. and Miller, J.A., SAND89-8009, Sandia national Laboratories, 1989.

15 Miller J.A. and G.A.Fisk, Special Report, C&EN, August 31, 1987.

16 Tomlin A.S., T. Turányi and M.J. Pilling, in: `Low temperature combustion and autoignition', eds. M.J. Pilling and G. Hancock, Elsevier, 1997

17 Sotudeh, R. Combustion of natural gas in a turbulent fluidzied bed reactor, Ph.D. Dissertation, Ecole Polytechnique de Montreal, 1998

18 Warnatz J., U. Mass and R.W. Dibble, "Combustion", Springer, 1996.

19 Frenklach M., "Reduction of Chemical Reaction Models", in Numerical Approaches to Combustion Modeling, Progress in Astronauts and Aeronautics, vol.135, AIAA, Washington, 1990.

20 Warnatz J., "Resolution of gas phase and surface combustion chemistry into elementary reactions", 24th Symposium (Int.) on Combust., 553-579, 1992.

21 Griffiths J.F., "Reduced kinetics models and their applications to practical combustion systems., Prog. Energy Combust. Sci., 21, 25-107, 1995.

22 Chang W.C., "Ph.D. Dissertation", University of California at Berkeley, 1995.

23 Kazakov, A. and Frenklach, M., http://diesel.fsc.psu.edu/~gri_mech/drm/home_drm.html.

24 Dennis J. S., Hayhurst A. N. and Mackley I. G., in Symposium (International) on Combustion, [Proc.], 19th, pp. 1205-1212, 1982.

25 van der Vaart, D. R., Combust. Flame, Vol. 71, pp. 35-39, 1988.

26 Hesketh, R. P. and Davidson J. F., Combust. Flame, Vol. 85, 449-467, 1991.

27 Markatou, P., L.D., Pfefferle and M.D. Smooke, Combus. Flame, 93:185-201, (1993).

28 Griffin, T.A., Ph.D thesis, Yale University, 1990

CHAPTER 3: NATURAL GAS COMBUSTION IN A TURBULENT FLUIDIZED BED OF INERT PARTICLES

Reference:

Sotudeh-Gharebaagh, R., J. Chaouki and R. Legros (1998), "Natural Gas Combustion in a Turbulent Fluidized Bed Reactor", Chemical Engineering Science, Manuscript ISCRE-91, Accepted for publication.

Keywords:

fluidized bed combustion, non-premixed, bubbling regime, turbulent regime, natural gas combustion, mixing.

3.1 Context[1]

In chapter II, combustion of methane was tested in a fixed bed reactor over inert particles. The aim was to evaluate the behavior of particles used in combustion studies. It has been shown that the combustion takes place of the order of 800 °C and under these conditions, the accelerating catalytic effects were not important. The general experimental findings helped us decide on the conditions needed for combustion studies, which is the subject of this chapter. Herein, combustion of natural gas was studied in a pilot plant fluidized of inert particles under bubbling and turbulent fluidized bed conditions. The experimental results showed that the turbulent fluidized bed reactor is an excellent reactor of choice to promote the oxidation and combustion processes.

---

[1] This section is not included in the original manuscript. It only serves as a transition between papers for the thesis.

3.2 Abstract

The combustion of natural gas has been studied in a pilot plant fluidized bed of inert particles at relatively high temperatures (800-1000°C). Experiments were carried out in both bubbling and turbulent regimes. Combustion can be completed in the flammability range with a suitable injection system to bring two gases into an intense contact sufficient to permit complete in-bed combustion. The experimental results show that the fluidized bed reactors offer excellent thermal uniformity and temperature control. This study also provides comprehensive data on gaseous fuel combustion and CO oxidation profile in a pilot plant fluidized bed of inert particles. Such data is required to develop a realistic model for combustion process in fluidized bed reactors.

3.3 Introduction

Safe control, efficient reduction and economical destruction of pollutant emissions from the devices burning fossil fuels are a major focus of environmental concern and legislation in various industrial nations. In response to such stringent regulations, and based on increased availability of natural gas (NG), different attractive and cost-effective technologies including basic co-firing, gas reburn have been initiated (American Gas association, 1991). The success of these devices depends strongly on their operating temperature, which is critical for thermal NO_x emissions. Thermal NOx are generated in conventional devices where the flame temperature is usually above 1200°C. Therefore,

the new generation devices should operate at temperatures well below 1200 °C. At temperatures below 800°C, no thermal NOx is formed and the combustion of gaseous fuel such as natural gas at such temperatures can be considered attractive. Unfortunately, this is not possible in a fluidized bed of inert particles at low fuel concentration, which is essential for safe operation. Low-temperature catalytic combustion of gaseous fuel has been so far reported in fixed beds for small-scale units (e.g. Mezaki and Watson, 1966). Although excellent gas-solid contact efficiency can be achieved in these reactors, the rise in bed temperature usually leads to the formation of hot spots, deactivation of the catalysts and even to conditions of homogeneous gas phase combustion. In addition, for very low gaseous fuel concentrations in the feed, auto-thermicity of a fixed bed reactor is difficult to achieve because of the creeping effect. Such undesired effect causes the movement of the reaction front towards the reactor outlet.

Fluidized bed technology can be widely used with natural gas for a wide range of applications e.g. co-firing, gas re-burn and direct combustion for heating fluidized beds in some industrial processes. In fluidized beds, high combustion efficiency can also be achieved at a remarkably low temperature (~900°C) as compared to conventional devices (over 1200 °C). The fluidized bed reactors could be operated isothermally without developing hot spots (Grace, 1990) and are capable of meeting all environmental requirements (Foka et al, 1994). Moreover, judicious selection of bed material can result in the in-bed elimination of gaseous pollutant species generated during combustion.

Various hydrodynamic regimes are observed in fluidized beds. So far, gaseous fuel combustion has been reported for the bubbling regime mostly for premixed combustion (e.g. Sadilov and Baskakov, 1973; Van der Vaart, 1992). For non-premixed combustion, no study has been reported in the open literature in which natural gas is injected directly to the bed. The turbulent fluidization regime is characterized by pressure fluctuations of low amplitude and of high frequencies (e.g. Kehoe and Davidson, 1971) and of small bubbles with high relative density. Turbulent fluidized beds (TFB) have a more homogeneous appearance and consequently high conversions are being achieved due to an improved gas-solid contact. These reactors also offer the advantages of exceptionally high heat transfer, excellent thermal uniformity and temperature control, high overall productivity and relatively short mean residence time as compared to the conventional combustion systems for a given throughput.

Concerning combustion of natural gas in TFB reactors, Foka et al. (1994) investigated the catalytic premixed combustion of natural gas (with a low inlet mixture of 4% methane) at moderately low temperatures (400-600°C). They further stated that the turbulent regime appears to be the most suitable one for complete combustion of natural gas. The success of the catalytic fluidized bed combustion of natural gas strongly depends on the nature of the catalyst used. Such a catalyst must be effective for combustion, resistant to attrition and have a low cost. Unfortunately, the combustion catalysts are expensive and subject to attrition. In addition, the combined cost of catalyst for the catalytic reactor is high. In

order to make turbulent fluidized bed reactors applicable for residential, industrial and waste-to-energy applications and to decrease this cost substantially, the catalysts should be replaced by inert materials. Therefore, the moderately high temperature combustion in fluidized bed reactors is needed in order to reduce the reactor size and to promote complete combustion. Despite the large impact of using inert particles as bed materials on industrial combustion applications, no information is available in the literature concerning the combustion mode and regime of fluidization in which the combustion takes place in pilot or industrial fluidized bed reactors at moderately high temperatures (< 1000 °C). Therefore, the outcome of this study may have implications for the combustion of volatile matters in fluidized bed coal combustors, since the presence of volatile matters is important in stabilizing the combustion process. Therefore, natural gas combustion process can provide insights into how volatiles burn inside of fluidized bed reactors.

In the present work, the combustion of natural gas with air in a pilot plant turbulent fluidized bed reactor of sand particles has been studied extensively. Due to safety concerns and also limited industrial applications of a premixed combustion mode, the non-premixed combustion is only considered in this investigation. The aim is to assess the experimental feasibility of natural gas combustion in a pilot turbulent fluidized bed of inert particles.

3.4 Experimental

3.4.1 Apparatus and bed materials

The apparatus used in this study is a 200 mm I.D. and 2 m tall refractory-lined combustor capable of withstanding high temperatures, as shown in Figure 3.1. The reactor is divided into four zones: the combustion inlet port (wind-box and a cap distributor), a fluidized bed zone, a freeboard zone and an expansion zone of 600mm I.D. An external natural gas burner with 20 kW nominal power located at the bottom of the bed provides the partial heat required for preheating the reactor to a desired temperature. Sand particles, which consist mainly of silica with an average particle size of 543 μm and a bulk density of 1400 kg/m^3 are used during the combustion tests. Several ports are provided along the axial position for pressure measurements, sampling and natural gas injection to the reactor. Natural gas may be supplied to the reactor either through the wind-box or at any elevation above the distributor by an injection probe pointing downward. Two injection probes of 6.33 mm in diameter were used throughout this study; a one-hole probe named the injection nozzle and a full sparger with 13 holes. Holes are 4.33 mm in diameter. These injection probes were kept free of particles during the preheating period using air as a purging fluid.

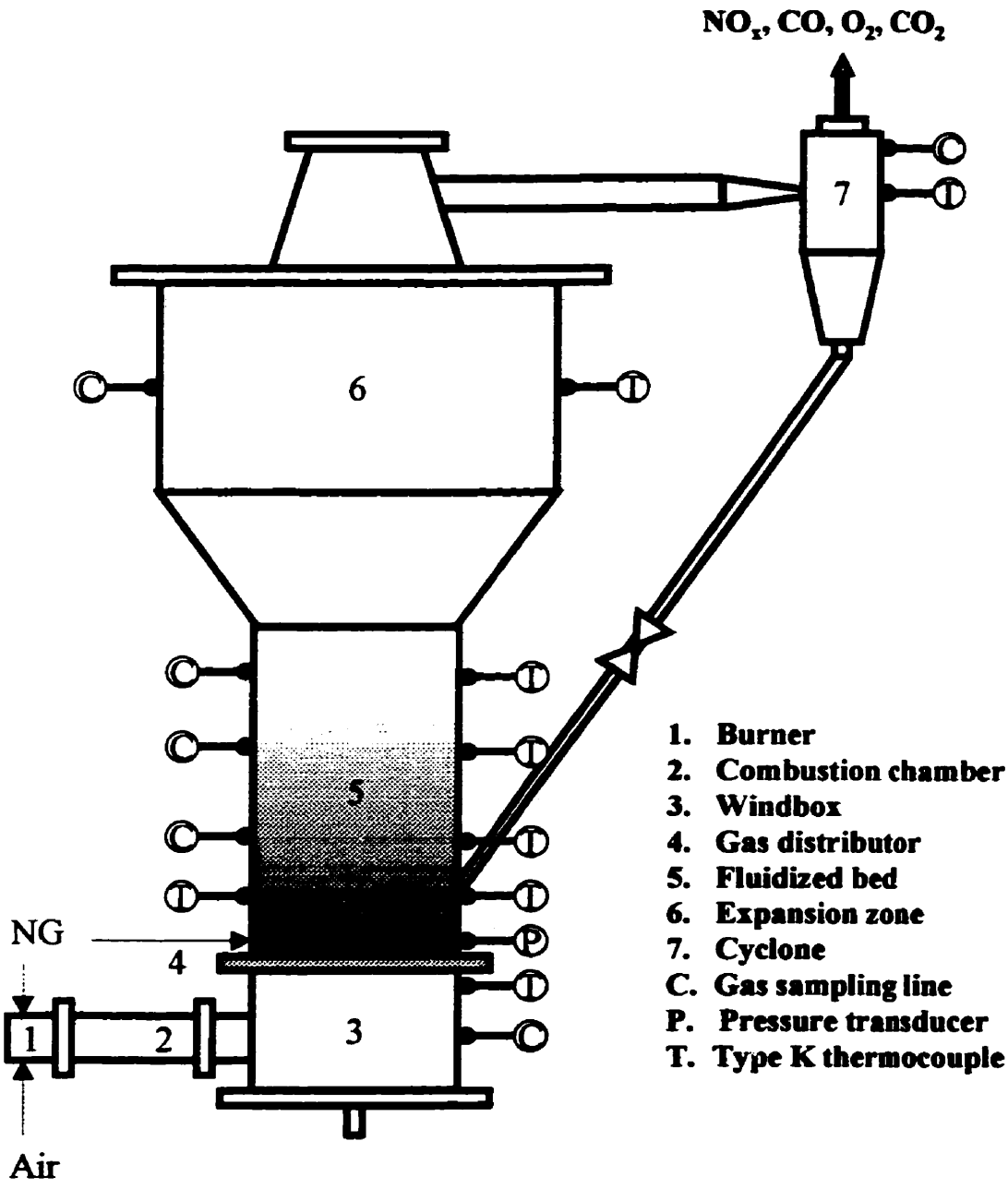

Figure 3.1 Schematic of pilot turbulent fluidized bed reactor

The reactor was also equipped for sampling and analysis of reaction products taken from the various ports and the reactor outlet. Sampling probes were placed along the reactor centerline with their tips protected from particle clogging by a filter. The probes were connected to the gas chromatograph (HP5980A) by a tube and the samples were withdrawn with a variable pressure vacuum system. Type-K thermocouples were also placed along the reactor centerline to monitor temperature profiles. An absolute pressure transducer was used to monitor the level of particles in the reactor by continuous recording of pressure fluctuations every 1s. Flow rates of air and natural gas were measured by orifice plates and rotameters, respectively. During the experiments, data are acquired by a PC acquisition system where temperatures and pressures are recorded at second and minute intervals, respectively. At relatively high superficial velocities, a significant amount of particles are entrained. These particles are separated from the gas by a 0.2m I.D. cyclone and recirculated to the bed. An initial bed height of 2.5D (about 20 kg sand particles) was used in all experiments.

3.4.2 Procedure

The experimental study began by cold fluidization tests to measure minimum fluidization velocity and the onset of turbulent fluidization. For hot hydrodynamics and reaction

studies, the following procedure was adopted to heat up the insulated pilot turbulent fluidized bed reactor to a desired temperature:

- Using the burner located at reactor base, the reactor temperature is raised up to 750°C.

- Using premixed combustion, which consists of natural gas injection to the wind-box, the reactor temperature is raised up to 850°C (under-bed combustion).

- Higher temperatures (850 to 1000°C) are reached using the non-premixed combustion mode, which consists of direct injection of NG to the reactor (over-bed and in-bed combustion).

3.4.3 Operational aspects

The following issues are of critical importance for successful operation of a pilot plant fluidized bed reactor:

- Prior to any experiment, all in-bed probes (including temperature, pressure, sampling and gas injection probes) must be carefully examined and positioned at their proper locations.

- A quite low superficial velocity based on cold conditions should be used to start-up the reactor.

- The solid inventory and temperature profile should be strictly controlled by means of pressure measurement and thermocouples, respectively.

- Attrition of particles in a fluidized bed reactor affects solid inventory of the reactor. At high sparger velocities, highly turbulent area is created around the sparger. This may result in generating of fine particles due to jet impingement. Under these conditions, the bed may easily become empty with excessive elutriation of resultant fine particles.

- Probes, thermocouples and sparger in fluidized bed reactors are liable to erosion and deformation. They should be frequently inspected and replaced.

3.5 Combustion and carbon monoxide trials

Prior to combustion tests in two fluidization regimes, the onset of turbulent fluidization, U_C, should be determined. This transition velocity has been extensively studied in the literature (e.g., Chehbouni et al. 1994) by means of pressure transducers, capacitance probe or by visual observations. Figure 3.2 shows the normalized standard deviation of pressure fluctuation measured at 150 mm above the distributor as a function of gas superficial velocity for sand particles of 543 μm at 25°C and 920 °C. The figure exhibits a well-defined maximum, which can be interpreted as the onset of turbulent fluidization. It is also important to note that at 920°C, U_C is slightly higher than that found for ambient temperature, which is consistent with the recent experimental findings in our laboratory (Gonzalez, 1995, Foka et al., 1994). For the operating conditions of interest in this study, the experimental and predicted values of U_C are presented in Table 3.1.

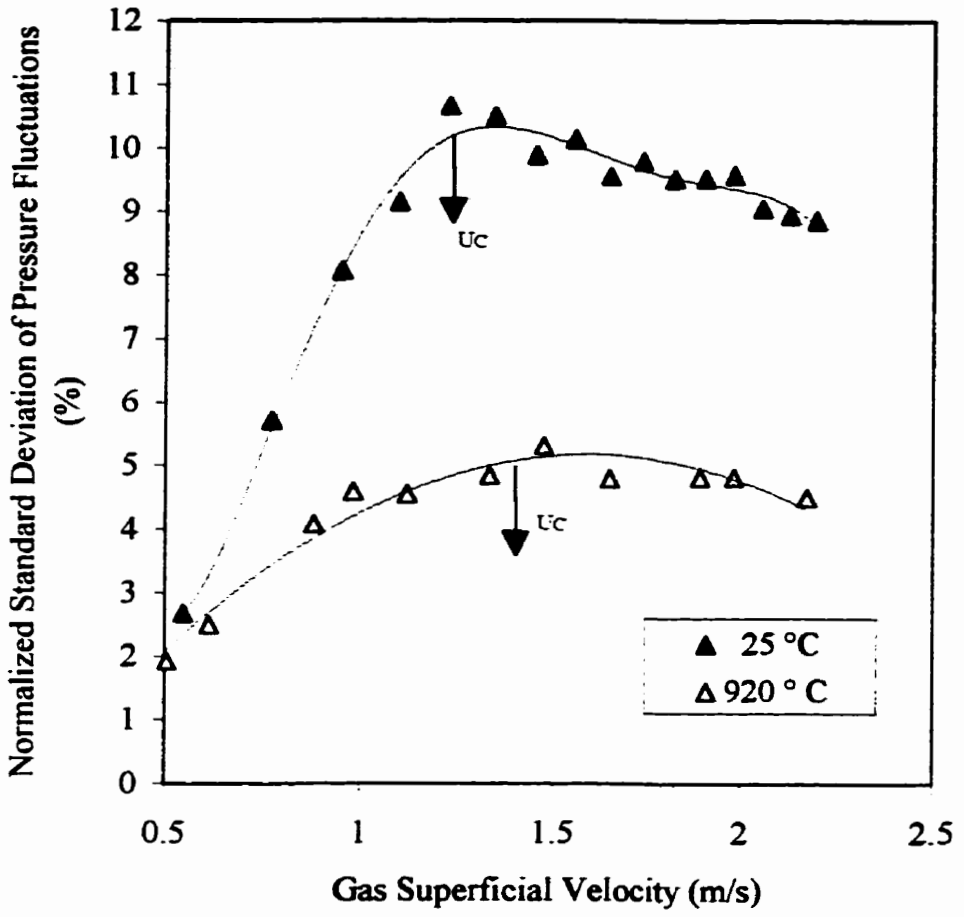

Figure 3.2 Normalized standard deviation of pressure fluctuation at 920 °C and 25°C (d_p= 543 μm, z=150 mm and D=200mm)

Table 3.1 Experimental and predicted values of U_C

Particle	U_C (m/s)		Reference
	25 °C	920 °C	
Sand particles (d_p=543 μm)	1.25	1.45	Experiments, this study
	1.00	1.74	Predicted, Cai et al., (1989)
	0.96	1.30	Predicted, Gonzalez (1995)

At 920 °C, U_C is about 10% higher than at ambient temperatures. It is important to mention that most measurements of U_c have been done at ambient temperature. Determination of U_C at high temperatures is very delicate and tedious since for every single point, the reactor must reach its steady state conditions prior to pressure signal measurements. Fewer data are available, such as Cai et al. (1989) and Gonzalez (1995), where the temperature and pressure effects on transition to turbulent fluidization were investigated mostly for group A particles. These correlations, which are presented in Table 3.1, either overestimate or underestimate U_C for group B particles at high temperature as compared to our experimental values.

Upon determining U_C, two values were chosen on either side of this transition velocity to represent the bubbling and turbulent regimes and then combustion tests were carried out in two steps. In the first step, or "***combustion trials***", the feasibility of non-premixed combustion was investigated in bubbling and turbulent fluidization conditions. Based on qualitative results obtained during these trials, a second series of tests or "***carbon***

monoxide trials", were conducted by further focussing on non-premixed combustion to measure CO profile inside of the bed. Description of these experiments and the corresponding results for both types of trials are discussed in the following sections:

3.5.1 Combustion trials

Natural gas was injected to the reactor in a series of experiments at two different temperatures (850 and 980 °C) and at two superficial velocities (0.5 and 1.5 m/s) to represent the bubbling and turbulent regimes, respectively. As mentioned earlier, a relatively deep bed was used in all experiments. In such a deep bed, natural gas inside the bubbles can exchange many times with the emulsion gas and considering the operating temperature and also the free radical recombination at the particle surfaces, the combustion becomes complete by the time gases reach the bed surface.

In order to determine the minimum temperature required for combustion trials, conditions for over-bed combustion were identified during the pre-heating period. Figure 3.3 shows the temperature profile during the preheating period, which can be divided into three periods. During period I, natural gas is directly injected to the wind-box,

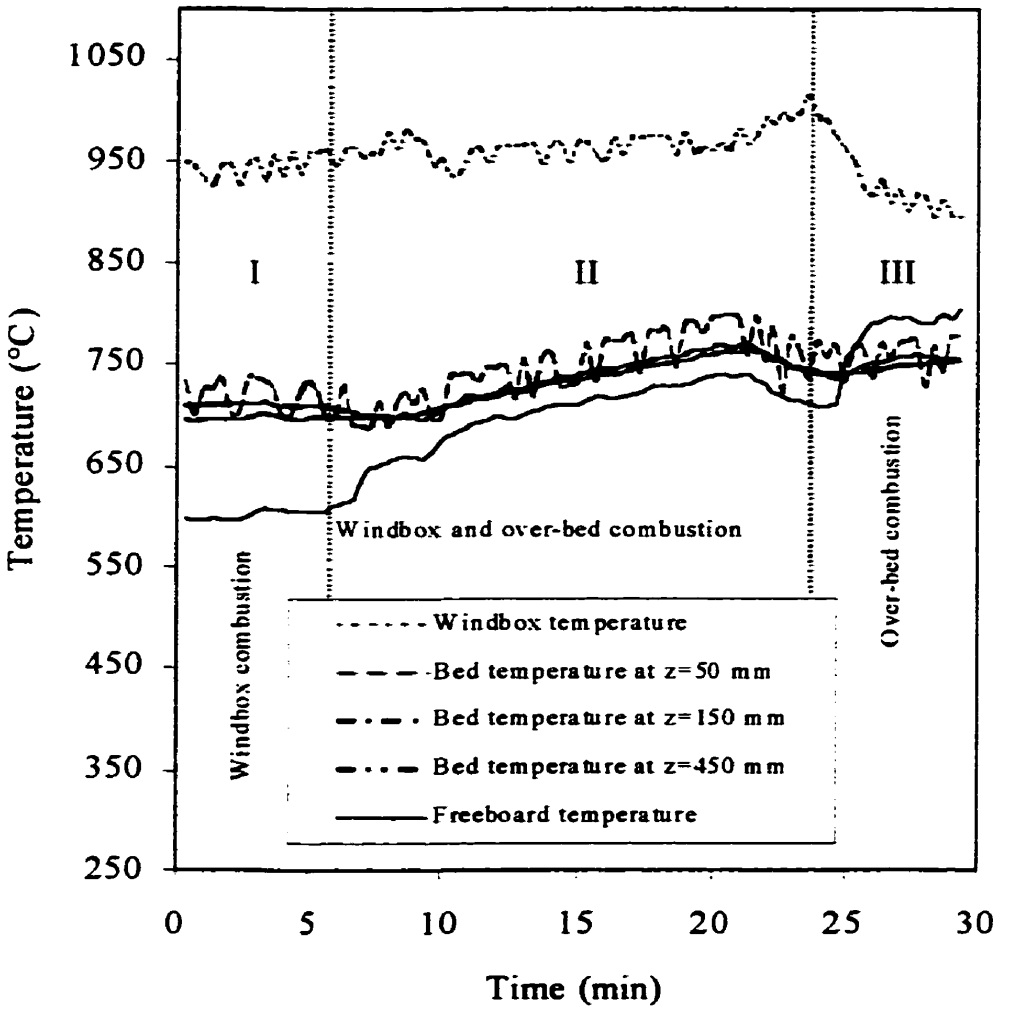

Figure 3.3 Temperature control during the pre-heating period

where its temperature is around 950 °C. The bed temperature is around 725 °C and the freeboard temperature is around 600 °C. A slight increase is observed in the bed and freeboard temperatures. During period II, natural gas is also gradually injected directly to the reactor and a slight increase in freeboard temperature is observed. During period III, the natural gas injected to the wind-box was interrupted and more natural gas is injected to the reactor. At this point the freeboard temperature becomes higher than the mean bed temperature and the bed serves as a heating medium for natural gas bubbles. For a bed temperature above 800 °C, combustion retreats to the bed only and this was considered as the minimal temperature for the operation of the pilot plant reactor.

For the pilot plant reactor used in this study, bed temperature variations are best within ±7 °C for turbulent and ±12°C for bubbling conditions. Figure 3.4 shows the radial and axial bed temperature profiles for turbulent fluidization regime during a typical experiment. Because of rapid solid mixing, temperatures in the turbulent fluidized bed are quite uniform in the presence of a highly exothermic reaction (natural gas combustion). With the pilot plant reactor of 20 cm in diameter, temperature differences in excess of 10°C were seldom seen. In fact, such temperature uniformity is of utmost importance in the operation of industrial fluidized bed reactors under turbulent fluidization conditions.

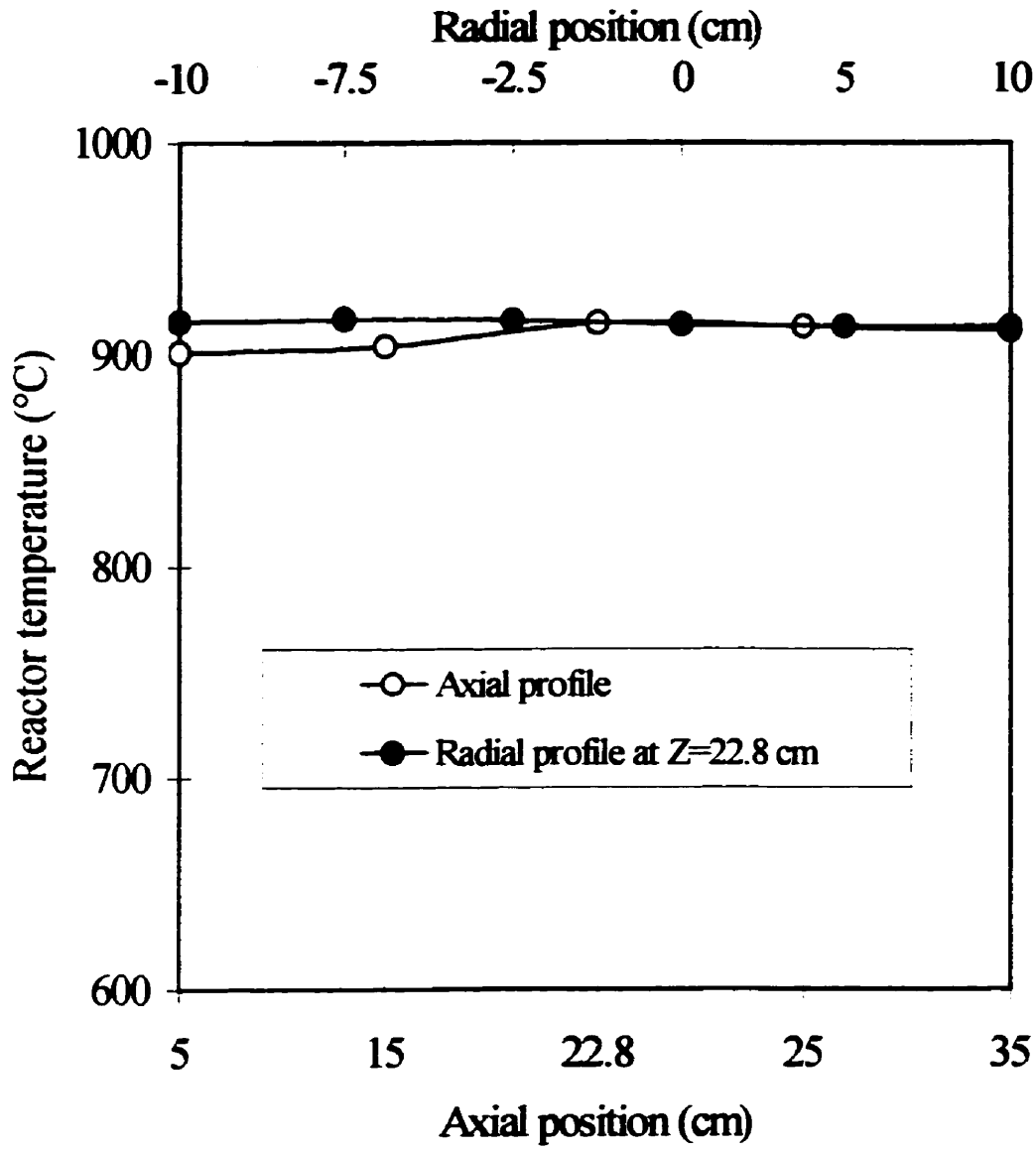

Figure 3.4 Axial and radial temperature profiles in turbulent flow regime for non-premixed combustion with one-hole sparger (z=17 cm, U_j=120 m/s, U=1.5 m/s)

A typical natural gas conversion profile obtained from the bubbling bed experiments is shown in Figure 3.5. For all experiments, the conversion is 100% at the top of the bed. As temperature increases, the 100% conversion point is reached within the bed and this can be attributed to the fact that the free radial formation dominates the inhibition process. The contribution of inhibition reactions to the overall combustion process has recently been investigated in details (Sotudeh-Gharebaagh et al, 1998). The combustion of hydrocarbons is a two step process. The first is the formation of CO and then CO gets converted into CO_2. At lower temperatures and also in the presence of inert particles, consumption of CO is very small compared to its formation, resulting in a maximum in CO emission level. Qualitative analyses showed that CO concentration rises sharply after the injection points and decreases as a function of height. Qualitative results obtained in this study also confirm the existence of a maximum. In order to convert CO to CO_2, bed temperature must be sufficiently high or otherwise, most of the CO will be converted in the splash zone. In order to avoid this situation, bed temperature for bubbling regime operation must be somewhat greater than 900 °C to have complete combustion within the bed. However, throughput of bubbling fluidized bed reactors is much lower than the industrial needs as compared to turbulent fluidized bed reactors for a given geometry.

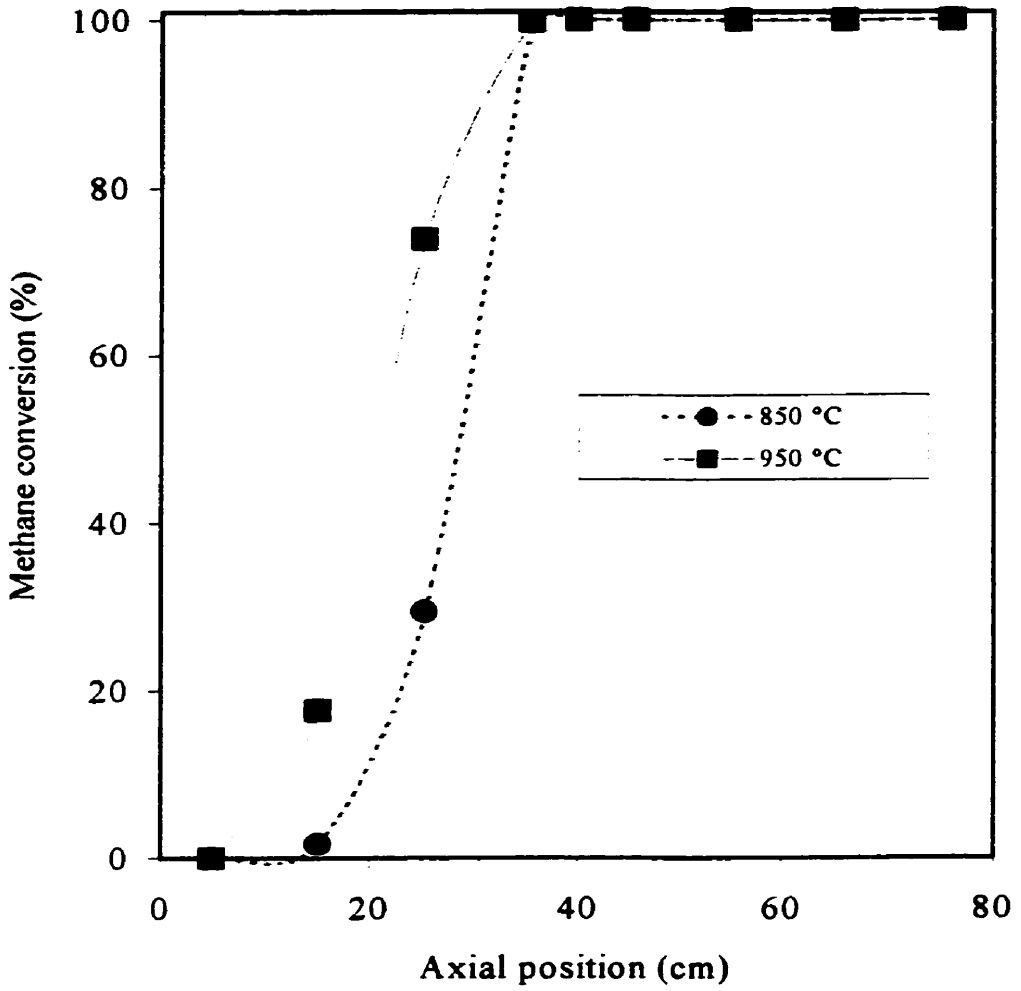

Figure 3.5 Methane conversion in the bubbling regime at various temperatures for non-premixed combustion with full sparger placed at the reactor base (U=0.5 m/s).

Figure 3.6 gives an example of conversion profiles obtained from the turbulent fluidization experiments. Once again, the conversion was completed within the bed. In this case also, CO levels undergo a maximum and because of good solid mixing, CO emission levels measured at the reactor outlet are quite small compared to those found in bubbling fluidized bed reactors.

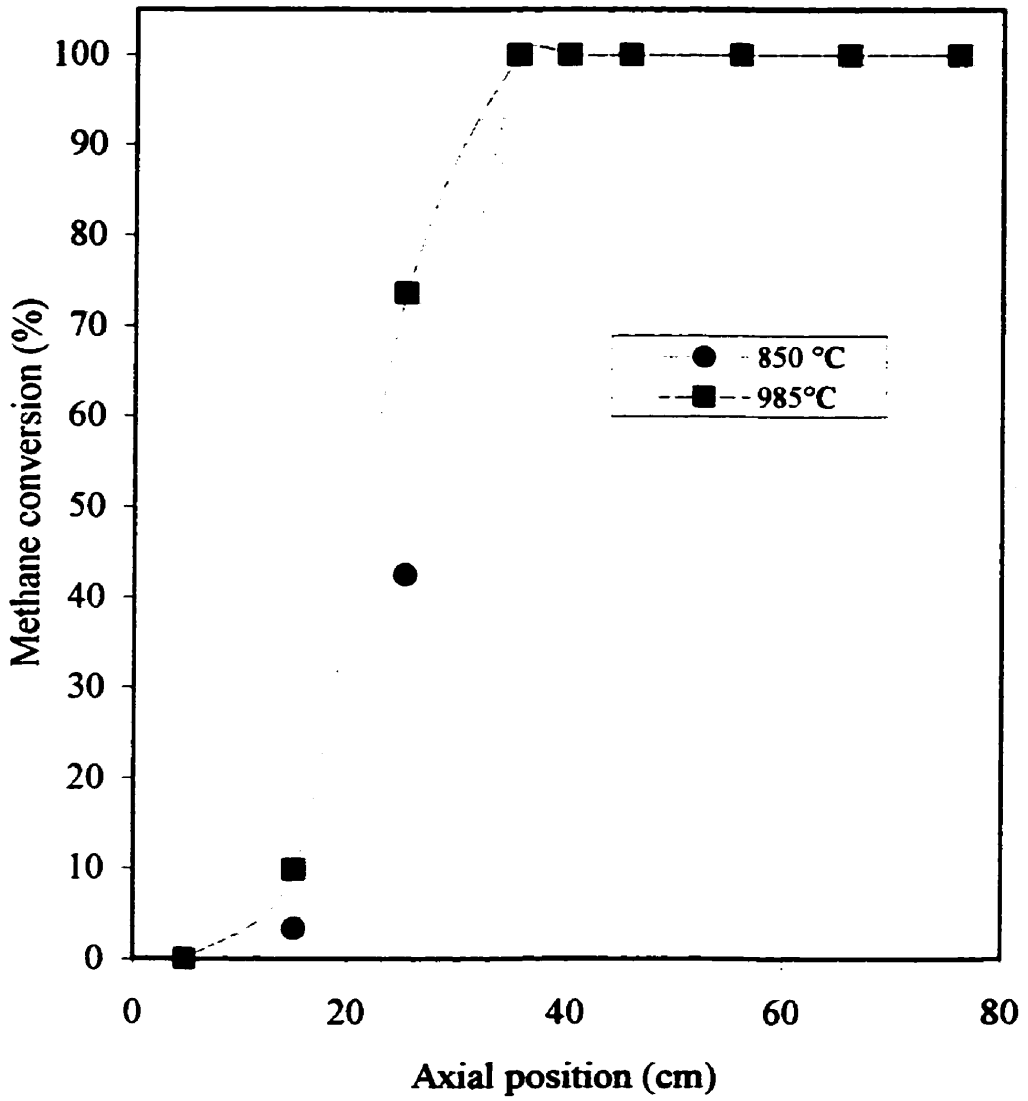

Figure 3.6 Methane conversion in the turbulent regime at various temperatures for non-premixed combustion with full sparger placed at the reactor base (U=1.5 m/s)

3.5.2 Carbon monoxide trials

Based on qualitative information obtained from the combustion trials, we further decided to test the behavior of CO formation and destruction inside the reactor. To this end, a new set of experiments was designed to focus on this subject. In these trials, an single-hole sparger with injection gas velocities of 30 and 120 m/s (through the sparger) and two gas superficial velocities of 0.7 and 1.5 m/s were tested at 900 °C. These sparger velocities were chosen to represent two different sparger hydrodynamics namely, bubbling and jetting based on the information from the literature. Existing correlations from the literature were examined to estimate the characteristic jet length for these sparger velocities and the predicted values are reported in Table 3.2

Table 3.2 Predicted characteristic jet length from the literature for the conditions of this study

U (m/s)	U_j (m/s)	Characteristic jet length (cm)						
		Yang (1981)	Hirsan et al. (1980)	Yates (1996)	Merry (1975)	Wen (1977)	Blake (1990)	Yang & Keairns (1979)
0.7	30	5.2	0.34	6.0	2.8	8.1	2.8	6.4
0.7	120	19.4	0.86	17.3	5.1	12.0	5.7	10.8
1.5	30	5.2	0.28	6.0	2.8	8.1	2.8	6.4
1.5	120	19.4	0.71	17.3	5.1	12.0	5.7	10.8

It is important to note that these correlations were mostly developed for upward streams and group A powders. Therefore, their applicability to downward spargers and group B particles are questioned, but due to lack of pertinent information, these values can be used to obtain an idea about jet penetration length. Among the correlations reported in Table 3.2, Hirsan et al., (1980) correlation is developed for group B powders. Massimilla (1985) states that the jet formation is more likely with the orifice velocity used. So far, Grace and Lim (1987) and Roach (1993) reported the criteria for the formation of permanent upward jets. None of these takes into account the orifice velocity and these can not be used to distinguish between jetting and bubbling for downward jets. Therefore, high jet penetration is referred to as jetting conditions while low penetration length being bubbling conditions around the sparger for this investigation.

Upon choosing the proper velocity for sparger and also gas superficial velocities, the experiments were performed at 900°C. This bed temperature was chosen to promote rapid CO destruction. The sparger is located at z=17 cm above main distributor, to avoid possible side effects caused by fluidizing gas coming from the distributor.

In figure 3.7, CO measurements along the reactor height for four conditions are reported. For the bubbling fluidized bed regime with jetting conditions (U=0.7 m/s and U_j=120 m/s), upon injecting the natural gas through a single point and due to the high turbulent area created around the sparger, excellent mixing were achieved between natural gas and air. In this region, the amount of O_2 is much lower than the stoichiometric value needed to convert the natural gas to CO_2 and almost all fuel was immediately converted to CO, leading to a peak in CO concentration and under this condition, CO rich bubbles were formed. CO bubbles must then come into contact with O_2 in order to get converted to CO_2 along the reactor length. Also, in the first stage of combustion, the fuel conversion to CO around the jet is much faster than the diffusion of oxygen through the surrounding layer. This is due to the excellent mixing between natural gas and air at the injection point. The second stage of combustion is the conversion of CO to CO_2, along the reactor height if the bed temperature is sufficiently high. This is achieved by diffusing oxygen to the CO bubbles. At these temperatures, no reaction can occur in the emulsion phase due to the quenching effect. Temperatures above 915 °C are needed for methane combustion in the emulsion phase (Hesketh and Davidson, 1991). Below this temperature for methane-air mixture, combustion is negligible.

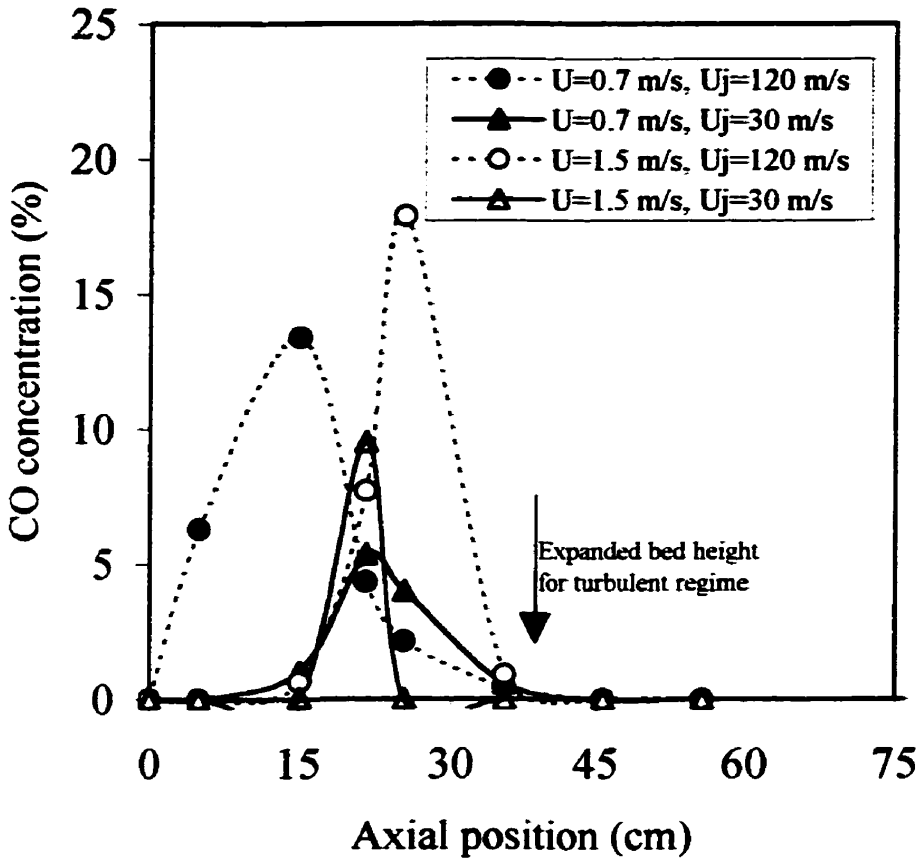

Figure 3.7 Axial CO profile at various operating conditions for non-premixed combustion with one-hole sparger placed at z=17 cm (T=900 °C).

The situation around the sparger is quite similar to the lower region in a circulating fluidized bed reactor, where a reducing zone is formed due to oxygen shortage. For the bubbling pattern (U_j=30 m/s), the overall trend remains the same, but no turbulence is formed around the sparger and the CO pick is lower. For the turbulent regime with jetting conditions, due to the high superficial gas velocity, the jetting zone shifts upwards and CO pick concentration was moved and pick concentration was observed as a higher position for the bubbling conditions. The same concept of two-stage combustion also remains valid here, and the CO oxidation becomes complete before reaching the bed surface, provided that the temperature is sufficiently high. The complete reaction length for CO oxidation in the turbulent fluidization is small as compared to bubbling conditions. This can be attributed to the fact that in turbulent fluidized beds, the gas mixing is improved. For low bed temperatures, the observation of CO profile in the reactor leads to the conclusion that CO burns in the freeboard. The overall trend reported in figure 3.7 is in close agreement with the predictions as well as with the experimental and theoretical findings of turbulent non-premixed combustion of methane in air (Masri et al., 1988) and of coal combustion (Lufei et al., 1993). Reported correlations in the literature also predict that CO is the dominant product at temperatures and particle size typically employed in fluidized bed combustion of coal particles (Gururajan et al, 1992). Under fluidized bed conditions, if temperature is kept sufficiently high, the subsequent oxidation of the CO occurs fast enough to convert it into CO_2 within bed.

3.6 Flue gas emissions

Our major environmental concern for fluidized bed systems is to control NO_x and CO emission levels. NO_x formation and destruction in combustion processes result from a combination of fuel nitrogen oxidation, thermal processes, and reactor hydrodynamics. In this study, the fuel is free of nitrogen and thermal generation of NO_x from the air nitrogen is the only source of NO_x. For the purpose of this study, the amount of thermal NO_x was predicted based on equilibrium conditions (for 8% oxygen in initial mixture, which is the case in turbulent fluidized bed conditions) using the detailed GRI (Gas Research Institute) mechanism for methane combustion. A detailed description of the complete GRI mechanism can be found in the GRI's annual reports (i.e. GRI, 1985). In this study, NO_x and carbon monoxide were recorded by a gas analyser at different temperatures from the reactor outlet and are reported based on 11% oxygen in the exit gas.

In Figure 3.8, normalized NO_x concentration is reported for turbulent and bubbling conditions along with predicted concentrations for the turbulent flow regime. The NO_x emissions levels for turbulent fluidized bed operation are quite high, but are still at the same order of magnitude as for the bubbling regime. This is attributed to the fact that the amount of oxygen available in the bed was almost 8% higher than that necessary to promote self-combustion for turbulent fluidization conditions of this study. For bubbling

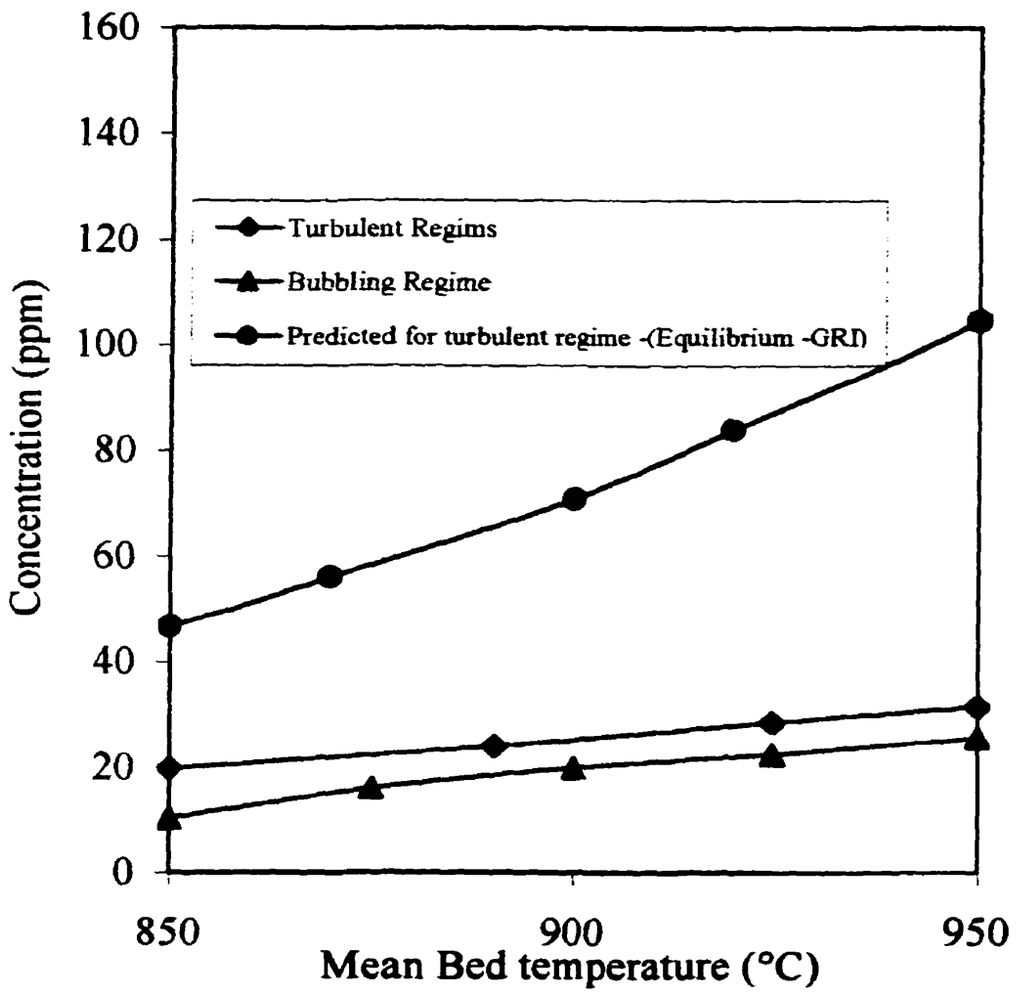

Figure 3.8 **Predicted and Normalized NO_X concentration at the reactor exit for non-premixed combustion with full sparger placed at the reactor base.**

conditions of this study, the excess oxygen in the bed is less than 1%, which consequently leads to lower measured and predicted NO_X formation. The maximum predicted NO_X value for bubbling conditions (T= 950 °C) does not exceed 30 ppm based on 11% oxygen, due to oxygen shortage, where 9% methane is injected to the reactor to obtain self-sustained combustion. It is important to note that the amount of NO_X generated for both fluidization regime is always lower than the value measured with the burner located at the reactor base (40 ppm based on 11% oxygen). For industrial reactors operating under turbulent fluidization regime with integrated heat exchanger inside of the reactor, due to low oxygen level, less NO_X may be measured as compared to those reported in this study.

Figure 3.9 shows the normalized concentration of CO (ppm) measured at the reactor outlet for turbulent and bubbling conditions. For temperatures less than about 850°C, high concentration of CO was generated since the temperature is not sufficiently high to complete the CO conversion within the bed. Within the temperature range used in this study (800 to 1000°C), both systems performed quite well. Turbulent fluidized bed generates less CO probably due to high gas-solid interactions, while the bubbling fluidized bed needs to operate above 900 °C for low CO emission levels.

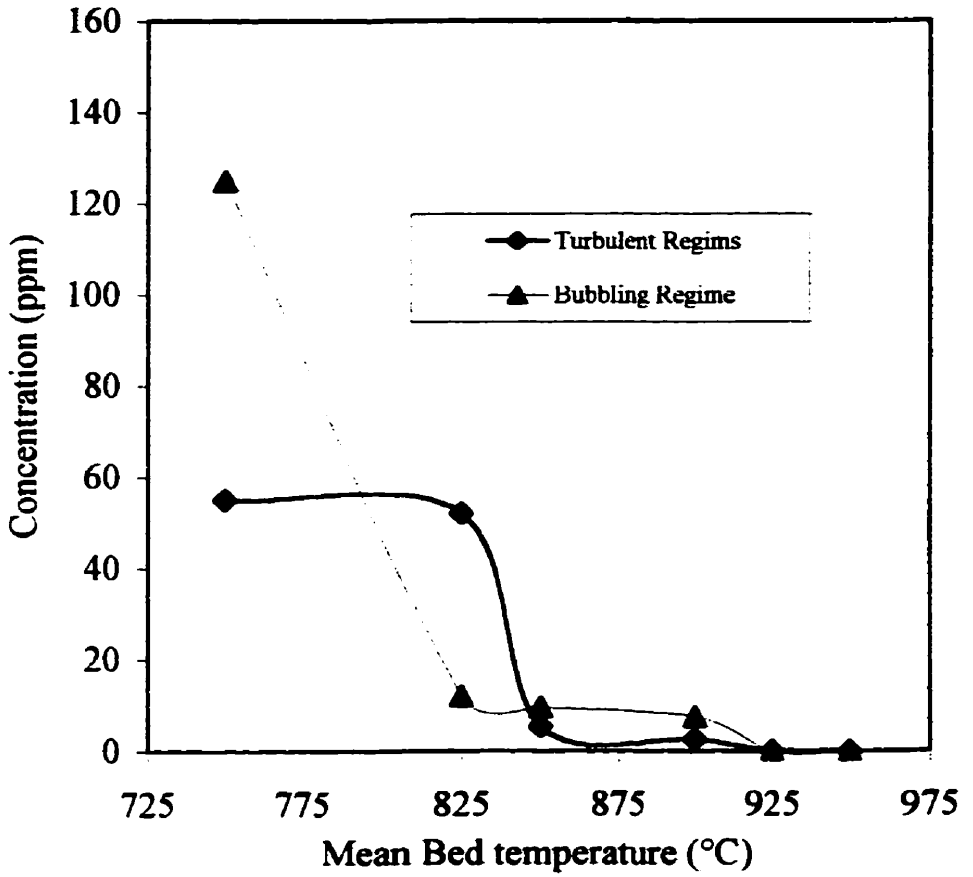

Figure 3.9 **CO emissions at reactor exit for the bubbling and turbulent regime for non-premixed combustion with full sparger placed at the reactor base.**

3.7 Auto-thermal combustion

Typically, when the reactor was operated in the bubbling regime, 9% of methane was injected to the reactor and the conversion was 100% at the temperature range of interest. Superficial gas velocity was 0.5 m/s and a maximum temperature of 950°C was used. It is interesting to note that under these conditions no external energy input power was needed to operate the reactor. When the reactor was operated in the turbulent regime, 6% of methane was injected to the reactor and the conversion was 100% at the temperature range of interest. Superficial gas velocity was 1.5 m/s and a maximum temperature of 980°C was used. In the turbulent regime due to its higher throughput, reactor power generation is higher than that of bubbling regime for the same operating temperature. The power generated in the combustion process is calculated using the following expression:

$$P = F_{CH_4} X \Delta H(T) \qquad (3.1)$$

The reactor power generated in this investigation was about 42 kW for the turbulent regime and 21 kW for the bubbling regime.

3.8 Conclusions

A promising generation of gas combustion technology has been proposed and tested using a turbulent fluidized bed reactor. The main results of this study as derived from the experimental observations are summarized as follows:

1. The turbulent fluidized bed reactor proposed in this study exhibits an excellent isothermicity.

2. Onset of turbulent fluidization was measured since the existing correlations can not be used to determine this velocity for the conditions of this study.

3. For both bubbling and turbulent fluidized bed reactors, the complete natural gas conversion can be achieved over 800 °C.

4. The power generated by turbulent fluidization regime is much higher than that for bubbling fluidized bed reactors while respecting all environmental requirements.

5. Measured CO profile with two different sparger velocities for the two fluidization regimes showed that a reducing zone similar to the lower region of circulating fluidized bed reactor was developed around the sparger.

6. The CO concentration within the bed passes through a maximum for both fluidization regimes, and after converting natural gas to CO, the CO oxidation

takes place along the reactor height as soon as it comes into intimate contact with oxygen.

7. The results of this study suggest areas for further investigations of fuel injection into fluidized beds, sparger hydrodynamics, optimal combustor design and gas-gas contact efficiency for flammable mixtures and also waste treatments.

3.9 Acknowledgements

The authors are grateful to Mr. P. Sauriol and Y. Segonne for their help with the experimental work. This work was supported by a grant provided by National Science and Engineering Research Council (NSERC) of Canada. The Ministry of Culture and Higher Education of I. R. of IRAN is also acknowledged for making Mr. R. Sotudeh-Gharebaagh's graduate studies possible in Canada.

3.10 References

American Gas Association, 1991, Cofiring and reburn keep emissions under control, Plant Eng., Spring.

Blake, T.R., H. Webb and P.B. Sunderland, 1990, The nondimensionalization of equations describing fluidization with applications to the correlation of jet penetration height, Chemical Engineering Science, **45**, 2, 365.

Cai, P., S.P. Chen, Y. Jin, Z.Q. Yu and Z.W. Wang, 1989, Effect of temperature and pressure on the transition from bubbling to turbulent fluidization, AIChE symp. Ser., 37.

Chehbouni A., Chaouki J., Guy C. and Klvana D., 1994, Characterization of the Flow Transition between Bubbling and Turbulent Fluidization, IEC J., **33**, 8, 1889.

Foka M., Chaouki J., Guy C. and Klvana D., 1994, Natural gas combustion in a catalytic turbulent fluidized bed, Chemical Engineering Science, **449**, 24A, 4269.

Gonzalez, A., 1995, PhD dissertation, Ecole Polytechnique de Montreal.

Grace J.R., 1990, High velocity fluidized bed reactors, Chemical Engineering Science, **45**, 1953.

Grace, J.R., and C.J. Lim, 1987, Permanent jet formation in beds of particulate solids, Canadian Journal of Chemical Engineering, **65**, 160.

GRI, Annual Report, September 1994 - August 1985, Gas research Institute.

Gururajan V.S., P.K. Agrewal and J.B. Agnew, 1992, " Mathematical modelling of fluidized bed coal gasifiers", Trans.I.Chem.E., **70**, 3, 211.

Hesketh R. P. and Davidson J.F., 1991, Combustion of methane and propane in an incipiently fluidized bed", Combustion and Flame, **85**, 449.

Hirsan, I., C. Shishlta, and K.M. Knowlton, 1980, The effect of bed and jet parameters on vertical jet penetration length in gas fluidized beds, 73rd Annual AIChE meeting, Chicago, Illinois.

Kehoe P. W. K. and Davidson J. F., 1971, Continuously slugging fluidised beds. Inst. Chem. Eng. Symp. Ser., **33**, 97.

Lufei J., H.A. Becker and R. K. Code, 1993, "Devolatilization and char burning of coal particles in a fluidized bed combustor", Can. J. Chem. Eng., **71**, 10.

Masri, A.R., R.W. Bilger, R.W. Dibble, 1988, "Turbulent non-premixed flames of methane near extinction; probability density function", Combustion and flame, **73**, 261.

Massimilla, L. 1985, Gas jets in fluidized beds, in Fluidization, 2nd ed., (Edited by Davidson, J., F. Clift, R. Harrison D.), Academic press, New York.

Merry J. M. D., 1975, Penetration of Vertical Jets into Fluidized Beds, AIChE, **21**, 3, 507.

Mezaki, R., C.C. Watson, 1966, Catalytic oxidation of methane, I & EC process design and development, **5**, 6.

Roach, P.E., 1993, Differentiation between jetting and bubbling in fluidized beds, Int. J. Multiphase Flow, **19**, 6, 1159.

Sadilov P. V. and Baskakov A. P., 1973, "Temperature fluctuations at the surface of a fluidized bed with gas combustion occurring therein", Int. Chem. Eng., **13**, 3, 449.

Sotudeh-Gharebaagh, R., J. Chaouki and R. Legros, 1998, Investigation of the heterogeneous and homogeneous combustion of methane, submitted to Comb. & Flame.

Van der Vaart D. R., 1992, Mathematical modeling of methane combustion in a fluidized bed, Ind. Eng. Chem. Res., **31**, 999.

Wen, C.Y., M. Horio, R. Kirshnan, R. Khosravi, P. Rengarajan, Proc., 1977, Second. Pacific Chem. Eng. Cong., 1182.

Yang, W.C. and D.L. Keairns, 1979, "Estimating the jet penetration depth of multiple vertical grid jets", IEC Fundamental, **18**, 4, 317.

Yang, W.C., 1981, "Jet penetration in a pressurized fluidized bed, IEC Fundamental, **20**, 297.

Yates, J.G., 1996, "Effects of temperature and pressure on gas-solid fluidization", Chemical Engineering Science, **51**, 2, 167-205.

CHAPTER 4: GAS MIXING IN A TURBULENT FLUIDIZED BED REACTOR

Reference:

Sotudeh-Gharebaagh, Rahmat and Jamal Chaouki (1998), "GAS MIXING IN A TURBULENT FLUIDIZED BED REACTOR", Submitted to Canadian Journal of Chemical Engineering (December 1998).

Keywords:

Mixing length, Mixing, Downward sparger, Turbulent fluidized bed, Hydrodynamic

4.1 Context[2]

In chapter III, combustion of natural gas was studied in a pilot plant fluidized of inert particles under bubbling and turbulent fluidized bed conditions. It was shown that the non-premixed combustion is a mode of choice to handle the flammable mixtures. Under these conditions, the mixing plays a vital role in the combustion process. Therefore, it has been decided to further evaluate the gas discharge modes and examine the effect of different variables on the mixing process. In chapter IV, gas mixing was investigated in a turbulent fluidized bed reactor with a sparger facing downward.

---

[2] This section is not included in the original manuscript. It only serves as a transition between papers for the thesis.

4.2 Abstract

A series of experiments has been conducted to study mixing and hydrodynamic behavior of a downward facing sparger in a turbulent fluidized bed reactor. Using pressure measurement technique, two flow discharge modes were identified around the sparger by injecting a gas tracer into the bed. These are bubbling and jetting conditions. Experimental results show that, under bubbling conditions, bubbles tend to keep their identity. While, under jetting conditions, a highly turbulent heterogeneous area is formed around the injection point. Due to attrition and erosion of internal heating or cooling surfaces in industrial reactors, the dominant discharge mode is the bubbling pattern. Therefore, in this investigation, the bubbling pattern is studied by measuring the radial and axial dispersion of gas tracer injected into a hot fluidized bed reactor of 20-cm diameter of FCC and sand particles. A three-phase model is also proposed in order to predict the *mixing length*. In addition, the effect of sparger configuration on tracer gas mixing was examined for FCC particles.

4.3 Résumé

Plusieurs séries d'expériences ont été menées pour étudier le mélange et le comportement hydrodynamique d'injecteurs de gaz dirigés vers le bas dans un lit fluidisé turbulent. En utilisant les fluctuations de pression, deux modes d'écoulement de gaz ont été identifiés autour des injecteurs en les alimentant d'un gaz traceur : le mode "bulle" et le mode "jet". En alimentant les injecteurs d'un gaz traceur, il a été démontré que dans le cas du mode "bulle", les bulles tendent à garder leur propre identité. Alors qu'en mode "jet", une zone turbulente hétérogène est formée autour des injecteurs. A cause de l'attrition et de l'érosion des échangeurs de chaleur internes dans les lits industriels, le mode bulle est prédominant. Ainsi, dans la suite du papier, seul le mode "bulle" a été étudié en injectant un traceur gazeux et en mesurant ses concentrations radiales et axiales dans un lit fluidisé turbulent . Ce lit a un diamètre de 20 cm et fonctionne à des températures variant de la température ambiante à 900°C en utilisant aussi bien des particules de sable que du FCC. Un modèle à trois phases a été proposé dans le but de prédire les longueurs de mélange. De plus, les plusieurs configurations d'injecteurs ont été examinées en utilisant des particules FCC.

4.4 Introduction

Commercial fluidized bed reactors employing spargers facing downward to separately inject fuels or reactives to the bed are finding increased applications in chemical, petrochemical and energy industries. In fact, the gas mixing coming from such spargers and the corresponding solid mixing are central features of fluidized bed reactors. Therefore, information concerning the flow pattern and mixing around the sparger is very important in design and scale-up practice. Interaction between a gas discharged from the sparger, the bed materials and in-bed gas becomes crucial to reactor performances in the case of fast chemical reactions. For highly exothermic reactions, creation of hot spot at the sparger region may lead to the solid agglomeration and mal-fluidization of bed materials. This reveals the importance of deep understanding of the flow pattern around the sparger. So far, several works have been reported in the literature attempting to describe the flow pattern, gas-solid and gas-gas contact in fluidized beds (e.g. Antimaty and Cakaloz, 1978) and characteristic jet penetration length (e.g. Yang et al., 1986; Yates et al., 1986; Merry 1975; Wen et al., 1977 and Blake et al., 1990). For mixing studies reported in the literature, a tracer gas (He, CO_2, H_2 or CH_4) was injected from mostly the main distributor and its concentration was analyzed using gas chromatography or mass spectrometry. All these studies were conducted at low temperatures by the upward injection system. Application of this information and the existing correlations to the downward gas sparger is questionable since these correlations may lead to an unjustified

characteristic jet penetration length considering the fact that such length for downward jets is rather small as compared to upward jets.

In industrial scale fluidized beds, where handling a flammable mixture is of critical importance, gas discharge through downward nozzles is commonly employed. The gas discharge in this way may lead to a number of patterns ranging from the periodic formation of single bubbles or permanent jet depending on the properties of the gas and solid particles, remote gas, gas discharge devices and the operating conditions. Under these conditions, the flow pattern around the discharge point plays a very critical role in gas-gas or gas-solid mixing. As already mentioned, a vast body of experimental data is available in the literature for vertically upward gas injection into the fluidized bed reactors, while the information regarding the downward nozzle is still lacking. Only reported study in the literature is that of Shen et al (1990), where they studied the downward sparger hydrodynamic in two-dimensional bed reactors at ambient temperatures. Benkrid and Caram (1989) showed that the physical behavior of two-dimensional fluidized bed reactor differs from three-dimensional fluidized beds. Therefore, measurements in three-dimensional beds are required to understand the flow structure around the injection point.

In this work, hydrodynamic and mixing behavior of a downward sparger were experimentally investigated at relatively high temperatures by injecting CH_4 or CO_2 as tracer. The flexible structure of experimental set-up also permitted measuring of radial

and axial concentration, pressure and temperature profiles. An attempt is also made to develop a realistic model, in order to estimate the mixing length around the sparger. Therefore, this paper presents the details of the experimental work and the model.

4.5 Experimental

4.5.1 Apparatus

Experimental conditions are summarized in Table 4.1 and Figure 4.1 shows the experimental set-up used throughout this investigation. As shown in Figure 4.1, the combustion products from the burner located at the base of the reactor were introduced from the "windbox" to the reactor to heat-up the bed of FCC or sand particles and also to maintain the bed temperature constant throughout the experiments. The gas leaving the entire reactor passes through a cyclone in which the entrained particles were recovered. The tracer gas was injected into the bed at the center at 17 cm above the distributor through a single-hole sparger with or without nozzle pointing downward. A pressure transducer was used to monitor bed level during the sampling period. The bed temperature was also measured radially and axially by several thermocouples located at different axial positions in the bed.

Table 4.1 Experimental conditions

Column (reactor):	(see Figure 4.1)	
Construction Material	304 Stainless Steel	
Diameter (cm)	20	
Length (m)	2	
Distributor:		
Type	Cap distributor	
Geometry	9 X 12.6 mm diameter caps	
Sparger:	(see Figure 4.2)	
d_j (mm)	5	
Experiments	**FCC**	**Sand**
Particles:		
d_p (μm)	70	533
ρ (kg/m³)	1450	2650
Fluidizing gas:		
U (m/s)	0.8	1.5, 0.8, 0.5
Onset of turbulent fluidization		
U_c (m/s)	0.7*	1.5*
Tracer gas:	CO_2 and CH_4	CH_4
U_j (m/s)	36 and 56	30
Gas analyzer:	HP5980A Gas Chromatograph TCD detector Molecular Sieve 5A and Porapak Q columns	

* Experimentally measured values by pressure fluctuation techniques

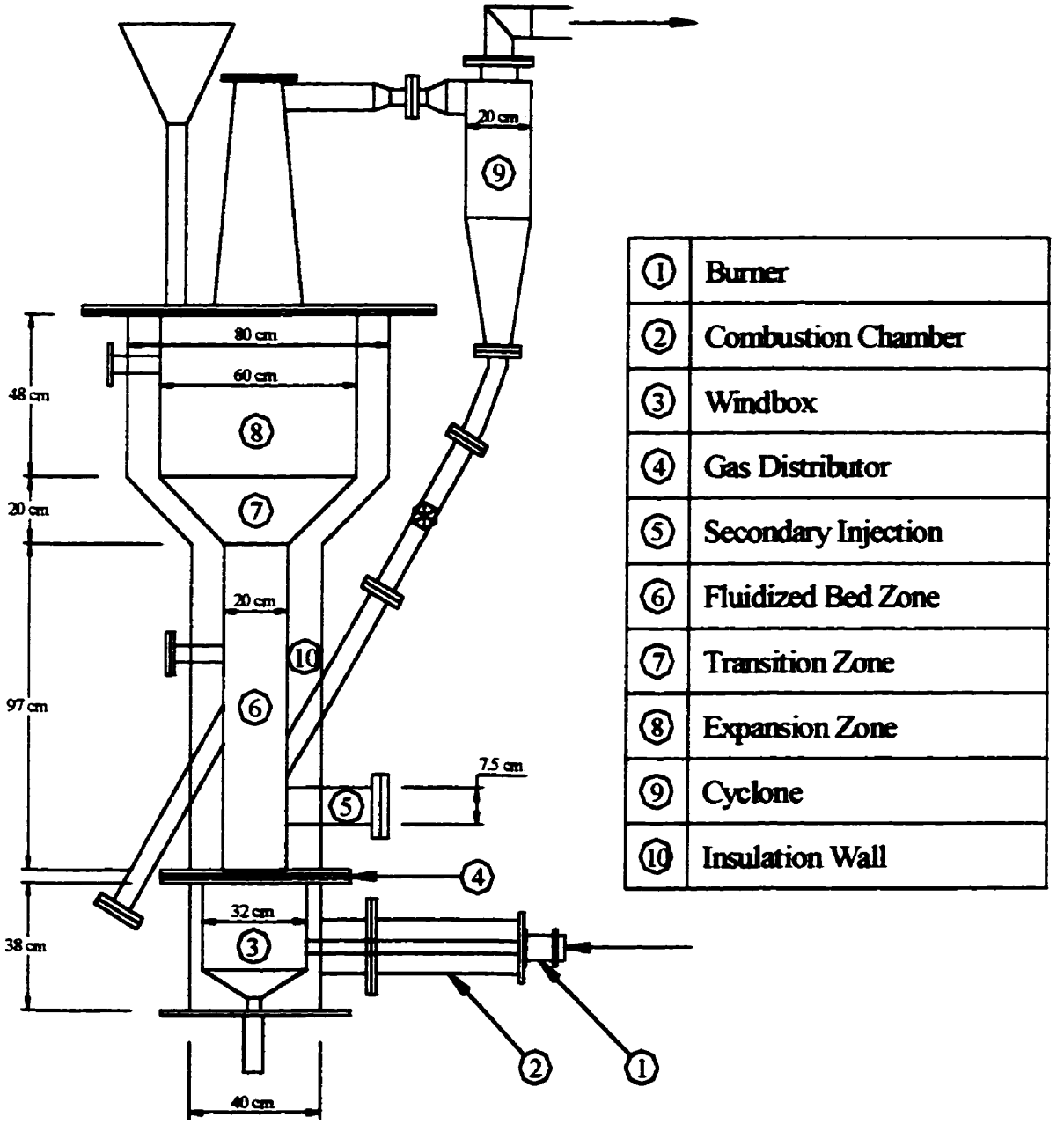

Figure 4.1 Schematic of a Pilot Plant Turbulent Fluidized Bed Reactor

The spargers, which were designed based on the information from the literature for commercial reactors, are shown in Figure 4.2.

4.5.2 Tracer gas supply and sampling

In order to obtain information on gas mixing in the bed, the tracer gas, namely methane, was supplied to the hot bed through a rotameter. The tracer gas temperature was estimated to be equal to bed temperature upon entering the bed. Figure 4.3 shows the sampling network to withdraw gas samples from varied axial and radial positions inside the reactor. The gas was sampled at steady state conditions through a sampling loop. The gas sampling does not disturb the gas flow in the bed, because the rate was negligibly small, compared with total gas flow rate in the bed. The sample was then passed through a drying agent to remove the water and the dry sample was sent to a gas chromatograph for tracer gas analysis. The drying agent does not absorb CH_4. Experiments were carried out at three different temperatures, (25, 400 and 900 °C). At 25 and 400 °C, which were devoted to mixing studies with no chemical reaction, CH_4 and CO_2 were injected as tracers to the bed and their axial and radial concentrations were measured. At 900 °C, methane was injected as fuel and the axial and radial methane and CO concentrations were measured.

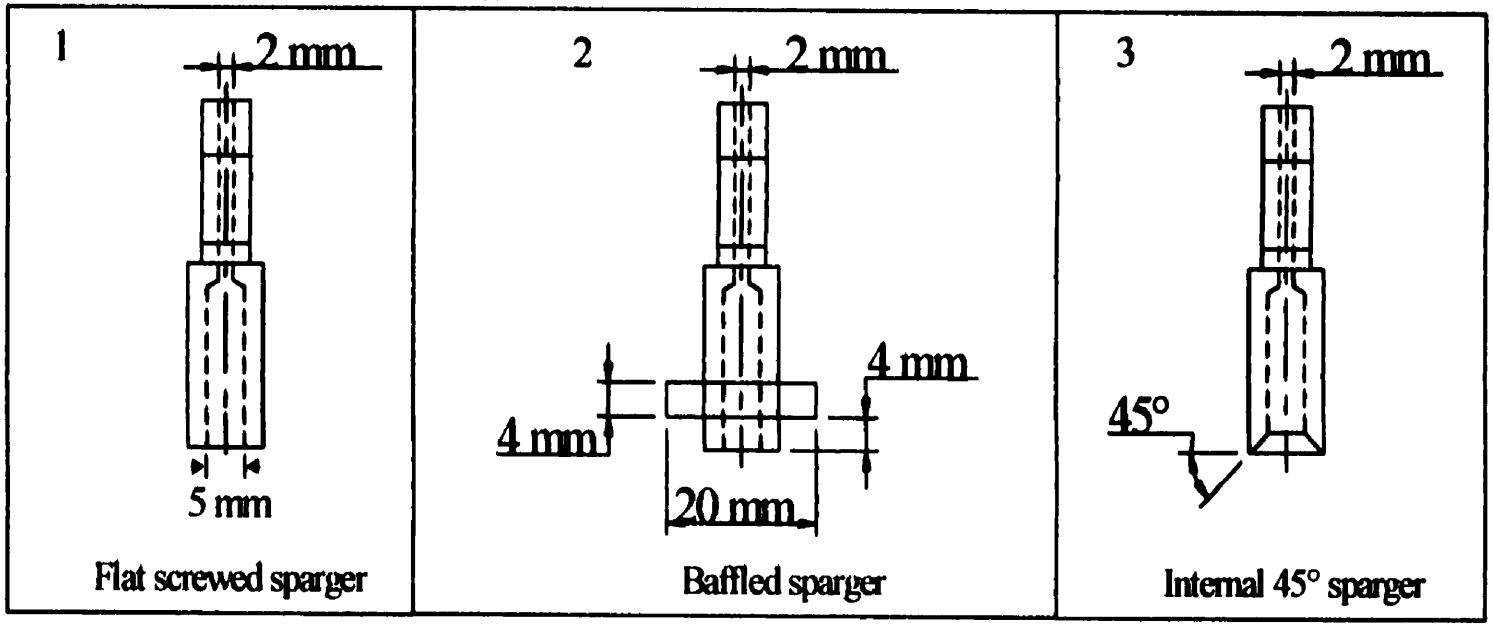

Figure 4.2 Configuration of Spargers used for Experiments

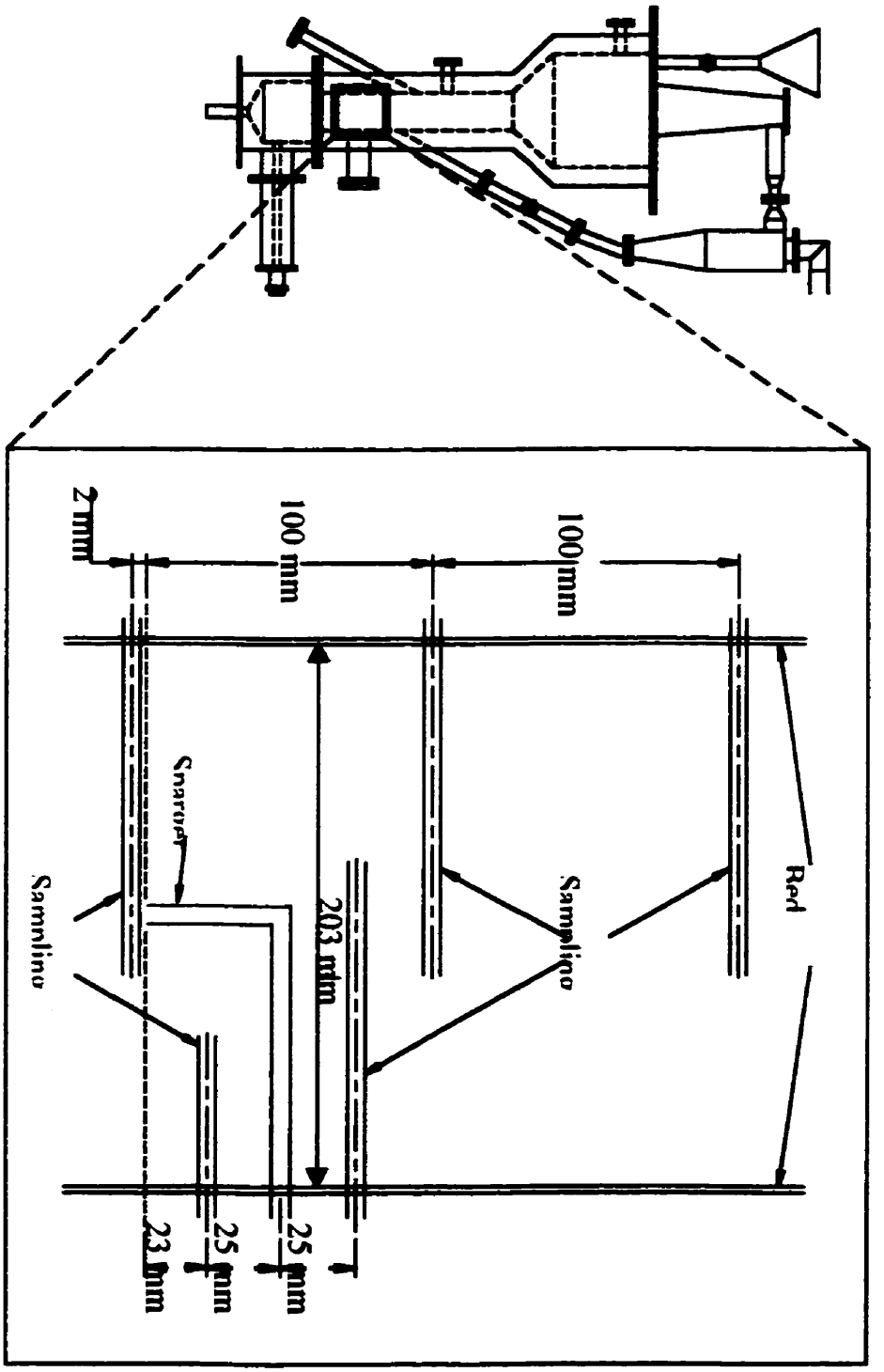

Figure 4.3 Schematic of the Gas Sampling Network

4.5.3 Experimental Procedure

In this investigation, the experiments were carried out for FCC and sand particles for: U= 0.2 and 0.8 m/s; Uj=25, 37 and 56 m/s and T=25, 400 and 900 °C. The concentration profiles were measured for 10 radial and 6 axial positions. Considering typical conditions for commercial reactors, where discharge velocity is kept around 30 m/s due to attrition considerations (e.g. Kunii and Levenspiel, 1991), the jet velocities for this study were chosen in order to have dynamic similarities between commercial conditions and the conditions of this study. The dynamic similarities mean that the operating conditions (i.e., particle type, temperature, pressure, superficial velocity and discharge velocity) should be chosen so that the jet characteristic length could remain the same. The existing correlations in the literature can not be confidently used to obtain the characteristic length for downward spargers, but in lack of pertinent information, this could be considered as a rough estimation of the jet length. The results of calculations obtained from the existing correlations reported in the literature are given in Table 4.2. This table permits us to decide on appropriate operating conditions for mixing and reaction studies.

Therefore, due to large industrial impact of understanding sparger hydrodynamics under bubbling conditions, the bubbling pattern was investigated in this study as an attempt to understand the gas mixing around the injection point.

Table 4.2 Characteristic jet length from existing correlation

Conditions	Industrial reactors	Poly mixing	Poly reaction	Poly mixing	Poly reaction	Reference	Correlation
U_j (m/s)	30	30	30	47.5	53		
Jet length (cm)	16.9	10.9	9.9	16.9	16.9	Yang (1986)	$\frac{L_j}{d_j} = 7.65\left[\left(\frac{U_{mf}(25°C)}{U_{mf}(T,P)}\right)\left(\frac{\rho_f U_j^2}{(\rho-\rho_f)gd_j}\right)\right]^{0.472}$
	16.2	11.4	10.5	16.1	16.1	Yates et al (1987)	$\frac{L_j}{d_j} = 9.7\left[\left(\frac{U_{mf}(25°C)}{U_{mf}(T,P)}\right)\left(\frac{\rho_f}{\rho-\rho_f}\right)\left(\frac{U_j^2}{gd_j}\right)\right]^{0.38}$
	25.4	16.9	14.3	20.4	18.0	Merry (1975)	$\frac{L_j}{d_j} = 5.25\left(\frac{\rho_f d_j}{\rho d_p}\right)^{0.3}\left(1.3\left(\frac{U_j^2}{gd_p}\right)^{0.2} - 1\right)$
	22.2	26.0	33.5	29.6	39.4	Wen (1977)	$\frac{L_j}{d_j} = 814.2\left(\frac{\rho_f d_j}{\rho d_p}\right)^{0.585}\left(\frac{\mu_g}{\rho_f d_j U_j}\right)^{0.654}\left(\frac{U_j^2}{gd_j}\right)^{0.47}$
	12.5	8.8	7.7	11.3	10.4	Blake et al (1990)	$\frac{L_j}{d_j} = 55.6\left(\frac{U_j^2}{gd_j}\right)^{0.251}\left(\frac{\rho_f}{\rho}\right)^{0.322}\left(\frac{\mu_g d_j}{\rho U_j d_p^2}\right)^{0.134}$
	12.5	10.2	9.2	12.1	11.4	Yang and Keairns (1979)	$\frac{L_j}{d_j} = 15\left(\frac{\rho_f U_j^2}{(\rho-\rho_f)gd_j}\right)^{0.187}$

4.6 Mixing Model

Experimental studies conducted so far in our laboratory show that the bubbles tend to retain their identity as they are purged on their way through the bed under bubbling flow pattern around the sparger. Considering this concept, for mixing model, we consider that the bed consists of three distinct phases, grid-bubble phase, sparger-bubble phase and emulsion phase. Upon injecting gaseous fuel into the bed through the sparger, small bubbles are formed in swarm of larger grid bubbles and the gas exchange immediately starts between different phases. It is important to note that since the gas superficial velocity chosen in this study is very close to the onset of the turbulent fluidization conditions, the use of expressions from the bubbling fluidized bed conditions remain valid (Gonzalez, 1995). An idealized version of model is presented in Figure 4.4. The differential equations representing the movement of gas tracer introduced into the bed through the sparger are given below:

Material balance of the tracer gas in the grid bubble phase is:

$$\frac{dC_g}{dz} = -\frac{K_{be}}{U_g}(C_g - C_e) \tag{4.1}$$

Material balance of the tracer gas in the sparger bubble phase is:

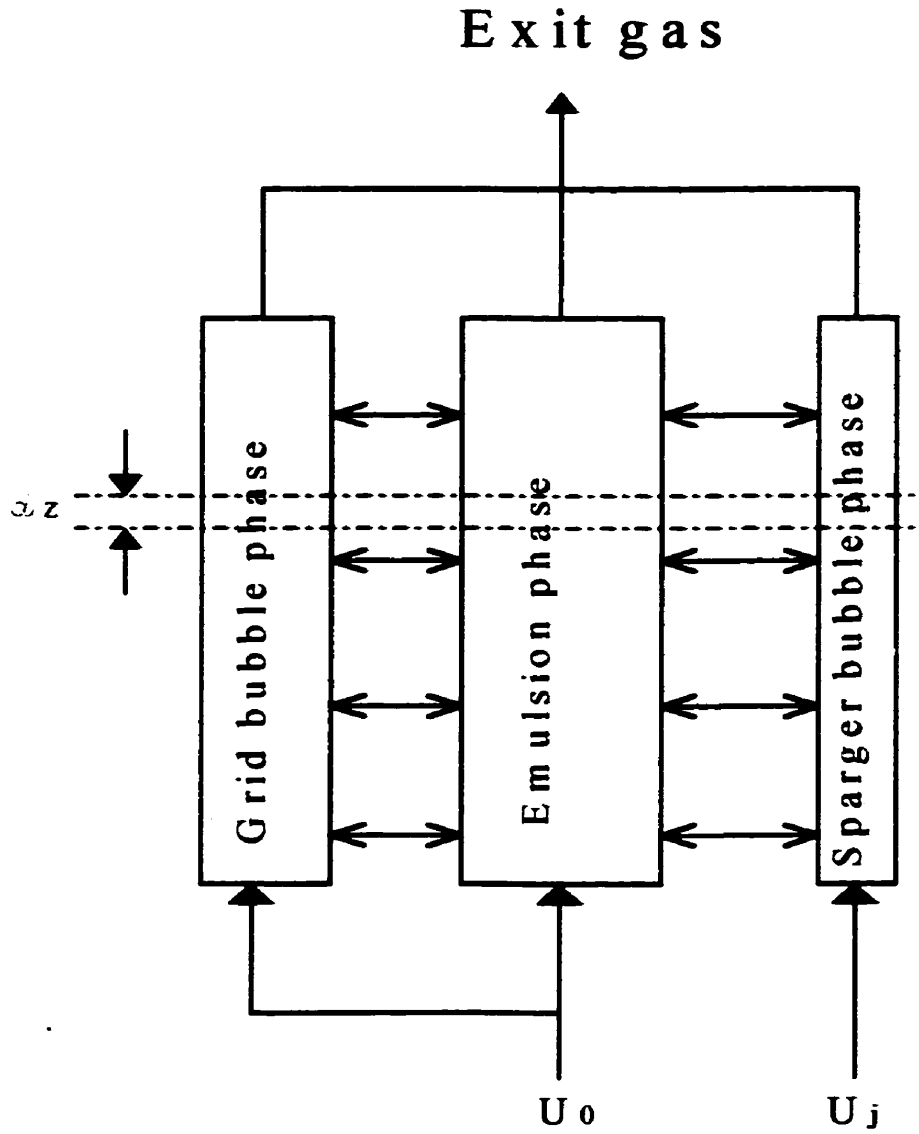

Figure 4.4 Features of a three-phase turbulent fluidized bed reactor model

$$\frac{dC_s}{dz} = -\frac{K_{be}}{U_s}(C_s - C_e) \tag{4.2}$$

Material balance of the tracer gas in the emulsion phase is:

$$\frac{dC_e}{dz} = \left[\frac{\delta_g \frac{K_{be}}{U_g}(C_g - C_e) + \delta_s \frac{K_{be}}{U_s}(C_s - C_e)}{1 - (\delta_g + \delta_s)} \right] \tag{4.3}$$

The interphase mass transfer coefficients from the bubble phases to the emulsion phase, which is different for sparger and grid bubbles due to different bubble size and physical properties, are derived from Davidson and Harrison (1963).

$$K_{be} = 4.5\left(\frac{U_{mf}}{d_b}\right) + 5.85\left(\frac{D_e^{0.5} g^{0.25}}{d_b^{1.25}}\right) \tag{4.4}$$

The bubble size at any height is obtained from Darton et al. (1977):

$$d_b = \frac{0.54(U - U_{mf})^{0.4}\left(z + 4\sqrt{5.52 \times 10^{-5}}\right)^{0.8}}{g^{0.2}} \tag{4.5}$$

By solving these equations simultaneously, the tracer concentration can be determined in all three phases. Based on the concentration profile, the characteristic mixing length can be estimated, which represents the length above the injection point, where the concentration in all phases becomes identical to the mean value considering the whole bed as a perfectly mixed reactor.

4.7 Results And Discussions

In this section, the transition velocity from the bubbling to jetting conditions is determined using pressure fluctuation measurements. The experimental results are also presented in detail for bubbling and jetting pattern around the sparger located in a fluidized bed of inert or FCC particles. The comparison is made between the experimental data and predicted values following a critical discussion on important findings of this investigation.

4.7.1 Transition velocity

Prior to mixing and reaction tests, the transition velocity or minimum jetting velocity (U_{mj}), from bubbling to jetting conditions around the sparger is determined at 400 and 900°C. So far, two correlations are suggested in the literature for the formation of permanent jets in fluidized bed reactors (Grace and Lim, 1987 and Roach, 1993). Grace and Lim (1987) suggested a very simple criterion with only the orifice and particle diameters. This correlation provides no information on operation, bed diameter, and jet angle away from the vertical. Roach (1993) suggested a critical Froude number to distinguish between jetting and bubbling in fluidized bed reactors. The correlation includes the effect of sparger porosity, particle density and size, fluid density and gas superficial velocity. Grace and Lim (1987) observed that increasing temperature destablizes the flow, where bubbles are more likely formed. Massimilla (1985)

qualitatively stated that the jet formation is likely achieved with coarser particles, low superficial velocity, high orifice velocity and high fluid density. It is well seen from the literature that the extent, integrity and coherence of jet flow in fluidized bed reactors is still not well understood and general experimental techniques for identifying the gas jet flow and bubble track region are still lacking. On the other hand, there is no single criterion in the literature to determine the onset of jetting conditions for downward spargers.

In this investigation, in order to obtain the bed behavior under bubbling and jetting pattern around the sparger, two jet velocities (low and high) were chosen and pressure fluctuation (PF) techniques is used to study the flow pattern around the injection point. The normalized standard deviation of PF (NSD) for these velocities is presented in Figure 4.5. The pressure probes are in stainless steel with an internal diameter of 2mm. This allows for rigidity and for a small dead zone volume. This choice subsequently eliminates signal damping and proper measurements of PF inside of the bed became possible (Chehbouni, 1993). As shown in this figure, the NSD for jetting conditions is one order of magnitude greater than that for bubbling conditions at the sparger tip. Upon obtaining the pressure profile for these velocities, pressure signals were measured for various jet velocities 3 mm below the center of the downward orifice. The signals were analyzed in terms of their mean values and the results are reported in Figure 4.6. The figure exhibits a well-defined change in the slope at around 100 m/s, which can be interpreted as the onset of jetting conditions.

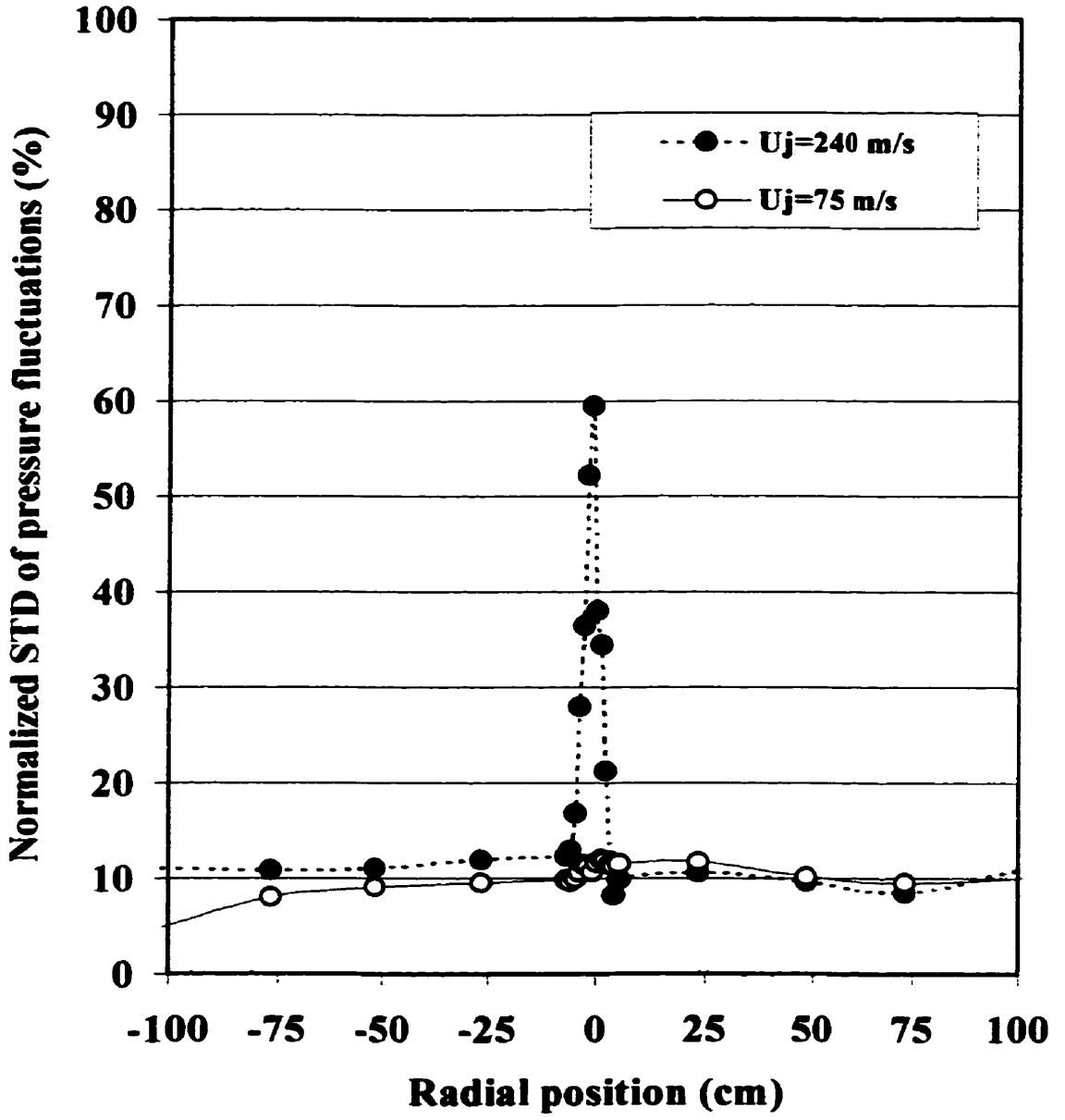

Figure 4.5 NSD of pressure fluctuations as a function of radial positions along the reactor (Single-hole sparger, z=20 cm, FCC particles, T=450 °C, U=0.25 m/s, d_{or}=2mm) for two different jet velocities.

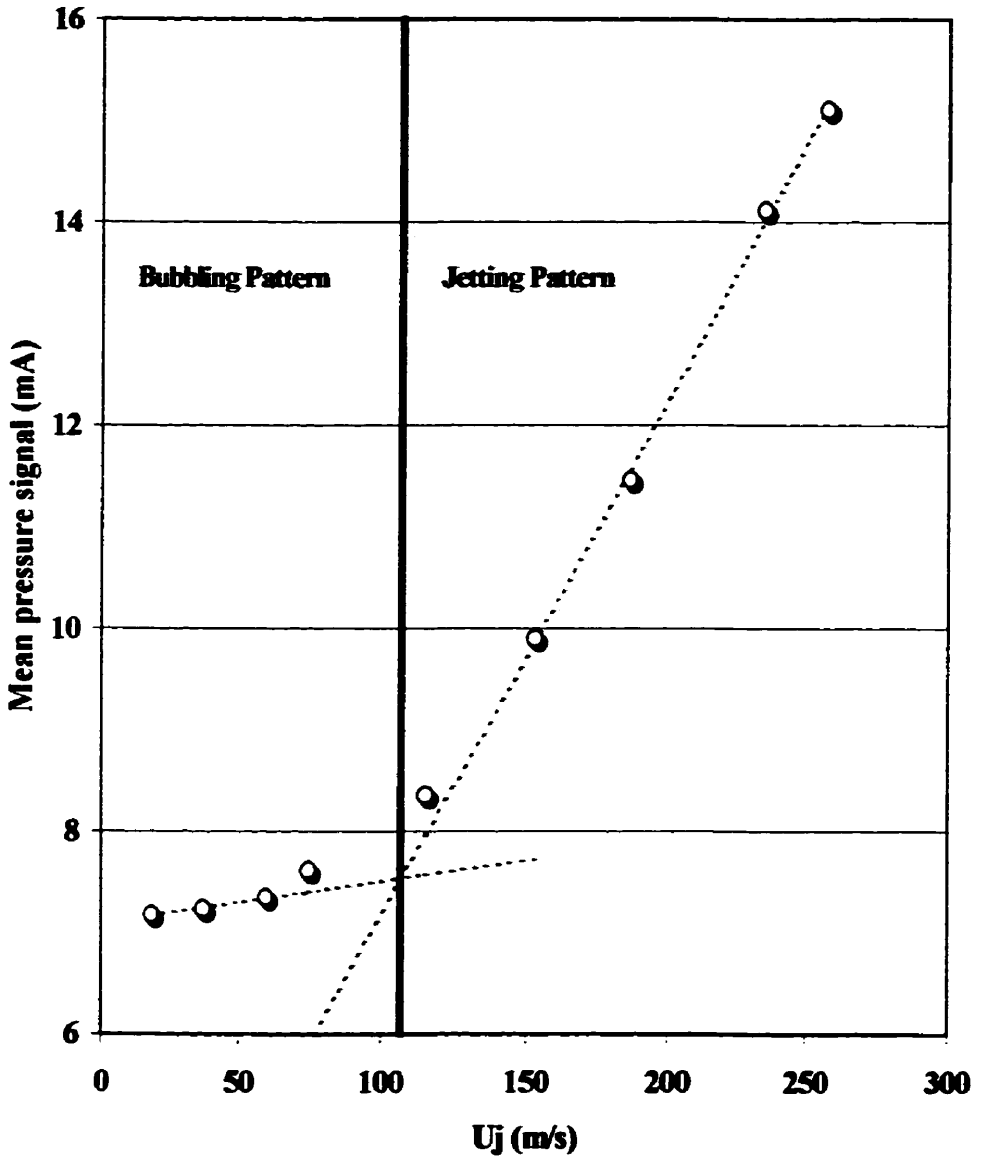

Figure 4.6 Transition from bubbling to jetting by mean pressure signal analysis (FCC particles, T=440 °C, U=0.25 m/s, d_j=2 mm and z=20 cm)

At discharge velocity 100 m/s, the mean pressure signal does not change so much. This could mean that the bubbles formed at the injection tip are very similar to those coming from the main distributor. Apparently, higher injection velocities lead to the formation of heterogeneous turbulent region around the injection point. This area is referred as the jetting zone. The experiments done with sand particles, which is presented in Figure 4.7 shows the similar trend. In Table 4.3, experimental and predicted values for permanent jet formation are presented for the condition of this study.

Table 4.3 Experimental and predicted values for permanent jet formation

Particle	d_p (μm)	Permanent jet		Reference
		Uj=30m/s	Uj=150 m/s	
Sand	543	no	yes	Experiments
		yes	yes	Grace and Lim (1987)
		yes	yes	Roach, 1993
FCC	70	no	yes	Experiments
		no	no	Grace and Lim (1987)
		transition	transition	Roach, 1993

As seen from this table, the correlations differ from the experiments. The difference can be attributed to the fact that the correlations do not consider the bed operating conditions (temperature, superficial velocity, discharge velocity and etc.). A comprehensive correlation, which is the subject of current investigation in our laboratory, is needed in

order to define the onset of jetting pattern around the sparger. Such a correlation is critical in practice if one needs to design internals and to safely operate the fluidized bed reactors.

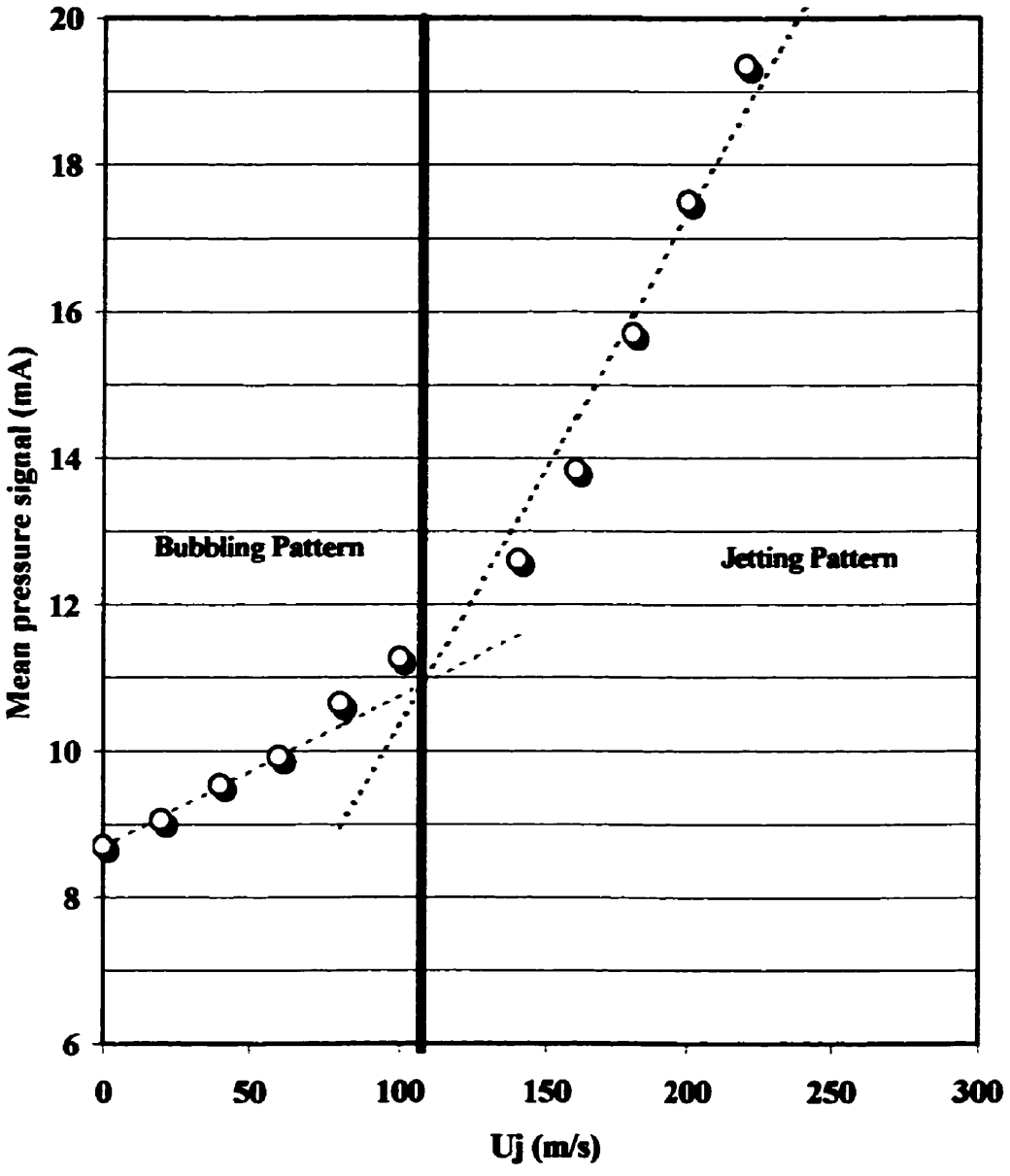

Figure 4.7 Transition from bubbling to jetting by mean pressure signal analysis (Sand particles, T=440 °C, U=0.25 m/s, d_j=2 mm and z=17 cm).

The pressure fluctuation data presented in figures 4.5 to 4.7 were obtained for U=0.25. Intuition suggests that at high gas superficial velocity, the change in bed density could have helped in jet formation. For experiments reported in the rest of this paper, the pressure fluctuation technique was used to insure the flow pattern around the sparger at the superficial gas velocities employed.

Upon determining the upper conditions for bubbling zone, the injection velocities reported in Table 4.2 were chosen and then reaction and mixing tests were being carried out for spargers shown in Figure 4.2. In the following section, the results are presented for experiments performed with FCC and sand particles followed by a critical discussion of major experimental findings for bubbling conditions.

4.7.2 Mixing and reaction studies for bubbling pattern

For commercial reactors, where gas is injected through a sparger with thousands of nozzles, the sparger is designed to operate under bubbling conditions to keep attrition very low so that control of the bed materials, which could be costly bed material, becomes possible. It is important to note that the downward jet attrition is significantly higher than that of the upward jet (Werther and Xi, 1993). This is probably due to very high interparticle collisions associated with downward jets, which cause the abrasion of the particle surfaces. For industrial scale reactors, downward discharge velocity is

usually kept around 30 m/s, which is quite lower than the jetting velocity. The experimental results show that with bubbling pattern around the sparger, the jet collapses forming gas bubbles and therefore subsequent bypassing around the sparger leads to poor mixing performances near the sparger tube.

Figure 4.8 shows radial methane concentration profile for different axial locations around a flat sparger at 400°C at U=0.8 m/s in turbulent fluidization conditions. The onset of turbulent fluidization conditions was measured to be 0.7 m/s. As shown in this figure, the sparger wall plays a vital role in mixing. High concentration of the tracer gas around the sparger wall can be attributed to the fact that the bubbles as formed at sparger tip, turn up forming a train of bubbles around the sparger wall. Under these conditions, the mixing is limited with the sparger wall. As soon as the bubbles reach the sparger level, due to an intense gas solid mixing at turbulent fluidization regime, the tracer gas is very well purged to the emulsion phase. This figure also shows the existence of three distinct mixing regions. These are *null*, *partial* and *complete* mixing zones. In the *null* mixing zone, the tracer gas is absent (just below the sparger). In the acceleration zone, where *partial* mixing exists, the axial and radial gas mixing is limited due to sparger-nozzle walls. In the fully developed mixing zone, quite uniform mixing pattern is developed (above the tracer injection level).

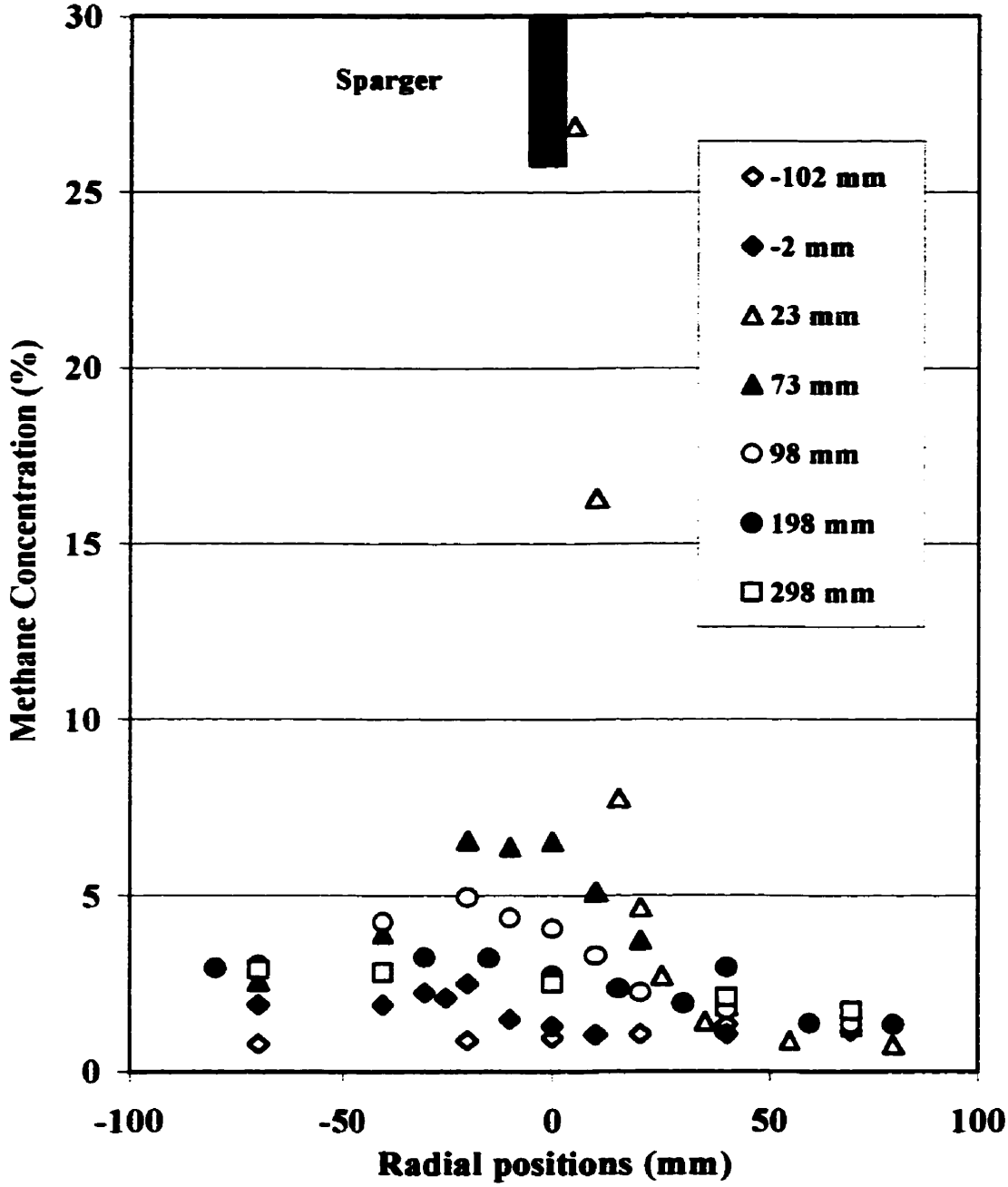

Figure 4.8 Radial methane concentration profile for different axial locations around the sparger (Flat sparger, 400 °C, U_j=37 m/s, U=0.8 m/s, FCC particles)

Figure 4.9 shows radial methane concentration profile for different axial locations around a flat sparger at 400 °C for a very dilute bed ($\varepsilon \cong 0.95$). In this figure, again, the tracer concentration is very high near the wall. Due to a very low bed density, solid particles are contributing less to the overall mixing process. As compared with Figure 4.8, the mixing is very poor in this condition. Even, above the injection level, the mixing is not improved. The results of this figure reveal the contribution of bed materials to the overall mixing process at different radial positions within the reactor.

Figure 4.10 shows the results of tracer concentration obtained during reaction at 825°C with flat sparger at discharge velocity of 56 m/s. This velocity is chosen in order to attain dynamic similarities with conditions expressed for Figure 4.8 as explained earlier. As shown in this figure, the overall results obtained for mixing studies remain valid here. Methane conversion is mostly achieved almost 100 mm above the injection level. It is important to note that for the pilot plant reactor used for reaction experiments with FCC particles, bed temperatures were measured in radial and axial positions. The variations are best within ±7 °C for axial and ±5 °C for radial positions.

In Figure 4.11, the predicted mixing length, which is estimated using the three-phase model, is reported. The centerline experimental data is also shown in this figure. It is important to note that for experimental mixing length of 150 mm above the sparger, the close to 95% of tracer gas in sparger bubble has been purged. On the other hand, the model estimates close to 95% of the mixing length. The difference between the

experimental and predicted mixing lengths can be attributed to the fact that mixing is improved in turbulent fluidization conditions, while in modelling, hydrodynamic properties were obtained based on bubbling fluidization correlations. Sotudeh (1998) was presented a simple approach to estimate the concentration of the individual phases. This analysis shows that at the points very close to the sparger, the sampling probe mostly captures the bubble from the sparger phase. At the axial positions far from the sparger, the gas is fairly dispersed in all phases. Sensitivity analysis shows that the mass transfer from the sparger bubble phase is of critical importance as compared with the mass transfer from the emulsion to the grid bubble phase.

4.7.2.1 Effect of gas superficial velocity

In Figure 4.12, CO_2 concentration profile for flat sparger at 25°C under bubbling fluidized bed conditions is presented. As seen in the figure, due to greater residence time, the gas coming from the distributor was not transporting the tracer gas. Still, the sparger wall effects are present and high CO_2 concentration was measured at z=23 mm. The result of this figure shows how important the effect of superficial gas is. In Figure 4.13, experimental axial profile is compared with the three-phase model predictions and the agreement is quite reasonable.

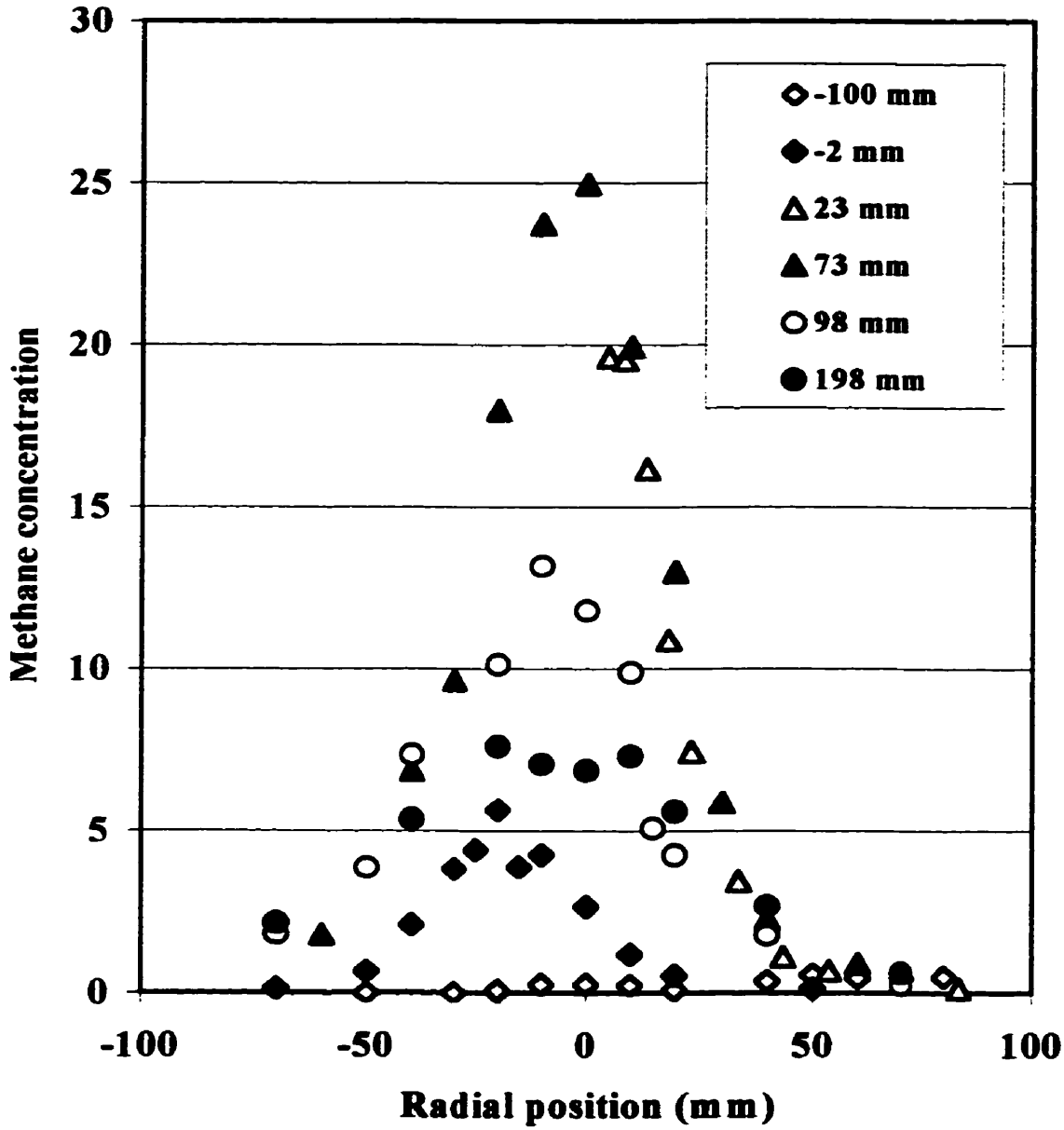

Figure 4.9 Radial methane concentration profile for a very dilute system (Flat sparger, 400 °C, Uj=37 m/s, ε=0.95, U=0.8 m/s, FCC particles).

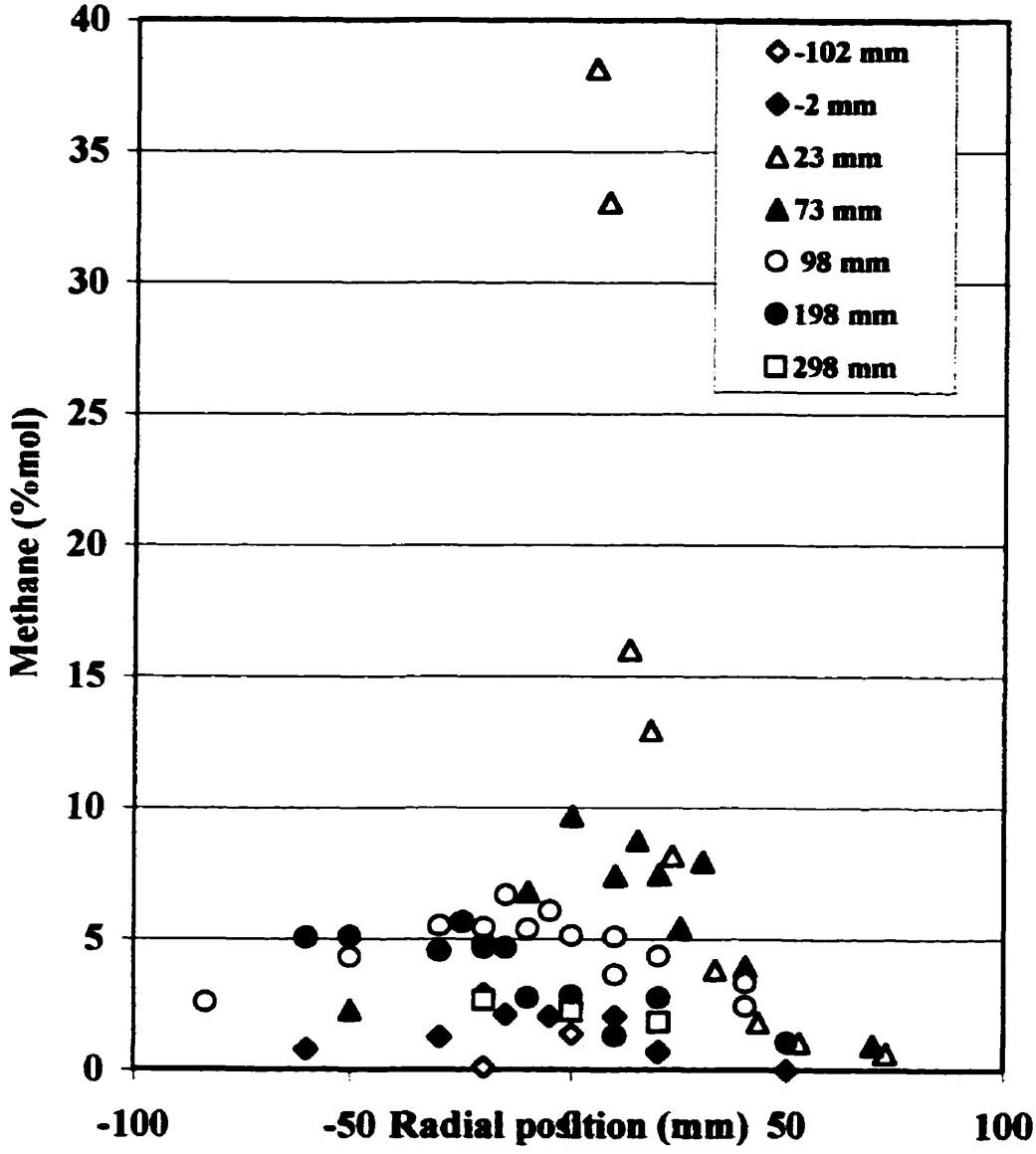

Figure 4.10 Radial methane concentration profile (Reaction, flat sparger, 825 °C, Uj=56 m/s, U=0.8 m/s, FCC particles).

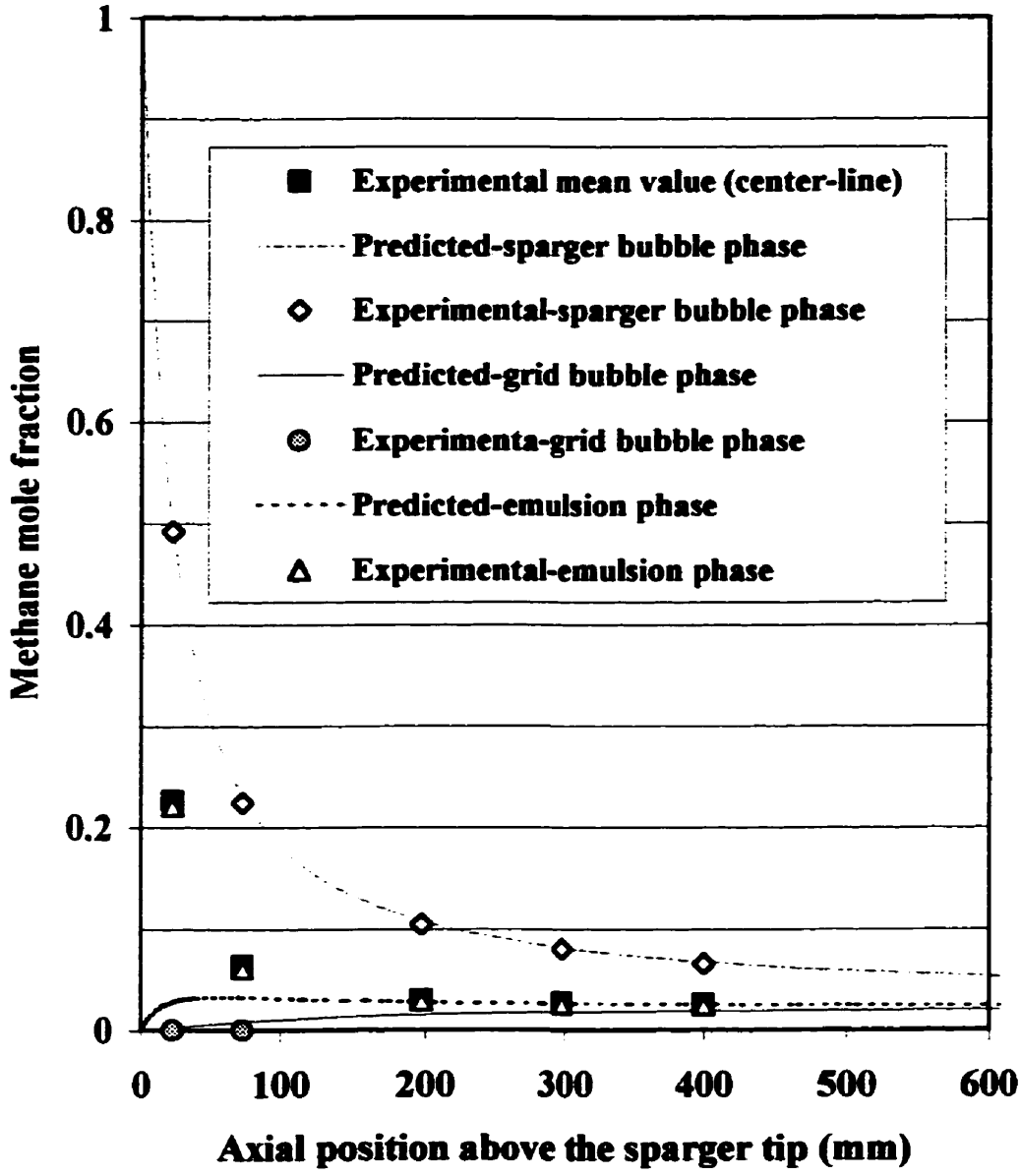

Figure 4.11 Prediction of mixing length using the three-phase model and experimental data (Flat sparger, 400 °C, Uj=37 m/s, U=0.8 m/s, FCC particles).

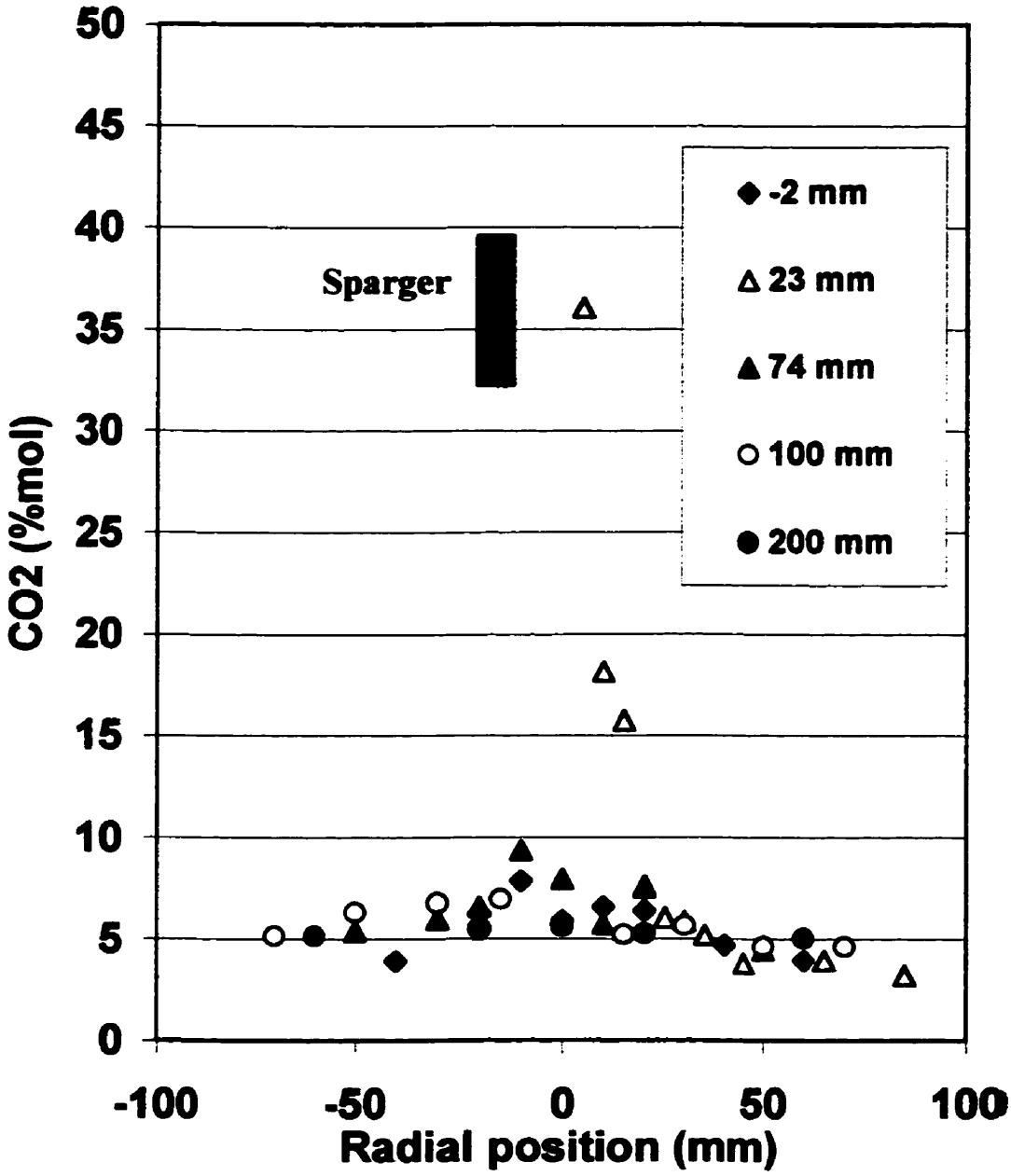

Figure 4.12 CO_2 profile (Flat sparger, 25 °C, U_j=25 m/s, FCC, U=0.2 m/s)

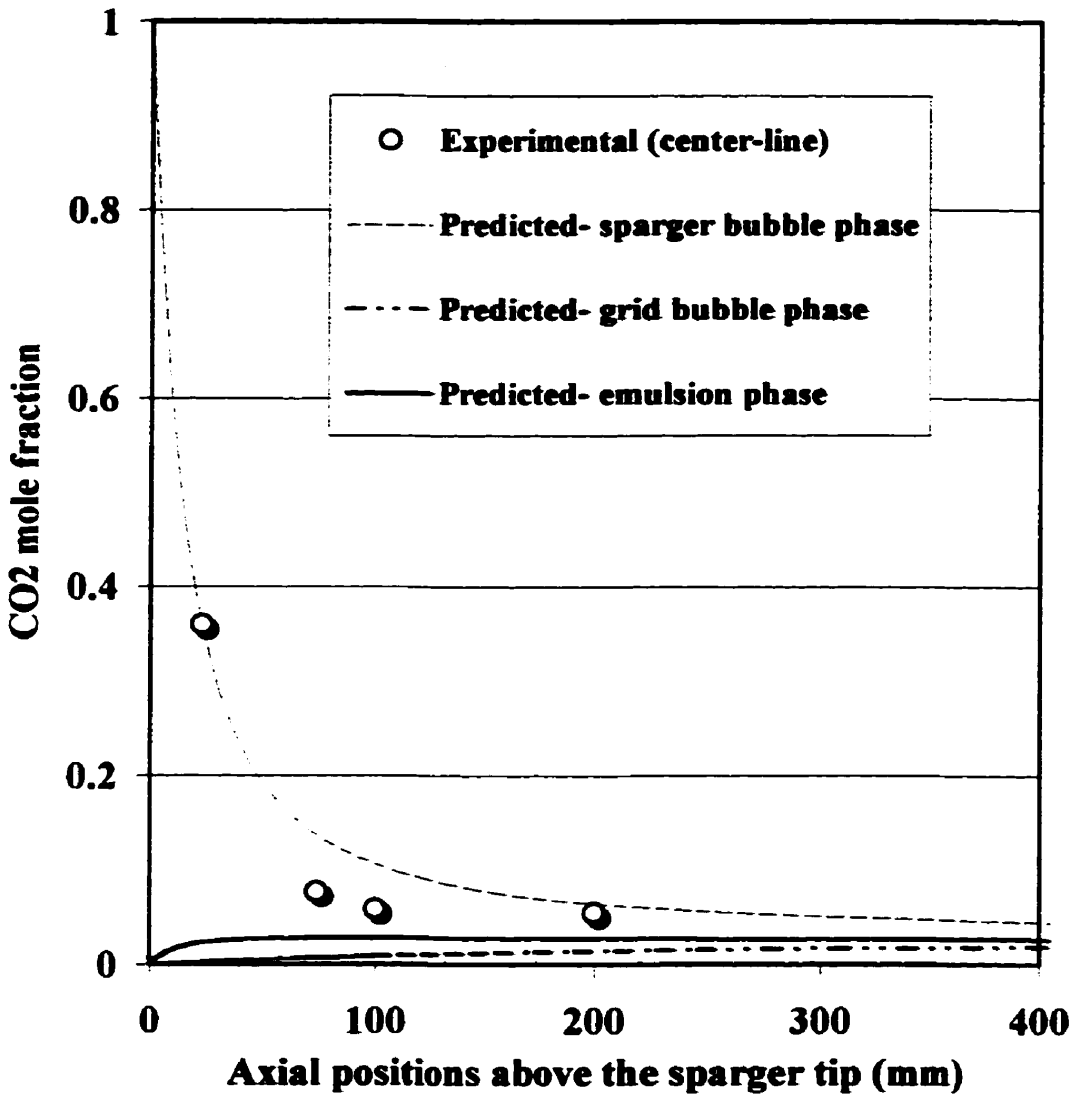

Figure 4.13 Prediction of CO_2 mixing length using the three-phase model and experimental data (Flat sparger, 25 °C, Uj=25 m/s, U=0.2 m/s, FCC particles).

4.7.2.2 Effect of sparger configuration

The effect of sparger configuration on mixing was tested for spargers shown in Figure 4.2. Figure 4.14 shows the normalized standard deviations of concentration data. The experimental results show that at -100 mm below the sparger tip, the tracer gas was not present. At 200 mm above the sparger tip, the concentration was quite uniform. At 2 mm below the sparger tip, for internal 45 ° and baffled spargers, the gas diffusion is deeper as compared to the flat sparger. This means that with the special configuration of these spargers, the gas has enough chance to be dispersed. The good performance of these spargers can be attributed to the fact that the momentum exerted by gas at the sparger tip is easily dispersed with these configurations and gas can diffuse to the bed at the injection point. In reactors with a larger number of nozzles placed in a downward sparger, this helps the efficient use of the region located below the sparger tip. However, it is important to note that before using these results in any design practice, their contributions to attrition should be examined carefully. At 23 mm above the sparger tip, the methane concentration for flat sparger is quite higher than that reported for others. This is consistent with the results obtained at 2 mm below the sparger. An important result of this study for all spargers is to confirm that the bubble rises very close to the sparger wall. The wall acts as a resistant to mixing, since it prevents the tracer gas contacting with bed (gas molecules or solid particles). It is important to note that this point is located at the middle of the downward nozzle.

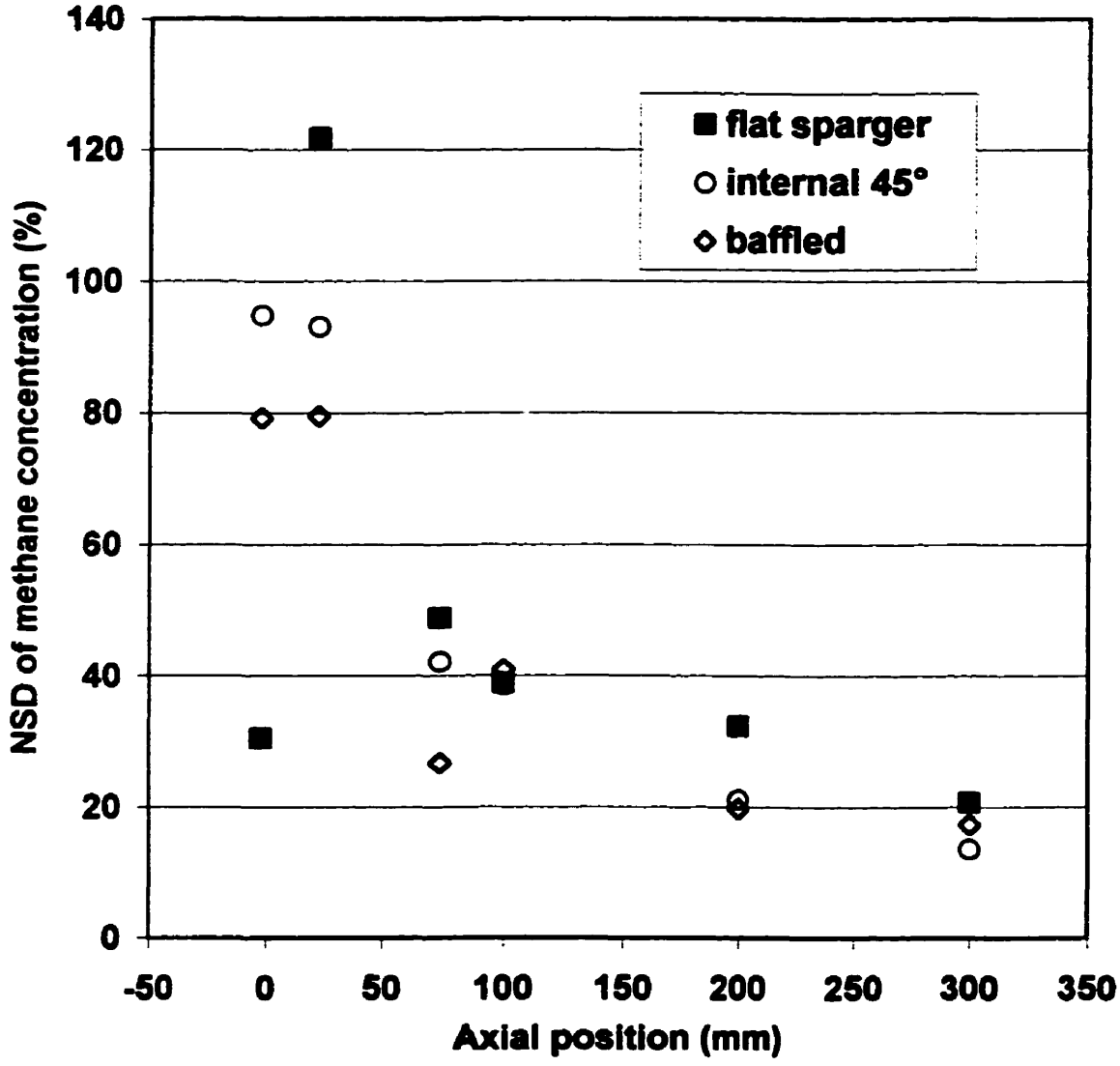

Figure 4.14 Comparison of normalized standard deviation of methane concentration profile for different spargers (FCC, 420 °C, U_j=36 m/s).

At 74 mm above the sparger tip, the concentration drops very rapidly. At these conditions, the turbulent bed hydrodynamics control the mixing process and the sparger effects are absent. It is also shown that due to sparger configuration at 74 mm, high concentration is seen for the flat sparger. Considering all results for these three spargers, we can conclude that the mixing for all spargers becomes almost complete about 100 mm above the sparger tip. Three mixing zones, as identified so far, are clearly shown in this figure again. Apparently, the spargers have different mixing behavior at sparger tip and near the sparger wall.

4.7.2.3 Effect of particle size

A series of experiments have been designed with sand particle of 543μm for methane oxidation reactions in order to examine the mixing behavior of these particles. It was found that the CO generated with sand particles (~10 %) as reported in Sotudeh-Gharebaagh et al (1998a) is greater than that of FCC particles (~2%). This can be attributed to the fact that the gas-solid mixing is very well improved with FCC particles of 70 μm rather than sand particles of 543 μm. With Sand particles, the reactions are mostly homogeneous, meaning that gas-solid mixing is less efficient, while the gas-gas contact efficiency is well enhanced. In Figure 4.15, radial methane concentration profile is reported for different axial locations around the sparger for sand particles. This figure shows that with sand particles mixing is very poor, since the high concentration of the tracer gas can be seen near the wall of the sparger and also 74-mm above the sparger tip.

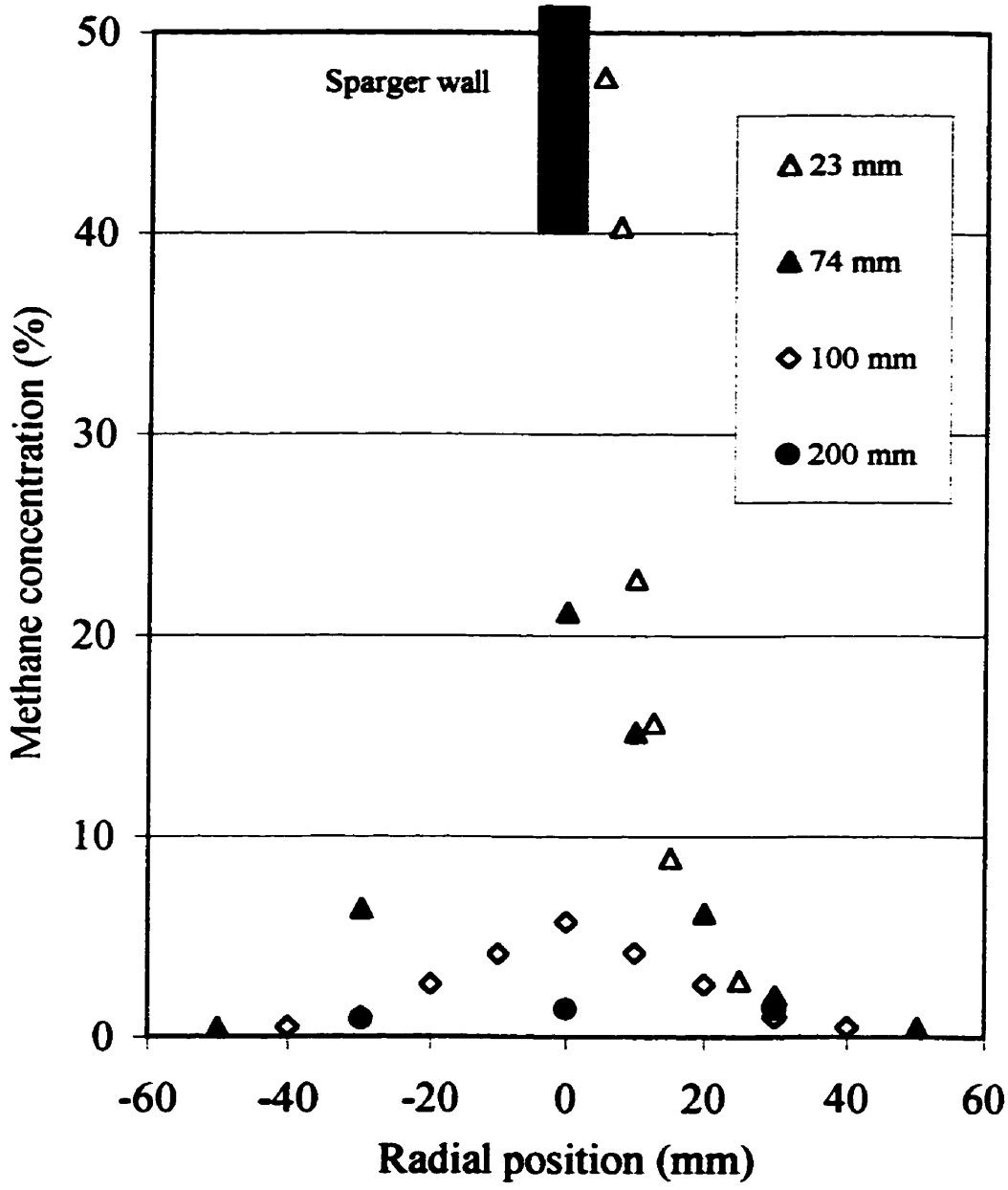

Figure 4.15 **Radial methane concentration profile for different axial locations around the sparger (Flat sparger, 400 °C, U_j=25 m/s, U=0.8 m/s, Sand particle)**

Comparison of results obtained for similar operating conditions for FCC and sand particles show that the fine particles have a definite contribution to the mixing process. Therefore, adding fine particles could significantly improve the mixing in reaction and selectivity in large industrial reactors, where one of the reactive is injected separately to the bed through the sparger.

4.8 Conclusions

The following conclusion can be directly drawn from the results of this investigation:

1. The characteristic jet length estimation shows that the behavior of flow pattern around the downward sparger is quite different from the spargers facing upward in fluidized bed reactors.

2. Depending on gas and solid properties, gas discharge devices and operating conditions, gas injection in fluidized bed reactors with a downward facing sparger leads to two distinct flow patterns: bubbling and jetting.

3. The experimental results showed that the downward gas injection under bubbling conditions forms three distinct regions in the fluidized bed reactors. These are *mull* mixing (just below the injection level), *partial* mixing (in the area adjacent to the nozzles and sparger), *complete* mixing (above the secondary injection level). In the partial mixing zone, the axial and radial gas mixing is limited due to sparger-nozzle tubes.

4. Under bubbling conditions at the sparger, bubbles, as formed on the sparger tip, turn upward, forming bubble trains along the nozzle wall. These bubbles are then purged with emulsion gas phase or coalesced with air bubbles coming from the main distributor within the bed.

5. Under bubbling conditions around the sparger, the pilot plant turbulent fluidized bed is quite isotherm in both axial and radial positions for oxidation of methane.

6. Under jet velocities less than 100 m/s, there is no permanent jet formation in the fluidized bed reactor at high temperatures for sand and FCC particles.

7. Sparger tubes limits gas-solid mixing. In fact, bubbles formed at the sparger tip have a tendency to follow the sparger wall, therefore, limiting the gas exchange between the bubble and emulsion phase.

8. Internal and baffled spargers give more mixing as compared to the flat sparger. For internal 45° sparger, diffusion at sparger tip is very high as compared to other configurations.

4.9 Acknowledgements

The authors are grateful to Mr. P. Sauriol and Mr. G. Malossi for their help with the experimental work. The Ministry of Culture and Higher Education of I.R. of IRAN is also acknowledged for making Mr. R. Sotudeh-Gharebaagh's graduate studies possible in Canada.

4.10 References

Atimtay A. and T. Cakaloz, Powder Technology, **20** pp.1-7 (1978).

Benkrid A. and S.H. Caram, AIChE J., **35**, 1328 (1989).

Blake T. R., H. Webb and P. B. Sunderland, Chem. Eng. Sci., **45**, 2, pp. 365-371 (1990).

Chehbouni, A., Ph.D. Dissertation, Ecole Polytechnique de Montreal, 1993.

Davidson, J.F., D. Harrison, "Fluidized particles", Cambridge university press, Cambridge, UK, 1963

Gonzalez, A., Ph.D. Dissertation, Ecole Polytechnique de Montreal, 1995.

Grace, J.R., and C.J. Lim, Can. J. Chem. Engng. **65**, 160, (1987).

Kunii D. and O. Levenspiel, "Fluidization Engineering", Butterworth-Heinemann, (1991).

Massimilla, L., in Fluidization,2nd edn., (Davidson & Clift Editon), Academic Press, (1985)

Merry, J.M.D., AIChE, **21**, 3, 507-510, (1975).

Roach, P.E., Int. J. Multiphase Flow, **19**, 6, 1159 (1993).

Shen Z., C. L. Briens, M. Kwauk and M. A. Bergougnou, Can. J. Chem. Eng., 68, pp. 534-540 (1990).

Sotudeh, R. Combustion of natural gas in a turbulent fluidzied bed reactor, Ph.D. Dissertation, Ecole Polytechnique de Montreal, 1998

Sotudeh-Gharebaagh R., J. Chaouki and R. Legros, "Natural gas combustion in a turbulent fluidized bed of inert particles", Submitted to Chemical Engineering Science (1998).

Wen, C.Y., M. Horio, R. Kirshnan, R. Khosravi, P. Rengarajan, Proc., Second. Pacific Chem. Eng. Cong., **1182**, (1977).

Werther J. and W. Xi, Jet Attrition of Catalyst Particles in Gas Fluidized Beds, Powder Technology,**76** , 39-46 (1993).

Yang W. C., B. Ettehadieh, T. C. Anestis, R. E. Gizzie and G. B. Haldipur, in K. Østergaard and A. Sørensen (eds), Fluidization V, Engineering Foundation, New York, pp. 95-102 (1986).

Yang, W.-C. and D. L. Keairns, Ind. Eng. Chem. Fundam., **18**, No. 4, pp. 317-320, (1979).

Yates J. G., V. Bejcek and D. J. Cheesman, in K. Østergaard and A. Sørensen (eds), Fluidization V, Engineering Foundation, New York, pp. 79-86 (1986).

CHAPTER 5: A MATHEMATICAL MODEL FOR NATURAL GAS COMBUSTION IN A TURBULENT FLUIDIZED BED OF INERT PARTICLES

Reference:

Sotudeh-Gharebaagh, R. and J. Chaouki (1998), "A Mathematical Model for Natural Gas Combustion in a Turbulent Fluidized Bed Reactor of Inert Particles", submitted to Ind. Eng. Chem. Res., December 1998.

Keywords:

modeling, mixing, turbulent fluidized bed, natural gas combustion, gas discharge.

5.1 Context[3]

In chapter II, the combustion of methane was tested in a fixed bed reactor over inert particles. A reduced reaction mechanism was also developed and tested using the fixed bed kinetic data. In chapter III, the experimental studies were reported for the combustion of natural gas in a turbulent fluidized reactor. It was shown that the mixing is critical for the success of non-premixed reactors. In chapter IV, gas mixing was characterized in turbulent fluidized bed conditions with sparger facing downward. All the information from chapter II, III and IV are used in last chapter in order to predict the behavior of turbulent fluidized bed reactors.

---

[3] This section is not included in the original manuscript. It only serves as a transition between papers for the thesis.

5.2 Abstract

A mathematical model is developed for combustion of natural gas and air fed separately into a Turbulent Fluidized Bed (TFB) reactor. The proposed model integrates bed-sparger hydrodynamics and reaction sub-models necessary to model the combustion phenomena. Hydrodynamic sub-model is derived from our experimental studies as well as using the information from the literature. While, kinetic sub-model is developed for natural gas combustion and pollutant formation using data from the combustion literature and our own experimental data. These sub-models are then combined together so that the TFB may be represented. The validity of the model was demonstrated using different sets of operating conditions for TFB reactor operated in Chemical Engineering Department at École Polytechnique de Montreal.

5.3 Introduction

Combustion of natural gas fuel in fluidized bed reactors can be considered as an economical method for heating fluidized bed reactors in some industrial processes, producing energy for industrial and residential sectors, sanitary purposes and upgrading low calorific fuels. Among the fluidized bed reactors, turbulent fluidized bed reactors (TFB) exhibits several advantages over conventional combustion. Operation of these reactors at industrial levels has confirmed many advantages that include fuel flexibility, high combustion efficiency, an improved gas-solid contact efficiency, low capital cost, potential applications in co-firing and gas-reburn. These characteristics can assure an increasing number of successful commercializations of TFB in chemical reaction engineering applications, power generation applications and co-firing as well. Although these reactors are becoming mature from these commercial applications, there are some significant uncertainties in predicting their performance in large-scale systems.

Technical knowledge about design and operation of TFB is not widely available for pilot plant and industrial units and also little has been done in the field of mathematical modeling and simulations with their validation. Sotudeh et al. (1998a) studied the feasibility of natural gas combustion in fluidized bed reactors experimentally. They showed that the turbulent fluidized bed is an excellent choice of reactor, where the non-premixed combustion can easily be achieved rather than premixed combustion. Few mathematical models have so far been reported for premixed combustion under bubbling

regime (e.g Yanata et al. 1975; van der vaart 1992; Pre et al., 1998). In these studies, in-bed pollutants (NO_x, N_2O and CO) formation and reduction were not fully integrated to the overall model. In addition, the bed is operated in bubbling fluidized bed conditions. The modeling of TFB reactors for non-premixed and premixed modes are quite modest and therefore, there is a strong need to simulate the behavior of these reactors, which are largely employed in industry.

So far, Sotudeh and Chaouki (1998) showed that depending on gas and solid properties, gas discharge devices and operating conditions, gas injection in fluidized bed reactors with a downward facing sparger leads to two distinct flow patterns; bubbling and jetting. In this work, two mathematical models are developed for bubbling-turbulent and jetting-turbulent fluidized bed reactors. Bubbling and jetting are refereed to sparger hydrodynamic and turbulent is referred to the bed hydrodynamics. A three-phase fluidization model was proposed by considering the sparger hydrodynamic in the modeling. An attempt is also made to integrate the proper reaction scheme in the overall model. This enables one to understand the formation and destruction of unwanted pollutants during the combustion process and at the reactor exit.

5.4 Experimental

The apparatus used in this study is a 200 mm I.D. and 2 m tall refractory-lined combustor, as shown in Figure 5.1. An external natural gas burner with 20 kW nominal

power located at the bottom of the bed provides the partial heat required for preheating the reactor to a desired temperature. Sand particles, which consist mainly of silica with an average particle size of 543 μm and density of 2650 kg/m^3 are used during the combustion trials. Several ports are provided along the axial position for pressure measurements, sampling and natural gas injection into the reactor. Natural gas is supplied to the reactor by an injection probe pointing downward. Two injection probes of 6.33 mm in diameter were used throughout this study; a one-hole and a thirteen-hole probe. Holes are 4.33 mm in diameter. The sparger scheme employed in the experimental studies is given in Figure 5.2. The reactor was also equipped for sampling and analysis of reaction products taken from the various ports and at the reactor outlet. Type-K thermocouples were also placed along the reactor centerline to monitor temperature profiles. An initial bed height of 2.5D (about 20 kg sand particles) was used in all experiments. The detail of the experimental work was reported elsewhere (Sotudeh et al. 1998a). The experimental data regarding the discharge modes leading to different flow pattern around the sparger is given by Sotudeh et al (1998b).

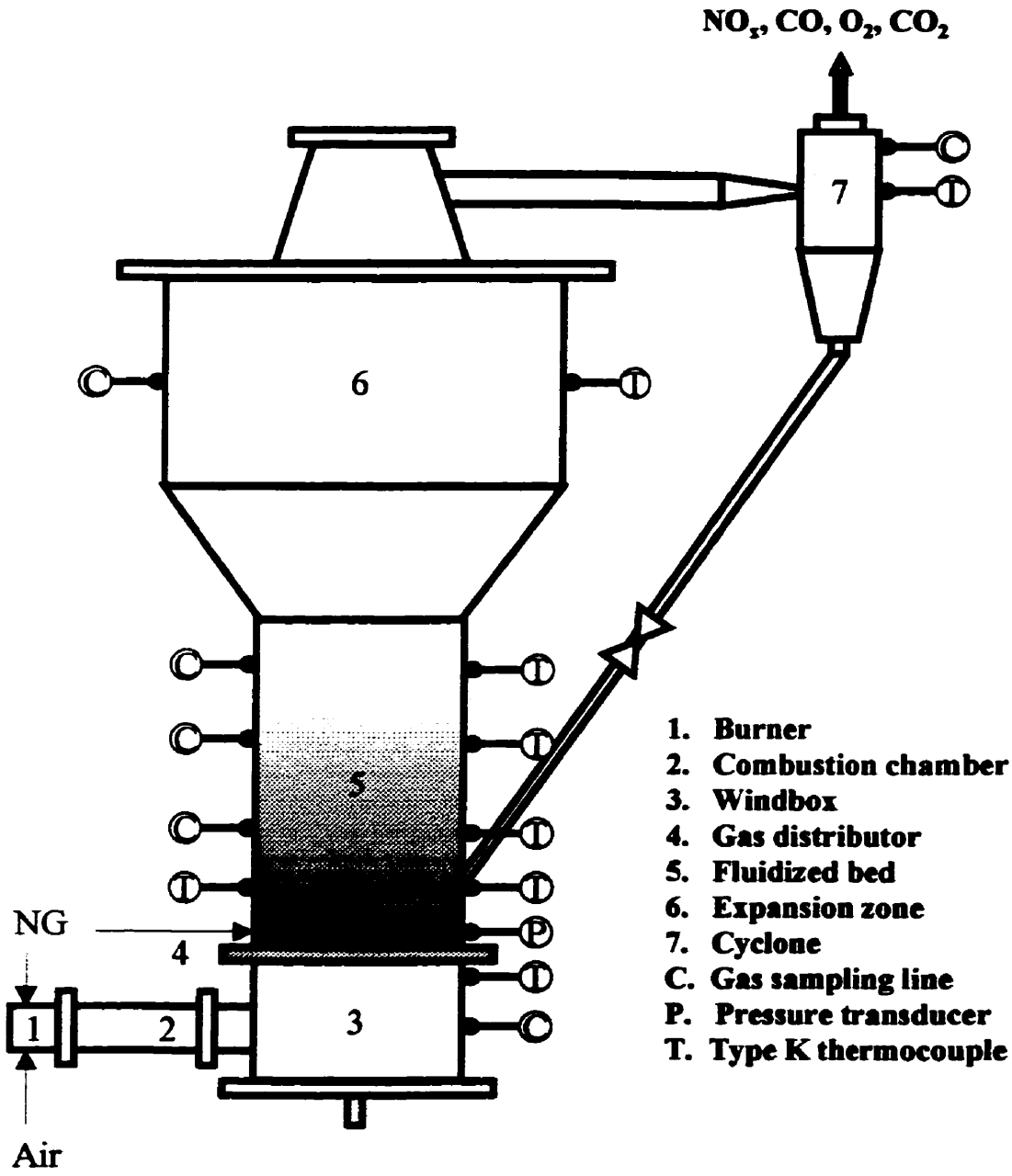

Figure 5.1 Schematic of pilot turbulent fluidized bed reactor

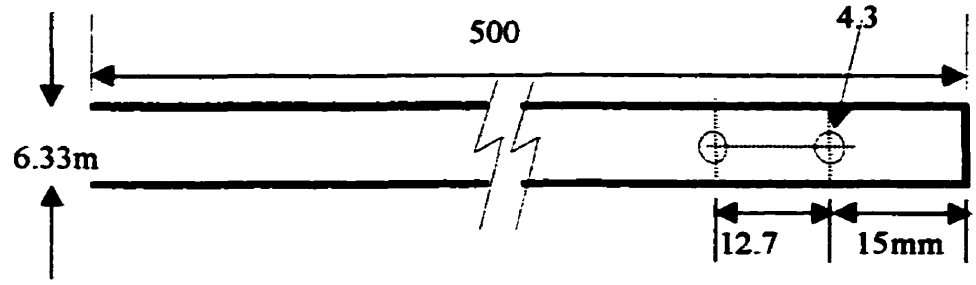

No. of holes=13

Figure 5.2 Schematic diagram of gas injector

Table 5.1 shows the experimental plan for the combustion of gaseous fuel in the pilot plant turbulent fluidized bed reactor.

Table 5.1 Experimental plan for non-premixed combustion in TFB reactors

Run	T (°C)	U (m/s)	U_j (m/s)	Sparger holes	Sparger hydrodynamics
1	850	1.5	15	13	Bubbling
2	900	1.5	15	13	Bubbling
3	950	1.5	15	13	Bubbling
4	900	1.5	30	1	Bubbling
5	900	1.5	120	1	Jetting

5.5 Reactor Model

The non-premixed reaction in turbulent fluidized bed reactors is mostly employed in industrial scale reactors. Despite their industrial application, no experimental data and modeling results are reported in the literature for small or large-scale units. Therefore, it is not possible to obtain the experimental data from the literature and one should generate his own data for building a realistic mathematical model to describe the behavior of these reactors. In this study, mathematical models are developed for bubbling-turbulent and jetting-turbulent fluidized bed reactors. Two mathematical models are presented here with following gross characteristics:

- Three phases air-bubble, natural gas bubble and emulsion phase with constant bubble size for bubbling-turbulent fluidized bed.

- Two step combustion process, conversion of CH_4 to CO bubbles and then three phases air-bubble, CO bubbles and emulsion phase with constant bubble size for jetting-turbulent fluidized bed reactor.

- Common to both mathematical models is the assumption of plug flow for all phases (van der vaart, 1992).

Additional assumptions common to the models are:

- The non-premixed fluidized bed is quite isothermal. For pilot plant reactor used throughout the experiments, bed temperatures were measured in radial and axial

positions. The variations are best within ±8 °C for bubbling and jetting experiments. Latter, in this paper, a jet suction model in developed in order to verify the jet isothermicity in jetting-turbulent fluidization conditions.

- The distribution of gases between the bubble and the emulsion phase is governed by the two-phase theory of fluidization.

- The bubbles are spherical.

- Bubbles in pilot plant reactors experience continual growth due to coalescence throughout the reactor. Clearly, the use of an average bubble size can only be the first approximation for these reactors. If these reactors were to be used to study the chemical reactions, this distinction would be very important. The model presented here takes bubble growth into account in the context of an extremely exothermic reaction.

In order to model the behavior of TFB reactor, the kinetic sub-model should be coupled with the hydrodynamic sub-model. In the following section, these sub-models are presented in detail.

5.5.1 Reaction sub-model

A global reaction rate expression is inadequate to describe the natural gas combustion process since it prevents the comparison of the experimental CO and NO_x profiles with the models. Natural gas combustion has been extensively studied in the literature and mechanistic reaction networks are available comprised of large numbers of elementary reactions. Efforts have also been devoted to develop the reduced mechanism. So far, Sotudeh et al (1998b) reported a modified reaction scheme by taking into account the inhibition process encountered due to presence of inert particles in the bed. In this study, an attempt is made to employ this modified reaction scheme within the reactor models described below. The reduced reaction scheme used is given in Table 5.2.

Table 5.2 Reduced reaction mechanism

i	Reactions Considered	k_i (cm-mol-s)	n_i	$E_i \times 10^{-3}$
1	$O+HO_2+M_4<=>OH+O_2+M_4$	2.00E+14	0	217.28
2	$O+H_2O_2+ M_4<=>OH+HO_2+ M_4$	9.63E+06	2.0	16.74
3	$O+CH_3<=>H+CH_2O$	8.43E+13	0	0
4	$O+CH_4<=>OH+CH_3$	1.02E+09	1.5	35.98
5	$O+CO+M_1<=>CO_2+M_1$	6.02E+14	0	12.55
6	$O+CH_2O+ M_4<=>OH+HCO+ M_4$	3.90E+13	0	14.81
7	$O_2+CH_2O<=>HO_2+HCO$	1.00E+14	0	167.41
8	$H+O_2+M2<=>HO_2+M_2$	2.80E+18	-.9	0
9	$H+2O_2<=>HO_2+O_2$	3.00E+20	-1.7	0
10	$H+O_2+H_2O<=>HO_2+H_2O$	9.38E+18	-.8	0
11	$H+O_2+N_2<=>HO_2+N_2$	3.75E+20	-1.7	0
12	$H+O_2+ M_4<=>O+OH+ M_4$	8.30E+13	0	60.31
13	$H+HO_2<=>O_2+H_2$	2.80E+13	0	4.47
14	$H+HO_2+ M_4<=>2OH + M_4$	1.34E+14	0	2.66
15	$H+H_2O_2<=>HO_2+H_2$	1.21E+07	2.0	21.76
16	$H+H_2O_2+ M_4<=>OH+H_2O+ M_4$	1.00E+13	0	15.1
17	$H+CH_4<=>CH_3+H_2$	6.60E+08	1.6	45.36
18	$H+CH_2O<=>HCO+H_2$	2.30E+10	1.1	13.7
19	$OH+H_2<=>H+H_2O$	2.16E+08	1.5	14.35
20	$2OH<=>O+H_2O$	3.57E+04	2.4	-8.83

Table 5.2 (continued)

21	$OH+HO_2<=>O_2+H_2O$	2.90E+13	0	-2.1
22	$OH+CH_4<=>CH_3+H_2O$	1.00E+08	1.6	13.05
23	$OH+CO<=>H+CO_2$	4.76E+07	1.2	0.29
24	$OH+CH_2O<=>HCO+H_2O$	3.43E+09	1.2	-1.87
25	$HO_2+CH_3<=>O_2+CH_4$	1.00E+12	0	0
26	$HO_2+CH_3+ M_4<=>OH+CH_3O+ M_4$	2.00E+13	0	0
27	$HO_2+CO+ M_4<=>OH+CO_2+ M_4$	1.50E+14	0	98.75
28	$HO_2+CH_2O<=>HCO+H_2O_2$	1.00E+12	0	33.5
29	$CH_3+O2+ M4<=>O+CH_3O+ M_4$	2.68E+13	0	120.5
30	$CH_3+O2<=>OH+CH_2O$	3.60E+10	0	37.4
31	$CH_3+H2O2<=>HO_2+CH_4$	2.45E+04	2.5	21.67
32	$CH_3+CH2O<=>HCO+CH_4$	3.32E+03	2.8	24.5
33	$CH_3+CH3OH<=>CH_3O+CH_4$	1.00E+07	1.5	41.59
34	$HCO+H_2O+ M_4<=>H+CO+H_2O+ M_4$	2.24E+18	-1.0	71.13
35	$HCO+M_3<=>H+CO+M_3$	1.87E+17	-1.0	71.13
36	$HCO+O_2<=>HO_2+CO$	7.60E+12	0	1.67
37	$CH_3O+O_2<=>HO_2+CH_2O$	4.28E-13	7.6	

5.5.2 Hydrodynamic sub-model

As stated earlier, two models are presented in this article. These are bubbling-turbulent and jetting-turbulent fluidized bed models. For both cases, a three-phase model is proposed considering that the bed consists of three distinct phases, grid-bubble phase, sparger-bubble phase and emulsion phase. The expressions needed to describe the bubble properties, expanded bed height, phase distribution are presented in Table 5.3. It is important to note that since the gas superficial velocity chosen in this study is very close to the onset of the turbulent fluidization conditions, the use of expressions from the bubbling fluidized bed conditions remain valid (Gonzalez, 1995).

Table 5.3 Expressions used to calculate the fluidized bed hydrodynamic properties

$$U_{mf} = \frac{\mu}{\rho_g d_p}\left[\sqrt{27.2^2 + 0.0408Ar} - 27.2\right] \text{(Grace, 1982)} \qquad (5.1)$$

$$Ar = \frac{d_p^{\,3}\rho_g(\rho_s - \rho_g)g}{\mu^2} \qquad (5.2)$$

$$d_b = \frac{0.54(U - U_{mf})^{0.4}\left(z + 4\sqrt{5.52\times10^{-5}}\right)^{0.8}}{g^{0.2}} \quad \text{(Darton et al., 1977)} \qquad (5.3)$$

$$U_{abs} = U - U_{mf} + 0.711\sqrt{gd_b} \quad \text{(Davidson and Harrison, 1963)} \qquad (5.4)$$

$$\frac{H - H_{mf}}{U - U_{mf}} = \int_0^{H_{mf}} \frac{dz}{U_{abs} - (U - U_{mf})} \quad \text{(Davidson and Harrison, 1963)} \qquad (5.5)$$

$$\delta = \frac{U - U_{mf}}{U_{abs}} \qquad \text{(Davidson and Harrison, 1963)} \qquad (5.6)$$

5.5.2.1 Bubbling-turbulent fluidized bed reactor model

Experimental studies conducted so far in our laboratory show that the bubbles tend to retain their identity as they are purged on their way through the bed under bubbling flow pattern around the sparger. In Figure 5.3, the idealized three-phase model is shown. The main feature of this model is the fact that bubbles from the sparger and main distributor form separate lean phases, respectively. Based on our experimental finding and model description, the proper model is built and the resulting differential equations for individual phases are given below:

Material balance of the specie *k* in the grid bubble phase is:

$$\frac{dC_{kg}}{dz} = \frac{R_{kg} - K_{be}(C_{kg} - C_{ke})}{U_{abs}} \qquad (5.7)$$

Material balance of the species *k* in the sparger bubble phase is:

$$\frac{dC_{ks}}{dz} = \frac{R_{ks} - K_{be}(C_{ks} - C_{ke})}{U_{abs}} \qquad (5.8)$$

Material balance of the species k in the emulsion phase is:

$$\frac{dC_{ke}}{dz} = \frac{1}{(1-\delta)U_{abs}}\left[\delta_g K_{be}(C_{kg} - C_{ke}) + \delta_s K_{be}(C_{ks} - C_{ke})\right] + \frac{\varepsilon_{mf} R_{ke}}{U} \qquad (5.9)$$

The interphase mass transfer coefficients from the bubble phases to the emulsion phase, which are different for sparger grid bubbles due to bubble size and physical properties, are derived from Davidson and Harrison (1963).

$$K_{be} = 4.5\left(\frac{U_{mf}}{d_b}\right) + 5.85\left(\frac{D_e^{0.5} g^{0.25}}{d_b^{1.25}}\right) \qquad (5.10)$$

The net reaction rate for species k is obtained based on the following expression considering all chemical reactions involved in the reaction scheme.

$$R_k = \sum_{i=i}^{I} (\nu''_{ki} - \nu'_{ki})\, r_i \qquad (k = 1,2,3,\ldots,K) \qquad (5.11)$$

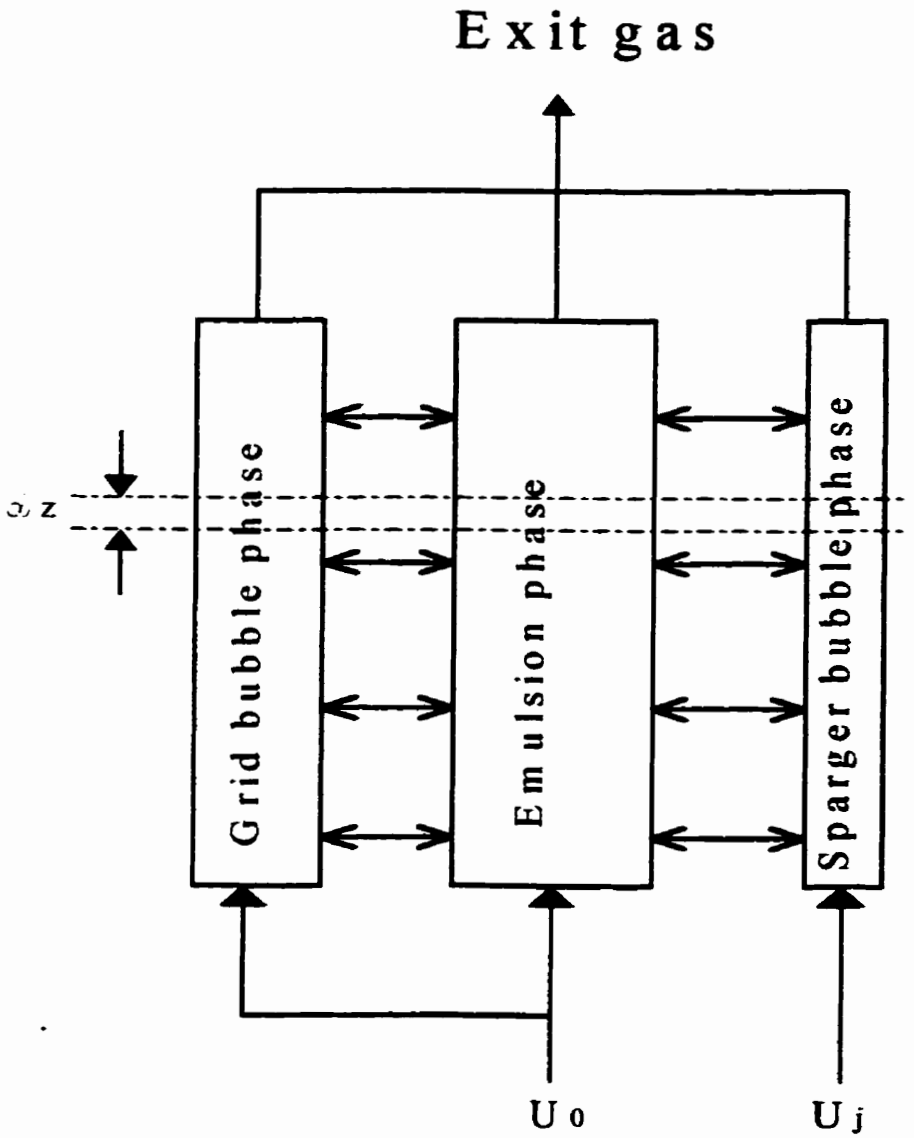

Figure 5.3 Features of a three-phase bubbling-turbulent fluidized bed model

5.5.2.2 Jetting-turbulent fluidized bed reactor model

Experimental studies reported by Sotudeh and Chaouki (1998) show that at quite high sparger velocity there is a creation of highly turbulent area at the injection point. This area, so called the jetting area, is the main characteristics of the jetting-turbulent fluidized bed reactors. Upon injecting the reactive gas into the sparger, the gas is only supplied to a limited cross section of the bed. At the jetting zone, the mixing is very well improved and therefore, the homogeneous combustion can easily be achieved. This means that all methane injected in this area is converted to CO due to oxygen shortage and the role of the jetting zone is to provide CO rich bubbles. These bubbles then travel upward in order to be purged along the reactor. Therefore, the jetting zone can be modeled with the three-phase model as described in the bubbling-turbulent section, with the condition that the methane is completely absent and CO bubbles should be considered as the sparger bubble phase. Obviously, the differential equations remain the same with the corresponding boundary conditions. These coupled differential equations are solved corresponding to their respective boundary conditions and therefore, the concentration profiles are predicted. In the following section, the calculated concentration profiles, which are compared to the experimental targets, are presented and discussed.

5.5.2.2.1 Modeling of jet suction

Fluidized bed gas, mainly air, is being sucked into a sparger jet due to relative vacuum created by the jet. Upon injecting the fluid into the bed, part of the sparger jet momentum is lost in presence of particles (Barghi, 1997). This deficit may be balanced with the momentum added by entrained gas. Assuming geometry for jet with no particles, axial momentum of the jet could be constant since no external force is involved. The momentum balance equation would be:

$$\rho_g u_j^2 A_j = \rho_{ff} \bar{u}_x^2 A_x \tag{5.12}$$

There is no correlation in the literature for defining the jet geometry (jet half angle or diameter) and the characteristic jet length for downward spargers. Directly applying the existing correlations developed for vertically upward jets overestimates the jet geometry. But in lack of the appropriate correlations, these could give a rough idea about the jet geometry. Merry (1975) proposed the following correlations in order to calculate the jet half angle θ and the characteristic jet penetration length:

$$\theta = 10.4\left[\frac{\rho d_p}{\rho_{gf} d_j}\right]^{0.3} \tag{5.13}$$

$$\frac{L_j}{d_j} = 5.25\left(\frac{\rho_{gf} d_j}{\rho d_p}\right)^{0.3}\left(1.3\left(\frac{U_j^2}{g d_p}\right)^{0.2} - 1\right) \tag{5.14}$$

Knowing the jet geometry, the jet cross-sectional area (A_x) is defined and the corresponding average velocity can be calculated:

$$\bar{u}_{jx} = \left(\frac{d_j}{d_j + 2x\tan\theta} \right) u_j \tag{5.15}$$

If one neglects the frictions of gas and entrained solids into the jet, the axial pressure profile in the jet-side, which is responsible for gas entraiment into the jet, can be:

$$P_{jx} = P_j + \frac{\bar{\rho}_{fj}}{2}\left[u^2_j - U^2_{jx} \right] \tag{5.16}$$

The pressure profile in the bed-side can be estimated from:

$$P_{bx} = P_0 + (1-\varepsilon)\rho g(h_0 + x) \tag{5.17}$$

For the purpose of modeling, we neglect the frictions caused by gas and solid for radial locations between the jet external surface and a point far from the external surface of the jet in the bed, where the radial velocity is assumed to be zero. Under this condition, the radial gas velocity created by relative vacuum between jet-side and bed-side would be:

$$U_r = \sqrt{\frac{2(P_{bx} - P_{jx})}{\rho_g}} \tag{5.18}$$

The induced gas flow rate to the jet can be found by numerical integration of this velocity over external jet surface:

$$q_{bj} = \int_0^{L_j} \left(\pi(d_j + 2x\tan\theta)\cos\theta\right) U_r dx \qquad (5.19)$$

5.6 Results And Discussions

In this section, experimental combustion data obtained in the pilot plant fluidized bed reactor is compared with concentration profiles predicted by the reduced mechanisms and hydrodynamic model for a variety of operating conditions.

Figure 5.4 gives an example of methane concentration profile obtained for the combustion of natural gas at 985°C under turbulent fluidization conditions. The combustion length, which can be defined as the length required to achieve almost complete combustion, can be characterized by this figure. As seen in this figure, methane and O_2 should first come into contact before the reaction starts. This means that the mixing controls the combustion process and that is why this should be carefully characterized.

In Figure 5.5, the combustion of methane is presented for two temperatures. The comparison between the model and the experimental data are quite satisfactory. One should also note that the performance of the three-phase model proposed here could be

improved by including a coalescence model between unlike air and fuel bubbles. Upon reaching those unlike bubble together, they coalesce together and they break-up. This could certainly have a certain effect on the prediction of the reactor performance.

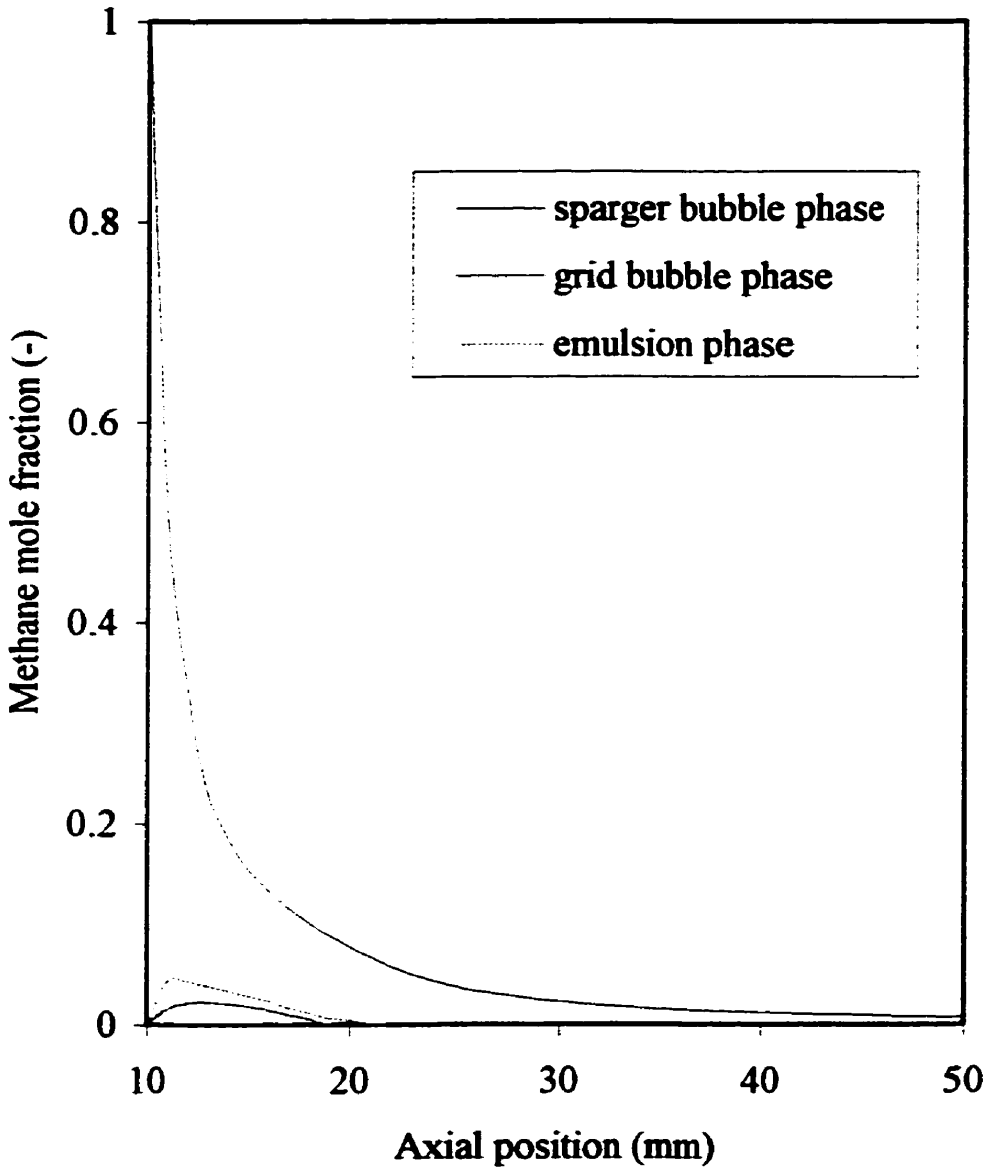

Figure 5.4 **Methane mole fraction in different phases predicted by the three phase model for T=985 °C, U=1.5 m/s, full sparger, sand particles.**

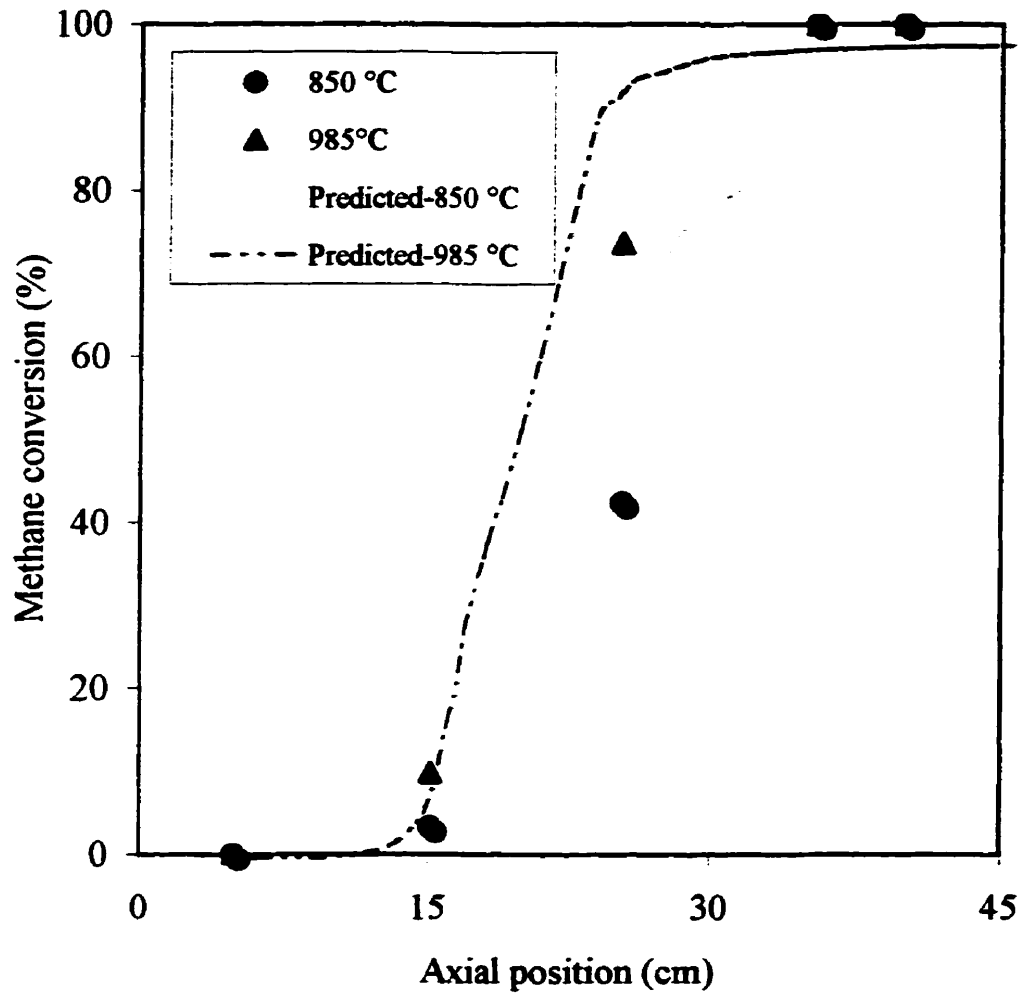

Figure 5.5 Methane conversion in the turbulent regime at various temperatures with 13 holes sparger placed at the reactor base (U=1.5 m/s).

In Figure 5.6, the CO profile is presented inside the bed for single sparger of 4.33 mm in diameter. It is seen that CO level undergoes a maximum and because of good mixing, CO emission levels measured at the bed exit is quite small. Both modelling and experiments confirmed the CO behavior inside of the bed. This also suggests that the methane combustion process inside the bed is a two step process through the sequence of elementary reactions. Initially methane converts to CO and as soon as this process becomes complete, the second step, which consists of CO combustion process, takes place. This combustion model was also confirmed by Sotudeh et al. (1998b) in fixed bed studies undertaken to evaluate the combustion behavior of inert particles. Comparing the experimental data with model prediction suggests that the concentration determined by the probe is very close to the CO concentration in the bubble phase. This can be attributed to the fact that the probes are located at the centreline of the reactor, where mostly the sparger bubbles have been captured by the sampling probe. Considering this explanation, the figure shows reasonable agreement between the experiments and modelling respecting all complexities involved in prediction of CO combustion behavior inside of the fluidized bed reactors. It is also worth mentioning that the predicted concentration reported in the figure is related to the concentration in the bubble phase. However, the results are not surprising. Since the amount of methane injected into the bed is quite small, the mean value of CO level inside of the bed in not significant and therefore, it has not been represented in the figure.

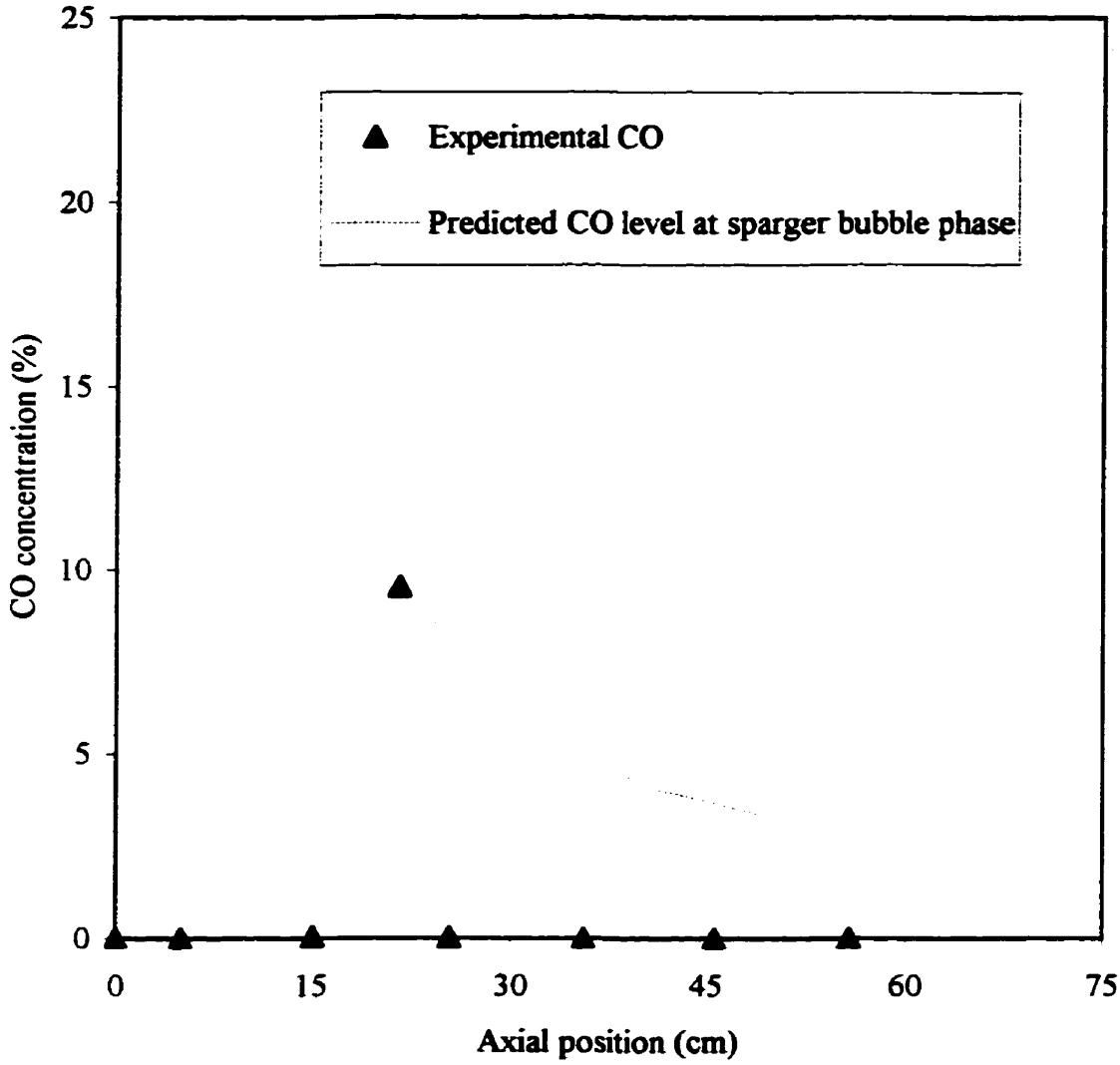

Figure 5.6 **Axial CO profile under bubbling-turbulent fluidized bed conditions for non-premixed combustion with one-hole sparger placed at z=17 cm, T=900 °C and U_j=30 m/s.**

In figure 5.7, by injecting a very high superficial velocity related to the jetting conditions around the sparger, the combustion behavior of jetting-turbulent fluidized bed reactor is studied. The results are encouraging, since no methane concentration was measured inside of the bed under this conditions. Therefore, it can be seen from the experimental data that the combustion process occurs in two steps. At the first step, all CH_4 injected into the bed with high jetting velocity is instantaneously converted to CO. This can be attributed to the fact that a highly turbulent area is formed at the injection point, where excellent contact can be achieved between CH_4 injected from the sparger and O_2 coming from the main distributor. At the jetting zone, due to less solid concentration as compared to the emulsion phase, homogeneous combustion takes place. Due to oxygen shortage, the combustion product is mainly CO. It can also be seen from the figure that CO oxidation becomes complete before reaching the bed surface, if the temperature is sufficiently high. The completion of the reaction completeness can be related to the fact that in turbulent fluidized beds, mixing is improved. In this figure, the experimental data is compared with model prediction for sparger bubble and mean value in the bed. It can be seen from the figure that the sampling probe mostly captures the CO bubble near the injection point and far from the injection point, the samples were taken from all phases. This can be attributed to the location of the sampling probe, which was in the centerline of the reactor.

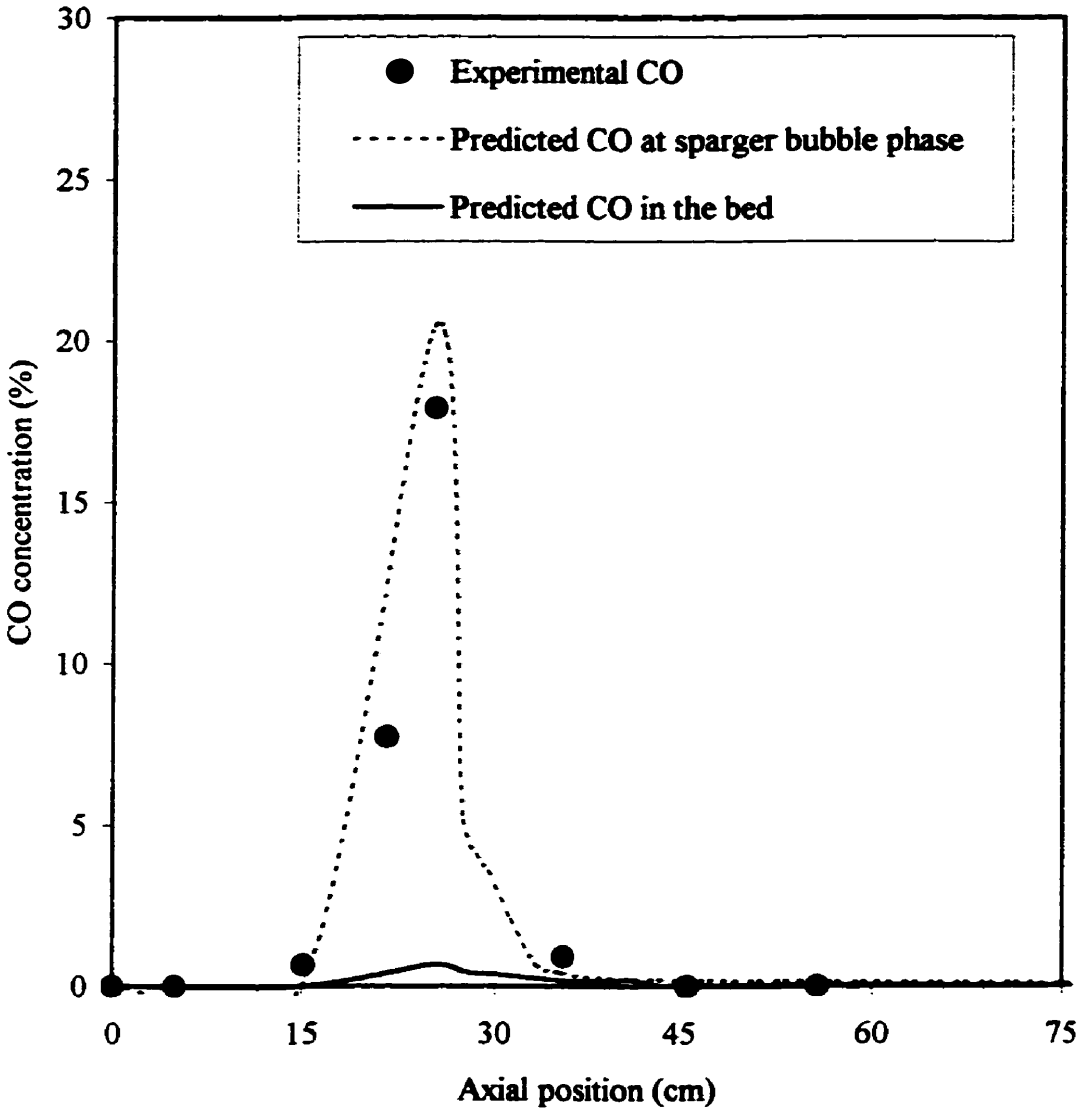

Figure 5.7 Axial CO profile under bubbling-turbulent fluidized bed conditions for non-premixed combustion with one-hole sparger placed at z=17 cm (T=900 °C).

In this paper, a model was proposed to estimate the induced gas flow caused by jet suction. The results show that the amount of air sucked into the jet is significantly high (7.75 times of the gas injected by sparger). Such high amount of air when enters into the jet leads to a very short mean residence time (in the order of 2 ms). The jet was then simulated considering an adiabatic CSTR reactor and the temperature increase was predicted to be less than 2 °C. It can therefore be concluded that the jetting zone is isothermal. This theoretical finding is in excellent agreement with our temperature measurements. This is also consistent with theoretical and experimental works reported in the literature (Bi and Kojima, 1996), where gas phase in jetting area was isothermal.

Considering these explanations, for jetting-turbulent fluidization condition, the comparison between the experimental data and modelling results are satisfactory. The jetting-turbulent fluidized bed reactor could be a new generation of turbulent fluidized bed reactors suitable for hazardous waste treatments since it could be possible to create non-isothermal beds if one chooses proper single step highly exothermic reaction. For the case of natural gas combustion, since the methane combustion is a two-step process, before any energy release due to combustion the mixing should be promoted, provided the residence time is sufficient.

In Figure 5.8, normalized experimental NO_x concentration emissions are compared with the thermal model predictions and under equilibrium conditions. As seen from this figure, the thermal NOx model underestimates the NO_x level, while the NOx predicted by

equilibrium conditions is quite high. The difference between thermal model predictions and experiments can be attributed to the small traces of fuel nitrogen coming from the natural gas. Simple calculations show that the amount of fuel nitrogen may vary between 0.05% and 0.03% for the experimental studies reported in this paper.

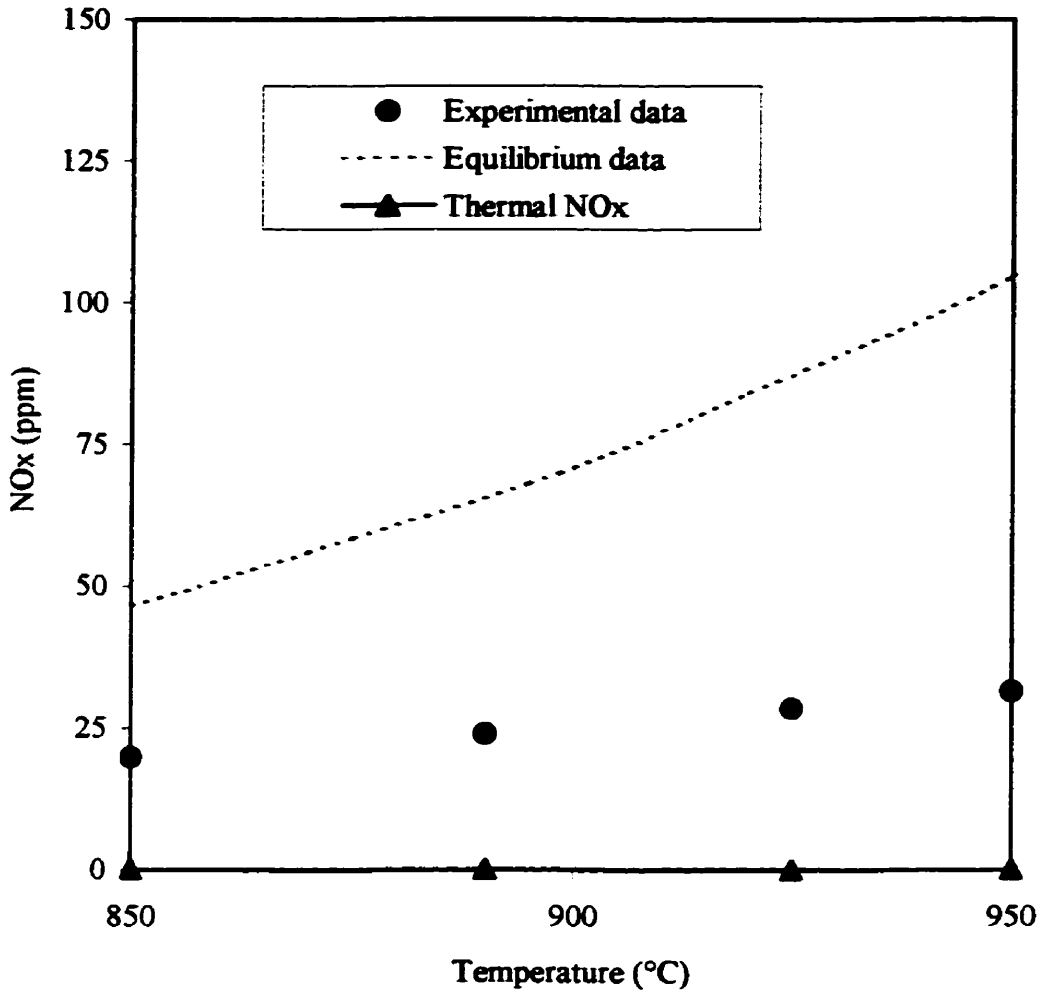

Figure 5.8 Predicted and Normalized NO_x concentration at the reactor exit for non-premixed combustion with full sparger placed at the reactor base.

5.7 Conclusion

In this study, models for non-premixed bubbling-turbulent and jetting-turbulent fluidized beds are proposed and reasonable agreement with experimental data was obtained. It is also shown that a detailed kinetic scheme, that takes into account the formation and destruction of pollutant and intermediate species, which are necessary to predict the concentration profiles. The model to represent the jetting and bubbling region around the injection point is compatible with detailed experimental observations reported so far in our laboratory. The model proposed in this work may also lead to proper understanding of existing mechanisms inside of the turbulent fluidized bed reactors.

5.8 Acknowledgements

This work was supported by a grant provided by National Science and Engineering Research Council (NSERC) of Canada. The Ministry of Culture and Higher Education of I. R. of IRAN is also acknowledged for making Mr. R. Sotudeh-Gharebaagh's graduate studies possible in Canada.

5.9 References

Barghi, S., Ph.D. Dissertaion, UWO, 1997.

Bi., J. and T. Kojima, Prediction of temperature and composition in a jetting fluidized bed coal gasifier, Chemical Engineering Science, 51, 11, 1996, 2745.

Darton, R.C., R.D. LaNauze, J.F. Davidson and D. Harrison, Bubble growth due to coalescence in fluidized beds, Trans. Inst. Chem. Eng., 1977, 55, 274-280.

Davidson, J.F., D. Harrison, "Fluidized particles", Cambridge university press, Cambridge, UK, 1963.

Gonzalez, A. Conversion du gaz naturel en éthylène dans un réacteur á lit fluidisé turbulent, PhD, dissertation, Ecole Polytechnique de Montreal. Canada, 1995.

Grace, J., in Handbook of multiphase systems, G. Hestroni, ed.p.8-1, Hemisphere, Washington, D.C., 1982

Merry J. M. D., Penetration of Vertical Jets into Fluidized Beds, AIChE, 21, 3, 507-510, 1975

Pre P., M. Hemati and B. Marchand, "Study on natural gas combustion in fluidized beds: modelling and experimental validation", Chem. Eng. Sci, 53, 16, 2871-2883, 1998.

Sotudeh-Gharebaagh, R. and J. Chaouki, "Gas mixing in a non-premixed turbulent fluidized bed reactor with a downward sparger", Submitted to Canadian Journal of Chemical Engineering, 1998.

Sotudeh-Gharebaagh, R., J. Chaouki and R. Legros, "Natural gas combustion in a turbulent fluidized bed of inert particles", Chem. Eng. Sci, Accepted, 1998a

Sotudeh-Gharebaagh, R., J. Chaouki and R. Legros, "Investigation of heterogeneous and homogeneous combustion of methane", Submitted to Combustion and flame, 1998b.

Van der Vaart D. R., "Mathematical modeling of methane combustion in a fluidized bed", Ind. Eng. Chem. Res., 31, 999-1007, 1992.

Yanata I., Makhorin K. E. and Glukhomanyuk A. M., "Investigation and modelling of the combustion of natural gas in a fluidized bed of inert heat carrier", Int. Chem. Eng., 15, 1, 68-72, 1975.

CONCLUSIONS

The main objective of this study was to assess experimentally the feasibility of natural gas combustion in a fluidized bed reactor of inert particles as an emerging technology capable of meeting all environmental requirements. A pilot plant turbulent fluidized bed reactor was modified to investigate the hydrodynamic and combustion studies. The operating parameters were chosen based on the results of kinetic studies performed in a fixed bed reactor.

Prior to combustion studies in the fluidized bed, the combustion behavior of inert particles was investigated in a fixed bed reactor with the objective of finding the appropriate operating conditions for combustion studies in a pilot plant reactor. The results showed that the sand particles have no accelerating catalytic effect. Inhibition caused by sand particles was important in the temperature range of 850 to 900 °C. The reduced reaction mechanism was also adapted to explain the experimental findings.

Combustion experiments were performed in two different fluidization regimes. The onset of turbulent fluidization regime was experimentally measured at the temperature range of interest. In both bubbling and turbulent fluidization regimes, a high degree of combustion was achieved. The turbulent fluidized bed reactor, as proposed in this study, exhibits an excellent isothermicity and the power generated in this regime is much higher

than that of bubbling fluidized bed reactors while respecting all environmental requirements.

In combustion studies, it has been found that the mixing plays a vital role in non-premixed fluidized bed reactors. Therefore, the tracer gas mixing and sparger hydrodynamic were investigated in order to characterize the flow pattern around the sparger. Two flow patterns around the sparger were identified. These are bubbling and jetting patterns. Under bubbling conditions, the bubbles keep their identity leading to low degree of attrition and therefore mixing controls the reaction process. This helps preventing hot spots. Under jetting conditions, the mixing was very high. But due to attrition level, industrial units can not be safely operated in these conditions. Due to importance of bubbling pattern in large-scale units, a set of mixing and reaction studies were completed for this pattern.

Finally, a model for a non-premixed turbulent fluidized bed was proposed and good agreements with experimental data have been obtained. It is also shown that a detailed kinetic scheme, that takes into account the formation and destruction of pollutant and intermediate species is necessary to predict the concentration profiles. The model to represent the jetting and bubbling region around the injection point is based on our detailed experimental observations. The model proposed in this work may also lead to proper understanding of existing mechanisms inside of the turbulent fluidized bed reactors.

RECOMMENDATIONS

We have shown in this study that the natural gas combustion in a turbulent fluidized bed is feasible and capable of meeting all environmental regulations. An attempt was also made to underline the importance of studying the natural gas combustion as an outstanding sample of highly exothermic reactions in fluidized bed reactors. A reduced mechanism was also integrated in fluidized bed reactors modelling to explain the formation and reduction of unwanted pollutants. The following points could be considered valuable in further understanding of governing phenomena in turbulent fluidized bed reactors:

1- The particles size distribution could have a significant effect on conversion and selectivity in turbulent fluidized bed reactors. There could be a critical particle size to be used in fluidized bed reactors since the inhibition effects might be dominant as compared to bubble size effect.

2- There is no unified correlation to predict minimum jetting velocity for separate injection of reactive into the bed of different particle size. Determination of such correlation would constitute a valuable contribution to the literature on fluidized bed reactors.

3- Understanding of natural gas combustion in turbulent fluidized bed reactor could be considered as an important step in understanding the co-firing and gas reburn. Attempts could be made to co-fire low calorific fuels, waste in fluidized bed reactor with natural gas co-feeding. This would help further development of new combustion devices.

GENERAL BIBLIOGRAPHY

AMERICAN GAS ASSOCIATION (1991 Spring). Cofiring and reburn keep emissions under control, Plant Eng.

ATIMTAY A. AND T. CAKALOZ (1978). Powder Technology, 20 1-7..

AVIDAN A. (1982 Sept. 19-22). Turbulent Fluid Bed Reactors Using Fine Powder Catalysts, in Jt. Meet. Chem. Eng., Chem. Ind. Eng. Soc. China Am. Inst. Chem. Eng. [Proc.], 1, 411-423.

BARGHI, S. (1997). Segregation and solid mixing in fluidized beds, Ph.D. Dissertaion, UWO, 1997.

BENKRID A. AND S.H. CARAM (1989). AIChE J., 35, 1328.

BLAKE, T.R., H. WEBB AND P.B. SUNDERLAND (1990). The nondimensionalization of equations describing fluidization with applications to the correlation of jet penetration height, Chemical Engineering Science, 45, 2, 365-371.

BROUGHTON, J. (1972), Ph.D. dissertation, Newcastle upon Tyne.

CAI, P., S.P. CHEN, Y. JIN, Z.Q. YU AND Z.W. WANG (1989). Effect of temperature and pressure on the transition from bubbling to turbulent fluidization, AIChE symp., 37.

CHANG W.C. (1995). Ph.D. Dissertation, University of California at Berkeley., U.S.A.

CHANTRAVEKIN P. AND HESKETH R. P.(1993). Chem. Phys. Processes Combust. 527-530.

CHEHBOUNI A., CHAOUKI J., GUY C. AND KLVANA D. (1994). Characterization of the Flow Transition between Bubbling and Turbulent Fluidization, IEC J., 33, 8, 1889.

DARTON, R.C., R.D. LANAUZE, J.F. DAVIDSON AND D. HARRISON (1977). Bubble growth due to coalescence in fluidized beds, Trans. Inst. Chem. Eng., 55, 274-280.

DAVIDSON, J.F., D. HARRISON (1963). Fluidized particles, Cambridge university press, Cambridge, UK.

DENNIS J. S., HAYHURST A. N. AND MACKLEY I. G. (1982). in Symposium (International) on Combustion, [Proc.], 19th, 1205-1212.

FEUGIER A., GAULIER C. AND MARTIN G. (1987). Some Aspects of Hydrodynamics, Heat Transfer and Gas Combustion in Circulating Fluidizing Beds, Proc. Int. Conf. Fluid. Bed Combust., (9th), 1, 613-618

FOKA M., CHAOUKI J., GUY C. AND KLVANA D. (1994). Natural gas combustion in a catalytic turbulent fluidized bed, Chemical Engineering Science, 449, 24A, 4269.

FRENKLACH M., (1990). Reduction of Chemical Reaction Models, in Numerical Approaches to Combustion Modeling, Progress in Astronauts and Aeronautics, 135, AIAA, Washington.

FRENKLACH M., H. WANG, C.T. BOWMAN, R.K. HANSON, G.P. SMITH, D.M. GOLDEN, W.C. GARDINER AND V. LISSIANSKI, 25th International Symposium on Combustion, Poster WIP-3-26.

GARDINER, W.C. (1984), Combustion Chemistry, Springer-Verlag, 1984.

GAS RESEARCH INSTITUTE (September 1994 - August 1985), Annual Report,

GONZALEZ, A. (1995). Conversion du gaz naturel en éthylène dans un réacteur á lit fluidisé turbulent, PhD, dissertation, Ecole Polytechnique de Montreal. Canada

GRACE J. R. (1986). Fluidized Beds as Chemical Reactors, Chapter 11 in Gas Fluidization Technology, Edited by Geldart, D., Wiley.

GRACE J.R. (1990). High velocity fluidized bed reactors, Chemical Engineering Science, 45, 1953.

GRACE, J. (1982). in Handbook of multiphase systems, G. Hestroni, ed. 8-1, Hemisphere, Washington, D.C.

GRACE, J.R., AND C.J. LIM (1987). Permanent jet formation in beds of particulate solids, Can. J. Chem. Eng., 65, 160.

GRIFFITHS J.F. (1995). "Reduced kinetics models and their applications to practical combustion systems., Prog. Energy Combust. Sci., 21, 25-107..

GRI-MECH, (1997). http://www.me.berekely.edu/gri_mech/data/rxn_table.html.

GURURAJAN V.S., P.K. AGREWAL AND J.B. AGNEW, (1992), Mathematical modelling of fluidized bed coal gasifiers, Trans.I.Chem.E., 70, 3, 211.

HESKETH R. P. AND DAVIDSON J.F., (1991), Combustion of methane and propane in an incipiently fluidized bed, Combustion and Flame, 85, 449-467.

HIRSAN, I., C. SHISHLTA, AND K.M. KNOWLTON (1980), The effect of bed and jet parameters on vertical jet penetration length in gas fluidized beds, 73rd Annual AIChE meeting, Chicago, Illinois. U.S.A.

KAZAKOV, A. AND FRENKLACH, M (1997). http://diesel.fsc.psu.edu/~gri_mech/drm/home_drm.html.

KEE, R. J., RUPLEY, F.M. AND MILLER, J.A. (1989), SAND89-8009, Sandia national Laboratories.

KEHOE P. W. K. AND DAVIDSON J. F. (1971). Continuously slugging fluidised beds. Inst. Chem. Eng. Symp. Ser., 33, 97.

KUNII D. AND O. LEVENSPIEL (1991), Fluidization Engineering, Butterworth-Heinemann.

LEEDS UNIVERSITY, (1997). http://chem.leeds.ac.uk/Combustion/Combustion.html.

LEWIS, B. AND G. VON ELBE, (1987). Combustion flame and explosions of gases, 3rd edition, Academic Press, London. U.K.

LUFEI J., H.A. BECKER AND R. K. CODE, 1993, "Devolatilization and char burning of coal particles in a fluidized bed combustor", Can. J. Chem. Eng., 71, 10.

MAKANSI J (1989-september)., Power.

MARKATOU, P., L.D., PFEFFERLE AND M.D. SMOOKE, Combus. Flame, 93:185-201, (1993).

MASRI, A.R., R.W. BILGER, R.W. DIBBLE, 1988, Turbulent non-premixed flames of methane near extinction; probability density function, Combustion and flame, 73, 261.

MASSIMILLA, L. (1985), Gas jets in fluidized beds, in Fluidization, 2nd ed., (Edited by Davidson, J., F. Clift, R. Harrison D.), Academic press, New York.

MERRY J. M. D., 1975, Penetration of Vertical Jets into Fluidized Beds, AIChE, 21, 3, 507-510.

MEZAKI, R., C.C. WATSON (1966), Catalytic oxidation of methane, I & EC process design and development, 5, 6.

MILLER J.A. AND G.A.FISK, (1987- August 31), Special Report, C&EN..

MOLERUS O. (1995). Particle Migration at Solid Surfaces and Heat Transfer in Bubbling Fluidized Beds, in Fluidization VIII (Proc. Eng. Found. Conf. Fluid., 8th),. 169-176.

PRE P., M. HEMATI AND B. MARCHAND (1998), Study on natural gas combustion in fluidized beds: modelling and experimental validation, Chem. Eng. Sci, 53, 16, 2871-2883.

ROACH, P.E. (1993), Differentiation between jetting and bubbling in fluidized beds, Int. J. Multiphase Flow, 19, 6, 1159.

SADILOV P. V. AND BASKAKOV A. P. (1973). Temperature fluctuations at the surface of a fluidized bed with gas combustion occurring therein, Int. Chem. Eng., 13, 3, 449.

SHEN Z., C. L. BRIENS, M. KWAUK AND M. A. BERGOUGNOU (1990). Can. J. Chem. Eng., 68, 534-540.

SOTUDEH-GHAREBAAGH R., J. CHAOUKI AND R. LEGROS (1998a), Natural gas combustion in a turbulent fluidized bed of inert particles, in print Chemical Engineering Science.

SOTUDEH-GHAREBAAGH, R. AND J. CHAOUKI (1998). Gas mixing in a non-premixed turbulent fluidized bed reactor with a downward sparger, Submitted to Canadian Journal of Chemical Engineering.

SOTUDEH-GHAREBAAGH, R., J. CHAOUKI AND R. LEGROS (1998b). Investigation of the heterogeneous and homogeneous combustion of methane, submitted to Comb. & Flame.

TOMLIN A.S., T. TURÁNYI AND M.J. PILLING (1997). in:Low temperature combustion and autoignition, eds. M.J. Pilling and G. Hancock, Elsevier.

TRINGHAM, D. J. (1982). Ph.D. dissertation, Leeds, U.K.

VAN DER VAART D. R. (1992). "Mathematical modeling of methane combustion in a fluidized bed", Ind. Eng. Chem. Res., 31, 999-1007, 1992.

VAN DER VAART, D. R. (1998). Combust. Flame, 71, 35-39.

VAN DER VARRT D.R. (1992), Ind. Eng. Chem. Res., 31, 999-1007.

VLACHOS, D. G., SCHMIDT, L. D. AND ARIS, R. (1994). AIChE, 40, 6.

WARNATZ J (1992). Resolution of gas phase and surface combustion chemistry into elementary reactions, 24th Symposium (Int.) on Combust. 553-579.

WARNATZ J., U. MASS AND R.W. DIBBLE (1996). Combustion, Springer.

WEN, C.Y., M. HORIO, R. KIRSHNAN, R. KHOSRAVI, P. RENGARAJAN (1987), Proc. Second. Pacific Chem. Eng. Cong., 1182.

WERTHER J. AND W. XI (1993), Jet Attrition of Catalyst Particles in Gas Fluidized Beds, Powder Technology,76 , 39-46.

YANATA I., MAKHORIN K. E. AND GLUKHOMANYUK A. M. (1975), Investigation and modelling of the combustion of natural gas in a fluidized bed of inert heat carrier, Int. Chem. Eng., 15, 1, 68-72.

YANG W. C., B. ETTEHADIEH, T. C. ANESTIS, R. E. GIZZIE AND G. B. HALDIPUR (1986). in K. Østergaard and A. Sørensen (eds), Fluidization V, Engineering Foundation, New York, 95-102.

YANG, W.C. (1981), Jet penetration in a pressurized fluidized bed, IEC Fundamental, 20, 297.

YANG, W.C. AND D.L. KEAIRNS (1979), Estimating the jet penetration depth of multiple vertical grid jets, IEC Fundamental, 18, 4, 317.

YATES J. G., V. BEJCEK AND D. J. CHEESMAN (1986). in K. Østergaard and A. Sørensen (eds), Fluidization V, Engineering Foundation, New York, 79-86.

YATES, J.G. (1996), Effects of temperature and pressure on gas-solid fluidization, Chemical Engineering Science, 51, 2, 167-205.

APPENDICES

APPENDIX I Complementary Detail for Chapter II

In this appendix, an energy balance for the preheating zone and a laminar flow reactor model for the reaction zone of empty annular region of the fixed bed reactor are presented in detail.

Energy balance for the preheating zone

Because the flow in the preheating zone is completely enclosed, an energy balance may be applied to determine how the mean temperature $T_m(z)$ varies with position along the concentric tube annulus (Figure 2.1). In this zone, fluid moves at a constant mass flow rate (w). Convection and radiation heat transfers occur at the outer surface, where constant wall temperature is assumed. Energy balance in inner tube shows that there is no temperature profile developed in inner surface. Typically, fluid kinetics as well as energy transfers by conduction in the axial direction are negligible. Applying conservation of energy to the differential control volume, we obtain:

$$\frac{dT_m}{dz} = \frac{2\pi R}{wc_p} h_T (T_s - T_m) \qquad \text{(A.1)}$$

In this equation, T_m is a bulk temperature, z is axial position, R is outer tube diameter, T_s is a surface temperature, C_p is the gas specific heat and h_T is a global heat transfer coefficient.

where h_T is:

$$h_T = h_c + h_r = \frac{K\,Nu}{R(1-k)} + \sigma\varepsilon_g (Ts + Tm)(Ts^2 + Tm^2) \qquad (A.2)$$

In this equation, K is thermal conductivity, Nu is the Nuselt number, k is ratio of outer tuber diameter to inner tube diameter, σ is Stefan-Boltzman constant and ε is emissivity. This ordinary differential equation can be solved subject to corresponding boundary conditions to obtain the mean temperature variation with position along the concentric tube annulus for the preheating zone. Typical profile obtained in this way is shown in Figure A.1. As shown in this figure, gas rapidly reaches to the surface temperature before entering to the reaction zone. This is justified considering low specific C_p and flow rate of mixture flowing in a very thin concentric tube annulus, where the radiation effects are also present.

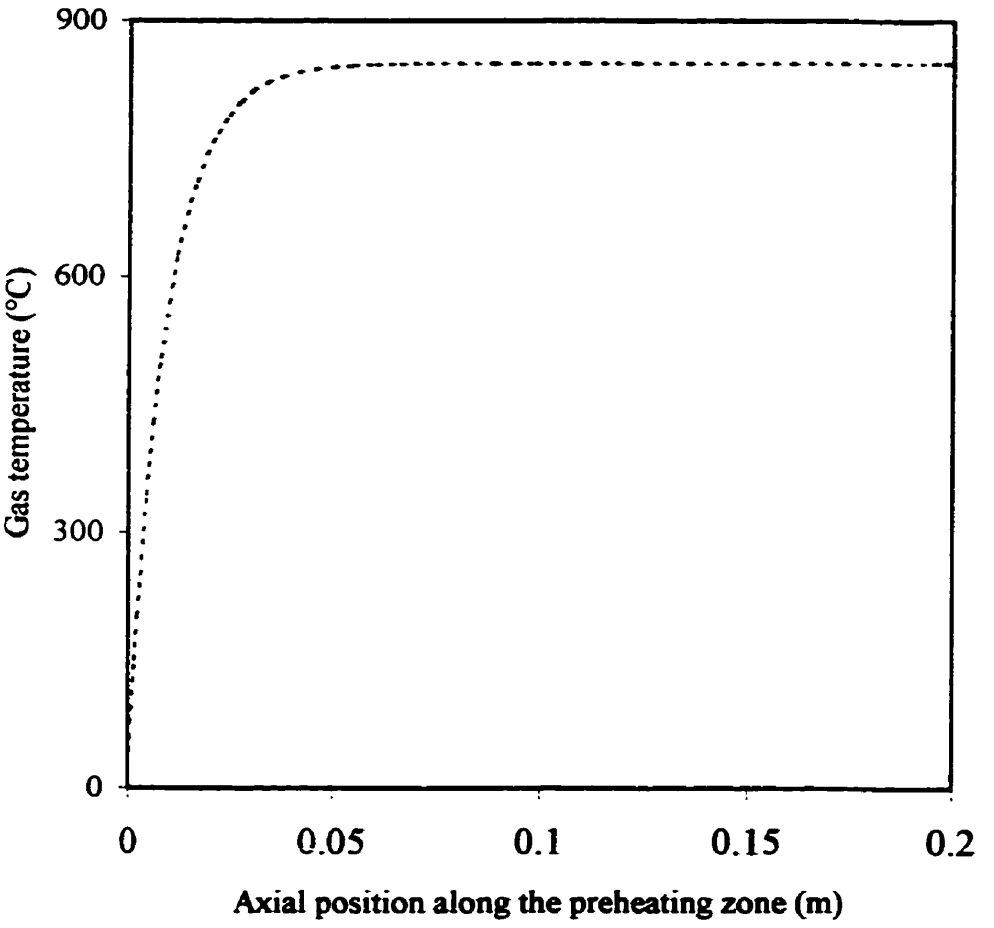

Figure A. 1 Variation of mean temperature with position along the concentric tube annulus for the preheating zone

Laminar flow reactor model for empty reactor experiments

For the annular region between two co-axial circular cylinders of radii kR and R (Figure 2.1) within the reaction zone, the radial velocity (u_r) distribution in radial position (r) is:

$$u_r = 2u_m \left[\frac{\left[1-\left(\frac{r}{R}\right)^2 + \left(\frac{1-k^2}{\ln(1/k)}\right)\ln\left(\frac{r}{R}\right) \right]}{\left[\left(1-k^2\right) - \frac{\left(1-k^2\right)}{\ln(1/k)} \right]} \right] \qquad \text{(A.3)}$$

In this equation, u_m is the mean velocity. The mean fractional conversion (X_m) of material converted in this zone in any axial position is:

$$X_m = \frac{\int_{kR}^{R} 2\pi X u_r r\, dr}{\int_{kR}^{R} 2\pi u_r r\, dr} \qquad \text{(A.4)}$$

Plug flow design equation (Eq. 2.13) can be used to evaluate the fractional conversion X as a function of radial position for a given radial velocity considering the reaction scheme in all grid points. The typical results of such calculations are presented in Figure 2.3.

APPENDIX II Protocole de Sécurité et d'Opération du Lit Fluidisé

Ce manuel regroupe les dispositions générales, les procédures ainsi que des données diverses (limite d'inflammabilité, toxicité, etc.) sur les composants principaux que l'on retrouve dans l'unité pilote du lit fluidisé turbulent qui est utilisé pour la combustion du gaz naturel à des témperatures relativement élevées (800-1000°C). Le but de ce document est de permettre aux utilisateurs de bien opérer l'unité et aussi d'être prêts à réagir devant toute anomalie.

Introduction

La combustion de gaz naturel dans un lit fluidisé turbulent est un procédé qui requiert plusieurs mesures de sécurité. Il s'agit d'un sujet complexe et multidisciplinaire qui demande des informations des sources variées telles chimiques, génie, médicales, et des expériences passées. A la lumière de ces informations, les dispositions générales et les procédures de sécurité, sont proposées dans le présent document afin d'opérer de façon sécuritaire l'unité expérimentale dans Centre de Recherche de BIOPRO. Tables AII.1, AII.2 aussi présentent les données diverses sur la limite d'inflammabilité et la toxicité pour les composants clés se retrouvant dans la combustion du gaz naturel dans un lit fluidisé turbulent.

Table A. 1 Risques inhérents à la présence de certains composés

Composé	Remarque	Seuil critique
He	Gaz asphyxiant	
CH_4	Inflammable, peut présenter un grand risque d'incendie et d'explosion.	
CO	Très inflammable, peut représenter un risque d'incendie et d'explosion, grande affinité pour l'hémoglobine.	TLV*: 50 ppm
CO_2	Peut représenter un danger limitant la réoxigénation cellulaire en trop grande concentrations.	TLV: 5000 ppm
NO	Composé nocif en trop grandes concentrations	TLV: 25 ppm
N_2O	Gaz asphyxiant utilisé pour ses propriétés anesthésiques, dommageable à des concentrations élevées	
NO_2	Gaz ayant un fort pouvoir oxydant, peut entraîner la mort même à de faibles concentrations.	TLV: 3 ppm ITLV**: 5 ppm

* Threshold Limit Value (TLV)

** Industrial Threshold Limit Value (ITLV)

Table A. 2 Données d'inflammabilité

Composé	Limite d'inflammabilité (fraction volumique dans l'air)		Température d'inflammation spontanée (°C)
	Inférieure	Supérieure	
CH_4	0.05	0.15	537
C_2H_6	0.03	0.125	515
H_2	0.04	0.742	400
CO	0.125	0.742	609

Ces valeurs de limites d'inflammabilité sont valides pour les gaz à TPN.

Dispositions générales

Les éléments suivants doivent être respectés en tout temps au laboratoire:

- Ne pas fumer;
- Porter lorsqu'à proximité du montage les éléments de protection personnels suivants: lunettes de sécurité, filtres respiratoires et survêtements protecteurs;
- Avoir en tout temps ce "*PROTOCOLE DE SÉCURITÉ ET D'OPÉRATION*" bien en vue;

- Afficher la liste des personnes (coordonnées) à aviser en cas d'anomalie.

- De façon générale, toujours aviser les personnes responsable du montage lorsque des manipulations sont en cours où prévues.

Étapes préliminaires

Les étapes suivantes, considérées comme étant essentielles au bon déroulement des expériences, doivent être effectuées avant chaque série d'expériences:

- Vérifier l'étanchéité du montage;

- Vérifier l'état des sondes et les changer au besoin;

- S'assurer du bon fonctionnement des détecteurs de sécurité;

- Faire une inspection générale au niveau des circuits électriques;

- Faire une inspection générale au niveau des circuits pneumatiques activant l'auvent;

- Veiller à ce que les électrovannes soient opérationnelles;

- S'assurer du bon fonctionnement du détecteur de flamme;

- Vérifier le niveau des bombonnes d'azote et d'hélium.

- Ne procéder au démarrage de l'unité que si les points 1 à 8 sont respectés, sinon remédier à la situation avant de poursuivre.

Procédure de préchauffage

Étant donné que la plupart des expériences se dérouleront à haute température, il faut préchauffer le lit en respectant la démarche qui suit:

- Démarrer le programme d'acquisition de données et le configurer, si nécessaire, de façon à ce que les mesures de température et de pression du lit et du windbox y soient présentées;

- Mettre en tension l'unité au moyen de l'interrupteur principal;

- S'assurer qu'il n'y ait pas de gaz combustibles présents dans le réacteur en purgeant avec de l'azote si nécessaire;

- Ouvrir l'électrovanne principale de l'air (interrupteur "AIR" à la position ON);

- Ouvrir et ajuster au besoin le débit d'air vers le brûleur à l'aide des vannes manuelles en s'assurant que le lit soit fluidisé au moyen des mesures de pressions (ATTENTION : un débit trop élevé résultera en des problèmes d'emportement et d'attrition importants à plus haute température).

- Appuyer sur le bouton "RESET" de la boîte du contrôleur de façon à ce que le voyant lumineux rouge s'éteigne (ceci permettra de procéder à l'allumage du brûleur);

- Mettre l'interrupteur "DÉMARRAGE" à la position "ON" suivi immédiatement de l'interrupteur "GAZ 2" à la position "ON" pour procéder à l'allumage du brûleur;

- Vérifier qu'il y a détection de flamme et ajuster au besoin les debits d'air et de gaz naturel, sinon remettre les interrupteurs "DÉMARRAGE" et "GAZ 2" à la position "OFF" et recommencer des étapes 5 à 7;

- Ajuster les débits de gaz naturel et d'air afin de contrôler le préchauffage du lit et s'assurer d'avoir une combustion complète;

- Continuer de préchauffer jusqu'à l'obtention d'une température de 775 à 800°C dans le WINDBOX, puis selon la température désirée, passer aux étapes suivantes :

- Si une température de lit entre 750 et 800°C est désirée, progressivement réduire le gaz du brûleur et l'injecter directement dans le WINDBOX jusqu'à obtention de la température voulue (à ce stade, la combustion peut avoir lieu dans le WINDBOX, l'utilisation du brûleur est discrétionnaire).

- Si une température de lit supérieure à 800°C est désirée, suivre ce qui est mentionné en (10.1) jusqu'à 800°C. A ce point, couper le gaz au WINDBOX et l'injecter directement dans le lit.

- Arrêter l'alimentation du gaz naturel au brûleur si ce n'est pas déjà fait :

- Mettre l'interrupteur "GAZ 2" en position "OFF", ceci entraîne une erreur et le voyant du contrôleur de flamme l'allume;

- Positionner l'interrupteur "DÉMARRAGE" à la position "OFF";

- Fermer la vanne manuelle du gaz naturel vers le brûleur.

Table A. 3 Schéma des interrupteur

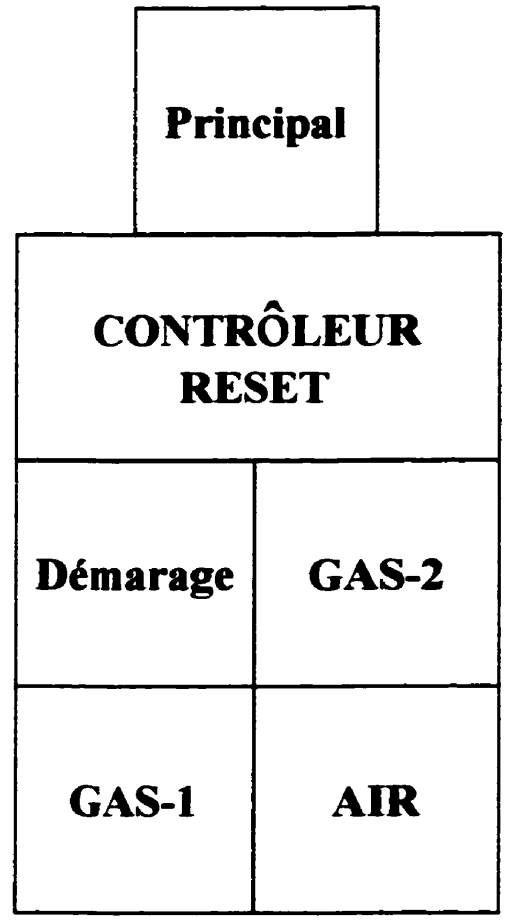

Procédure d'opération

Il existe deux modes d'opération pour la combustion du gaz naturel dans un lit fluidisé turbulent : le cas "PREMIXED" et le cas "NON-PREMIXED". Quand la température désirée du lit est obtenue à l'aide de la procédure de préchauffage, la combustion peut avoir lieu. Voici selon le cas, la procédure à suivre :

A) CAS "PREMIXED"

- Dans ce cas ci, la combustion peut avoir lieu dans le WINDBOX. Avant d'alimenter le gaz naturel, s'assurer que le WINDBOX est à une température inférieure à 500°C pour éviter que la combustion s'y propage;
- Alimenter progressivement l'air et le gaz naturel au réacteur (le gaz naturel est alimenté au niveau du WINDBOX);
- Ajuster la vitesse superficielle du gaz et aussi le ratio air/gaz naturel au niveau désiré;
- Poursuivre l'opération suffisamment longtemps afin de dresser un portrait représentatif.

B) CAS "NON-PREMIXED"

- Dans ce cas ci, on alimente directement dans le lit. Alimenter progressivement l'air et le gaz naturel au réacteur (le gaz naturel est alimenté au niveau du lit);
- Ajuster la vitesse superficielle du gaz et aussi le ratio air/gaz naturel au niveau désiré;

- Poursuivre l'opération suffisamment longtemps afin de dresser un portrait représentatif.

Procédure d'arrêt

- Couper l'alimentation en gaz au réacteur et au brûleur.
- Maintenir un débit d'air suffisant pour assurer la fluidisation du lit.
- Mettre tous les interrupteurs et les vannes manuelles en position "OFF" jusqu'aux prochaines expériences.

Guide de dépannage

Ce tableau présente le guide de dépannage pour l'opération du lit fluidisé turbulent. Pour chaque anomalie, on propose une démarche de remédiation.

Table A. 4 Guide de dépannage pour l'opération du lit fluidisé turbulent

Observation	Diagnostique	Démarche
CO > 50 ppm	Fuite dans le TFBC.	1. Mettre un masque à gaz. 2. Procéder à l'arrêt* de l'unité. 3. Ouvrir les fenêtres du laboratoire. 4. Quitter la zone.
Hydrocarbures > 2 %	Fuite dans le TFBC.	1. Procéder à l'arrêt de l'unité. 2. Ouvrir les fenêtres du laboratoire. 3. Quitter la zone.
T> 1100°C	Mauvaise fluidisation ou perte des particules.	1. Procéder à l'arrêt de l'unité. 2. Quitter la zone.
P > 5 psia	Obstructions des conduits. Conditions explosives. Risque de défluidisation.	1. Procéder à l'arrêt de l'unité. 2. Quitter la zone.
Fumée à la sortie du TFBC.	Formation de carbone solide.	1. Vérifier les conditions d'operation.
Poussière dans l'aire de travail.	Haut taux d'entrainement. Attrition des particules.	1. Vérifier la vitesse superficielle de gaz. 2. Vérifier l'état des particules.
Érosion de la couche réfractaire de la paroi interne du réacteur.		1. Procéder à l'arrêt de l'unité. 2. Remplacer la couche réfractaire.

- Selon la procédure déjà décrite

Références

Hawley G.G., N. I. Sax and R.J. Lewis, " Hawley's Condensed Chemical Dictionary", 11th ed., New York, 1987.

CRC, " CRC Handbook of Chemistry and Physics : a Ready-Reference Book of Chemical and Physical Data", 75th ed., Cleveland, CRC, 1995.

APPENDIX III Pressure Fluctuation Signal Processing

In order to process the experimental pressure fluctuation data, a sampling time interval of 50 ms was selected for the conversion of the analog signal to the digital signal. The sampling interval ensured a good quality and undistorted character of the measured frequency up to 10 Hz. From the data collected for about 120s the mean pressure drop over the bed and the mean deviation of the pressure fluctuation signal from the mean pressure drop were computed. The power frequency spectrum was obtained by the fast Fourier transform of the pressure fluctuation signal. The frequency corresponding to the maximum power in the spectrum was called the dominant frequency and the other local maximums were called the side frequencies. The spectral power density can be used as a measure of the "quality" of the fluidization under various operating conditions. Typical examples of the pressure fluctuation signal from the bed of sand particles and the corresponding power spectrum of frequencies are shown in Figures A.2 and A.3. For original signal reported in these figures, the pressure probe location was 16.7 cm above the main distributor and 3mm below the sparger, where the tracer is injected separately to the bed.

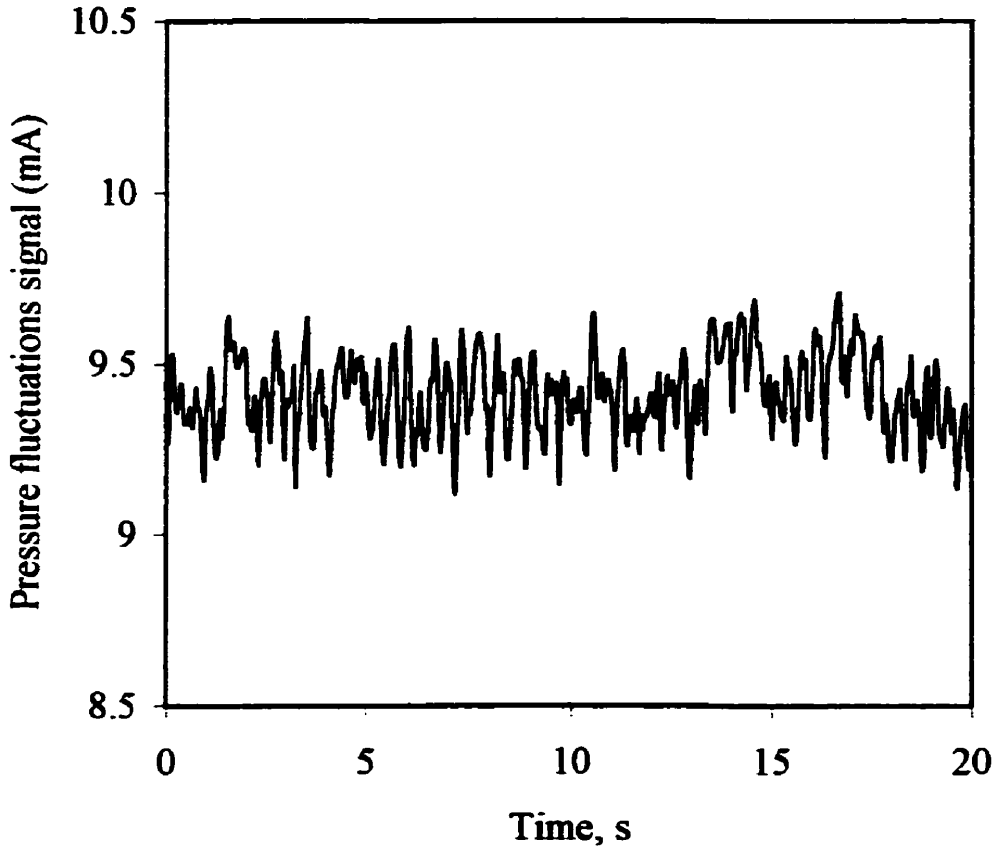

Figure A. 2 **Pressure fluctuation in the fluidized bed of sand particles (dp=230μm, T=440 °C, dj=2mm, U=0.25 m/s , Uj=200 m/s)**

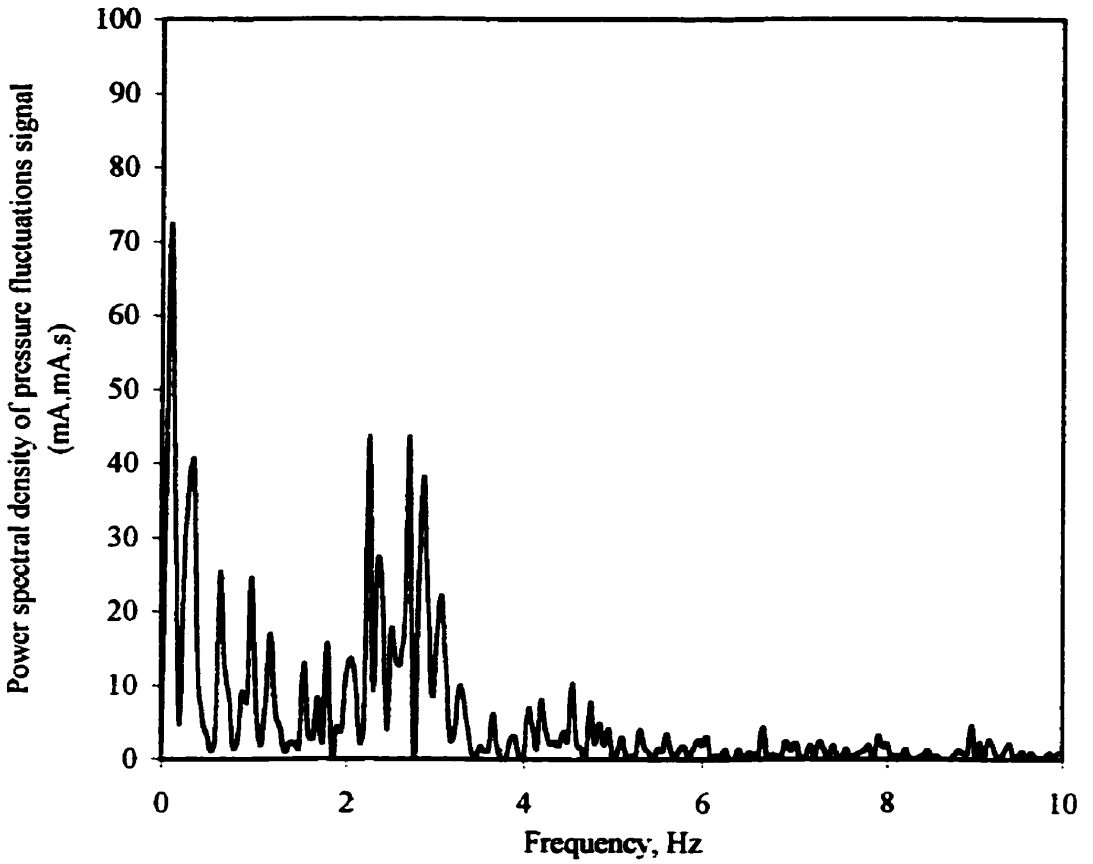

Figure A. 3 Power spectrum of the pressure fluctuation signal shown in Figure A.2

APPENDIX IV Calculation of Sample Concentration for Three-Phase Model

It is assumed that the rate of gas drawn through the sampling probe is constant and hence the composition of sampled mixture (C_{probe}) is:

$$C_{probe} = \delta_s C_s + \delta_g C_g + (1-(\delta_g + \delta_S))C_e \qquad \text{(A.5)}$$

For the axial positions far from the sparger the sparger, comparing the sparger bubble phase concentration with concentration at grid bubble phase and emulsion phase, intuition suggests that the grid bubble phase concentration and emulsion phase concentration may be considered very close together. This can be justified considering the fact that these concentrations are one order of magnitude smaller than that of sparger bubble phase. By this hypothesis, the equation (A.5) is reduced to:

$$C_{probe} = \delta_s C_s + (1-\delta_S)C_e \qquad \text{(A.6)}$$

Knowing the bubble size issued by sparger and also the corresponding equations as presented in chapter 4 and 5, one can calculate the concentration of the sparger bubble

phase. Know by applying the equation (A.6), the concentration profile for emulsion phase can be estimated by:

$$C_e = \frac{C_{probe} - \delta_s C_s}{1 - \delta_S} \qquad \text{(A.7)}$$

This concentration is also considered for grid bubble phase. The typical concentration profiles calculated in this way are shown in Figure 4.11 for flat sparger at 400 °C, U_j=37m/s and U=0.8 m/s. As seen from this Figure, at the point in the vicinity of the sparger, the emulsion phase concentration should be very high. Such high value can be attributed to the fact that the concentration of tracer in grid bubble phase is very low, since the grid bubbles are unlikely present at the vicinity of the sparger. It can also be concluded that at the axial positions well below 100mm, the probe mostly captures the bubbles from the sparger phase.